CNN Pincer Ruthenium Complexes for Efficient Transfer Hydrogenation of Biomass-Derived Carbonyl Compounds

Rosario Figliolia, Paolo Cavigli, Clara Comuzzi, Alessandro Del Zotto, Denise Lovison, Paolo Strazzolini, Sabina Susmel, Daniele Zuccaccia, Maurizio Ballico, Walter Baratta

Supporting Information

Table of Contents:

Figure S1. ^{1}H NMR spectrum of 6-(4-methoxyphenyl)pyridine-2-carbaldehyde oxime Pag. S1

Figure S2. ^{13}C{^{1}H} NMR spectrum of 6-(4-methoxyphenyl)pyridine-2-carbaldehyde oxime Pag. S2

Figure S3. (+)-ESI-MS and MS/MS spectra of 6-(4-methoxyphenyl)pyridine-2-carbaldehyde oxime Pag. S3

Figure S4. ^{1}H NMR spectrum of (6-(4-methoxyphenyl)pyridin-2-y)methanamine (HCNN^{OMe}) Pag. S4

Figure S5. ^{13}C{^{1}H} DEPTQ NMR spectrum of (6-(4-methoxyphenyl)pyridin-2-y)methanamine (HCNN^{OMe}) Pag. S5

Figure S6. (+)-ESI-MS and MS^{n} spectra of (6-(4-methoxyphenyl)pyridin-2-y)methanamine (HCNN^{OMe}) Pag. S6

Figure S7. ^{31}P{^{1}H} NMR spectrum of *cis*-[RuCl(CNN^{OMe})(PPh$_3$)$_2$] (**1**) Pag. S7

Figure S8. ^{1}H NMR spectrum of *cis*-[RuCl(CNN^{OMe})(PPh$_3$)$_2$] (**1**) Pag. S8

Figure S9. ^{13}C{^{1}H} DEPTQ NMR spectrum of *cis*-[RuCl(CNN^{OMe})(PPh$_3$)$_2$] (**1**) Pag. S9

Figure S10. ^{13}C{^{1}H} QUATD NMR spectrum of *cis*-[RuCl(CNN^{OMe})(PPh$_3$)$_2$] (**1**) Pag. S10

Figure S11. ^{31}P{^{1}H} NMR spectrum of [RuCl(CNN^{OMe})(dppb)] (**2**) Pag. S11

Figure S12. ^{1}H NMR spectrum of [RuCl(CNN^{OMe})(dppb)] (**2**) Pag. S12

Figure S13. $^{13}C\{^{1}H\}$ DEPTQ NMR spectrum of [RuCl(CNN^{OMe})(dppb)] (**2**) Pag. S13

Figure S14. ^{1}H-^{1}H COSY 2D NMR spectrum of [RuCl(CNN^{OMe})(dppb)] (**2**) Pag. S14

Figure S15. Aromatic region of the ^{1}H-^{1}H COSY 2D NMR spectrum of [RuCl(CNN^{OMe})(dppb)] (**2**) Pag. S15

Figure S16. Alkylic region of the ^{1}H-^{1}H COSY 2D NMR spectrum of [RuCl(CNN^{OMe})(dppb)] (**2**) Pag. S15

Figure S17. ^{1}H-^{1}H NOESY 2D NMR spectrum of [RuCl(CNN^{OMe})(dppb)] (**2**) Pag. S16

Figure S18. ^{1}H-^{13}C HSQC 2D NMR spectrum of [RuCl(CNN^{OMe})(dppb)] (**2**) Pag. S17

Figure S19. Aromatic region of the ^{1}H-^{13}C HSQC 2D NMR spectrum of [RuCl(CNN^{OMe})(dppb)] (**2**) Pag. S18

Figure S20. Alkylic region of the ^{1}H-^{13}C HSQC 2D NMR spectrum of [RuCl(CNN^{OMe})(dppb)] (**2**) Pag. S18

Figure S21. ^{1}H-^{31}P HMBC 2D NMR spectrum of [RuCl(CNN^{OMe})(dppb)] (**2**) Pag. S19

Figure S22. ^{1}H-^{15}N HSQC 2D NMR spectrum of [RuCl(CNN^{OMe})(dppb)] (**2**) Pag. S20

Figure S23. $^{31}P\{^{1}H\}$ NMR spectrum of [RuCl(CNN^{OMe})(dppf)] (**3**) Pag. S21

Figure S24. ^{1}H NMR spectrum of [RuCl(CNN^{OMe})(dppf)] (**3**) Pag. S22

Figure S25. $^{13}C\{^{1}H\}$ DEPTQ NMR spectrum of [RuCl(CNN^{OMe})(dppf)] (**3**) Pag. S23

Figure S26. $^{31}P\{^{1}H\}$ NMR spectrum of [RuCl(CNN^{OMe})(CO)(PPh$_3$)] (**4**) Pag. S24

Figure S27. ^{1}H NMR spectrum of [RuCl(CNN^{OMe})(CO)(PPh$_3$)] (**4**) Pag. S25

Figure S28. $^{13}C\{^{1}H\}$ DEPTQ NMR spectrum of [RuCl(CNN^{OMe})(CO)(PPh$_3$)] (**4**) Pag. S26

Figure S29. $^{31}P\{^{1}H\}$ NMR spectrum of *trans*-[Ru(CNN^{OMe})(CO)(PCy$_3$)(PPh$_3$)][BAr$^{f}_4$] (**5**) Pag. S27

Figure S30. ^{1}H NMR spectrum of *trans*-[Ru(CNN^{OMe})(CO)(PCy$_3$)(PPh$_3$)][BAr$^{f}_4$] (**5**) Pag. S28

Figure S31. $^{13}C\{^{1}H\}$ DEPTQ NMR spectrum of *trans*-[Ru(CNN^{OMe})(CO)(PCy$_3$)(PPh$_3$)][BAr$^f_4$] (**5**) Pag. S29

Figure S32. ^{1}H-^{1}H COSY 2D NMR spectrum of *trans*-[Ru(CNN^{OMe})(CO)(PCy$_3$)(PPh$_3$)][BAr$^f_4$] (**5**) Pag. S30

Figure S33. Aromatic region of the ^{1}H-^{1}H COSY 2D NMR spectrum of *trans*-[Ru(CNN^{OMe})(CO)(PCy$_3$)(PPh$_3$)][BAr$^f_4$] (**5**) Pag. S31

Figure S34. Alkylic region of the ^{1}H-^{1}H COSY 2D NMR spectrum of *trans*-[Ru(CNN^{OMe})(CO)(PCy$_3$)(PPh$_3$)][BAr$^f_4$] (**5**) Pag. S31

Figure S35. ^{1}H-^{1}H NOESY 2D NMR spectrum of *trans*-[Ru(CNN^{OMe})(CO)(PCy$_3$)(PPh$_3$)][BAr$^f_4$] (**5**) Pag. S32

Figure S36. ^{1}H-^{13}C HSQC 2D NMR spectrum of *trans*-[Ru(CNN^{OMe})(CO)(PCy$_3$)(PPh$_3$)][BAr$^f_4$] (**5**) Pag. S33

Figure S37. Alkylic region of the ^{1}H-^{13}C HSQC 2D NMR spectrum of *trans*-[Ru(CNN^{OMe})(CO)(PCy$_3$)(PPh$_3$)][BAr$^f_4$] (**5**) Pag. S34

Figure S38. Aromatic region of the ^{1}H-^{13}C HSQC 2D NMR spectrum of *trans*-[Ru(CNN^{OMe})(CO)(PCy$_3$)(PPh$_3$)][BAr$^f_4$] (**5**) Pag. S34

Figure S39. ^{1}H-^{31}P HMBC 2D NMR spectrum of *trans*-[Ru(CNN^{OMe})(CO)(PCy$_3$)(PPh$_3$)][BAr$^f_4$] (**5**) Pag. S35

Table S1. Further data regarding the catalytic TH of lignocellulose biomass carbonyl compounds to alcohols with **2**, **3**, **5** (S/C = 1000-10000) Pag. S36

Figure S40. ^{1}H NMR spectrum of γ-valerolactone (GVL) obtained from TH reduction of ethyl levulinate in 2-propanol catalyzed by ruthenium pincer complexes **2**, **3** and **5** Pag. S37

Figure S41. GC-FID chromatograms of the reaction mixture of the TH of cinnamaldehyde **g** in 2-propanol at reflux promoted by complex **2** at S/C 1000 Pag. S38

Figure S42. ^{1}H NMR spectrum of furfuryl alcohol obtained from TH of furfural Pag. S39

Figure S43. ^{13}C{^{1}H} NMR spectrum of furfuryl alcohol obtained from TH of furfural Pag. S40

Figure S44. ^{1}H NMR spectrum of 2,5-bis(hydroxymethyl)furan (BHMF) obtained from TH of 5-HMF Pag. S41

Figure S45. ^{13}C{^{1}H} DEPTQ NMR spectrum of 2,5-bis(hydroxymethyl)furan (BHMF) obtained from TH of 5-HMF Pag. S42

Figure S46. Comparison between the GC-FID chromatograms of levoglucosanol obtained from TH of Cyrene **e** i promoted by complex **2** (A), **3** (B) and **5** (C) at S/C 10000 Pag. S43

Figure S47. ^{1}H NMR spectrum of levoglucosanol obtained from TH of Cyrene **e** promoted by complex **2** at S/C 10000 (*erithro*/*threo* ratio 1/1.2) Pag. S44

Figure S48. ^{13}C{^{1}H} DEPTQ NMR spectrum of levoglucosanol obtained from TH of Cyrene **e** promoted by complex **2** at S/C 10000 (*erithro*/*threo* ratio 1/1.2) Pag. S45

Figure S49. GC-FID chromatogram of γ-valerolactone (GVL) obtained from TH of ethyl levulinate **f** promoted by complex **2** at S/C 1000 Pag. S46

Figure S50. ^{1}H NMR spectrum of γ-valerolactone (GVL) obtained from TH of ethyl levulinate **f** promoted by complex **2** at S/C 1000 Pag. S47

Figure S51. ^{13}C{^{1}H} DEPTQ NMR spectrum of γ-valerolactone (GVL) obtained from TH of ethyl levulinate **f** promoted by complex **2** at S/C 1000 Pag. S48

Figure S52. ^{1}H NMR spectrum of cinnamyl alcohol obtained from TH of *trans*-cinnamaldehyde **g** Pag. S49

Figure S53. ^{3}C{^{1}H}NMR spectrum of cinnamyl alcohol obtained from TH of *trans*-cinnamaldehyde **g** Pag. S50

Figure S54. ^{1}H NMR spectrum of veratryl alcohol obtained from TH of veratraldehyde **h** Pag. S51

Figure S55. ^{1}H NMR spectrum of the dibenzyl alcohol obtained from TH of 4,4'-[ethane-1,2-diylbis(oxy)]bis(3-methoxybenzaldehyde) (EDOMB) **i** Pag. S52

Figure S56. $^{13}C\{^{1}H\}$ DEPTQ NMR spectrum of the dibenzyl alcohol obtained from TH of 4,4'-[ethane-1,2-diylbis(oxy)]bis(3-methoxybenzaldehyde) (EDOMB) **i** Pag. S53

Figure S57. ^{1}H NMR spectrum of vanillyl alcohol obtained from TH of vanillin **j** Pag. S54

Figure S58. $^{13}C\{^{1}H\}$ DEPTQ NMR spectrum of vanillyl alcohol obtained from TH of vanillin **j** Pag. S55

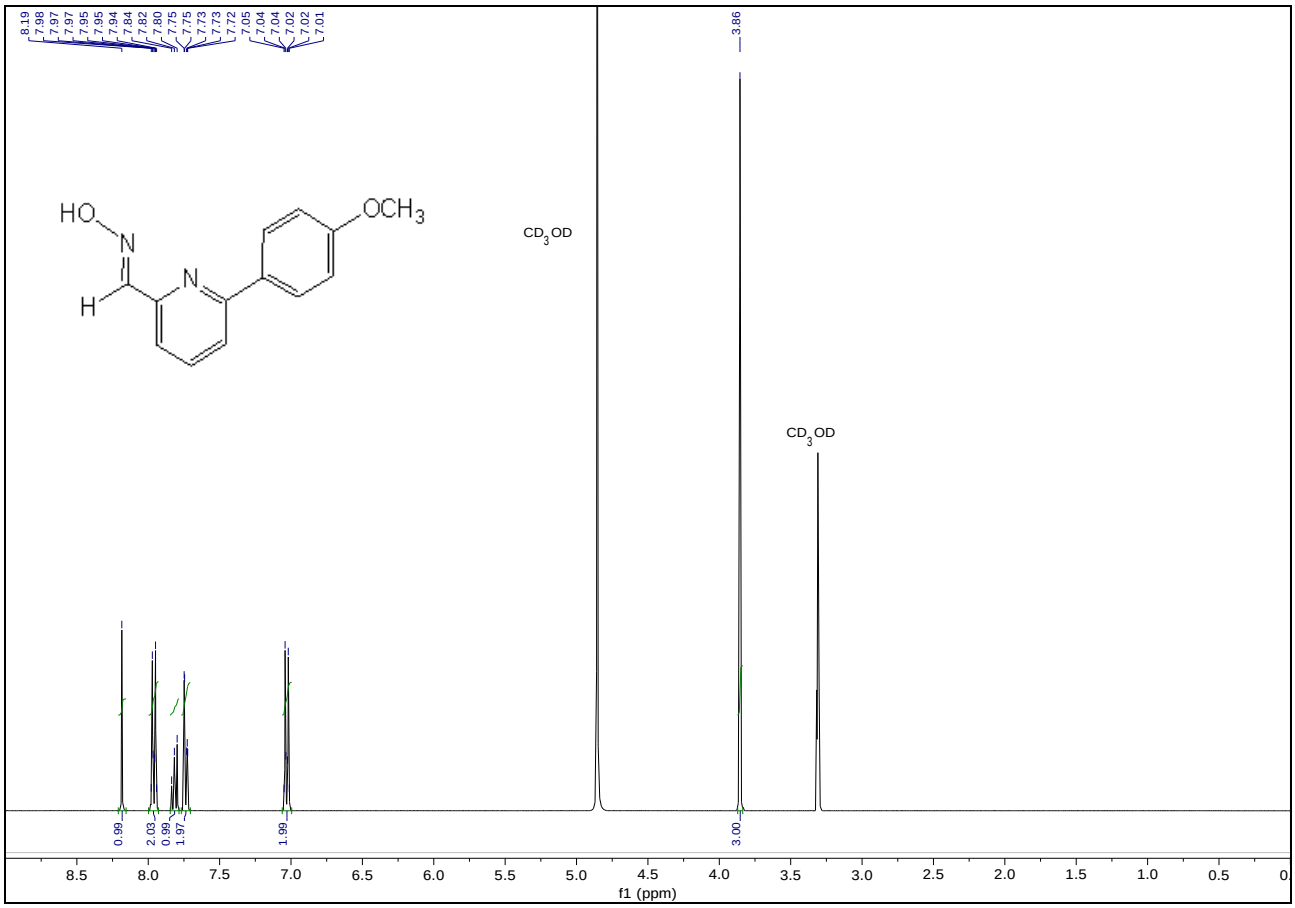

Figure S1. ^{1}H NMR spectrum (400.1 MHz) of 6-(4-methoxyphenyl)pyridine-2-carbaldehyde oxime in CD_3OD at 25 °C.

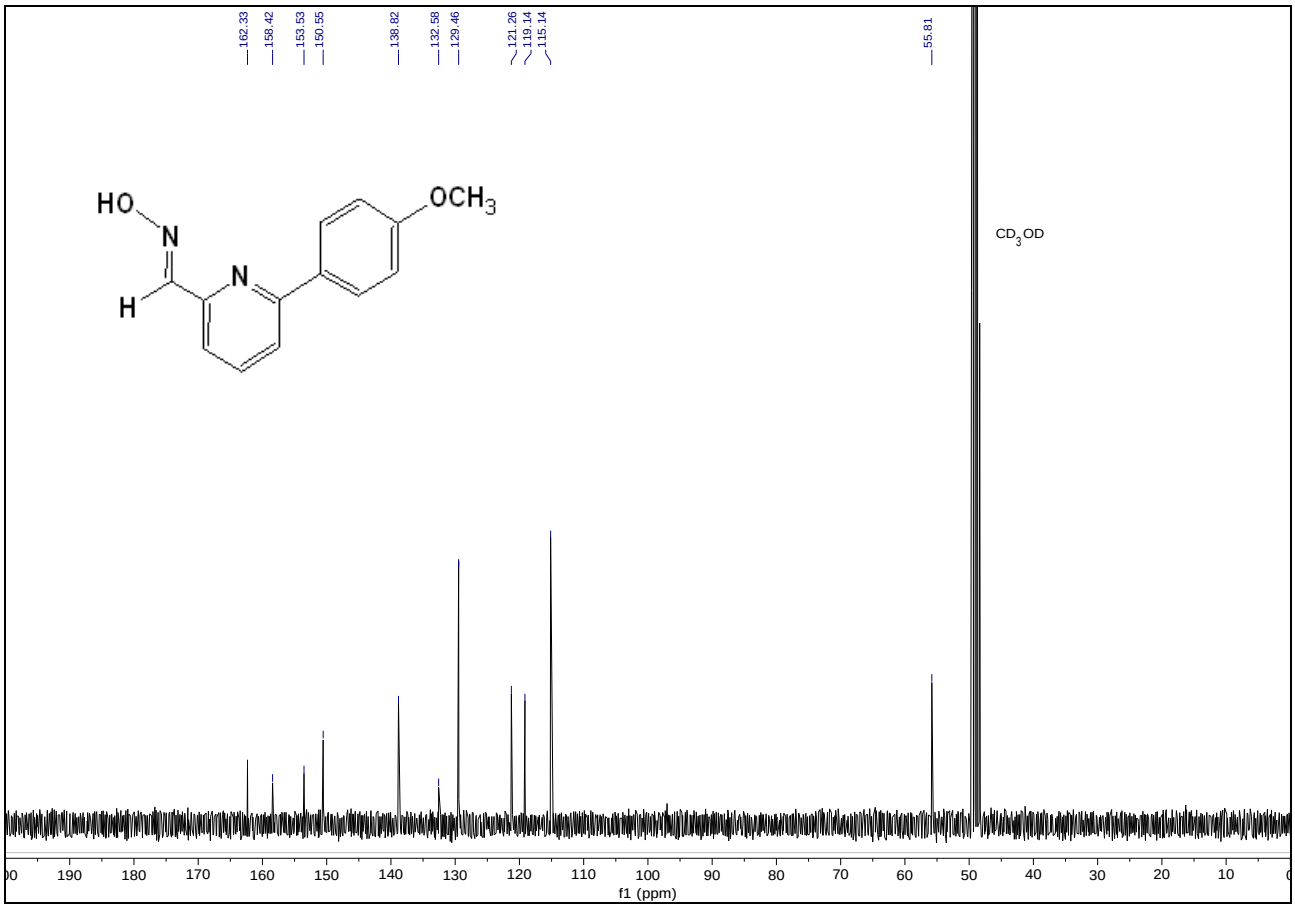

Figure S2. $^{13}C\{^{1}H\}$ NMR spectrum (100.6 MHz) of 6-(4-methoxyphenyl)pyridine-2-carbaldehyde oxime in CD_3OD at 25 °C.

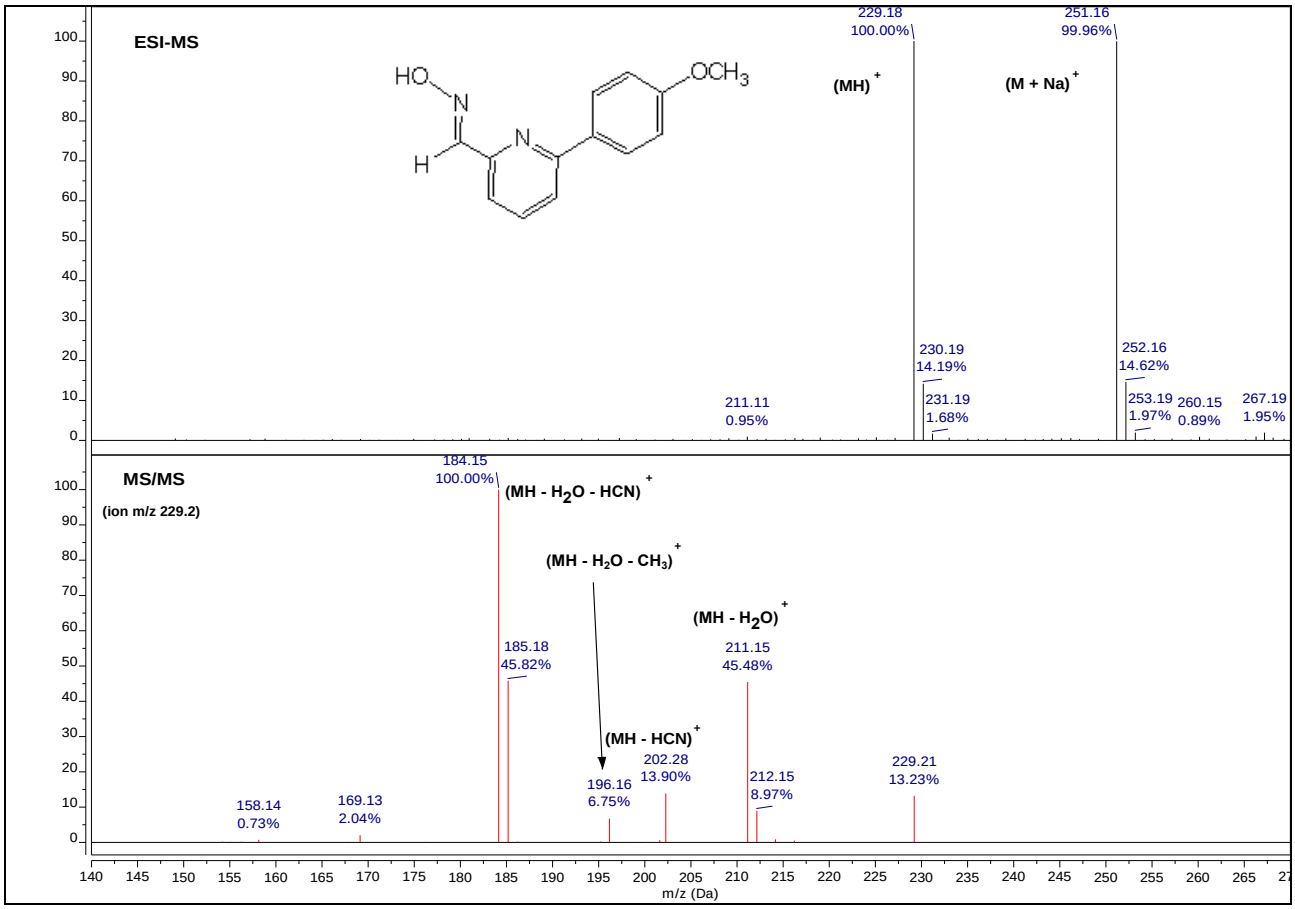

Figure S3. (+)-ESI-MS and MS/MS spectra of 6-(4-methoxyphenyl)pyridine-2-carbaldehyde oxime in CH_3OH

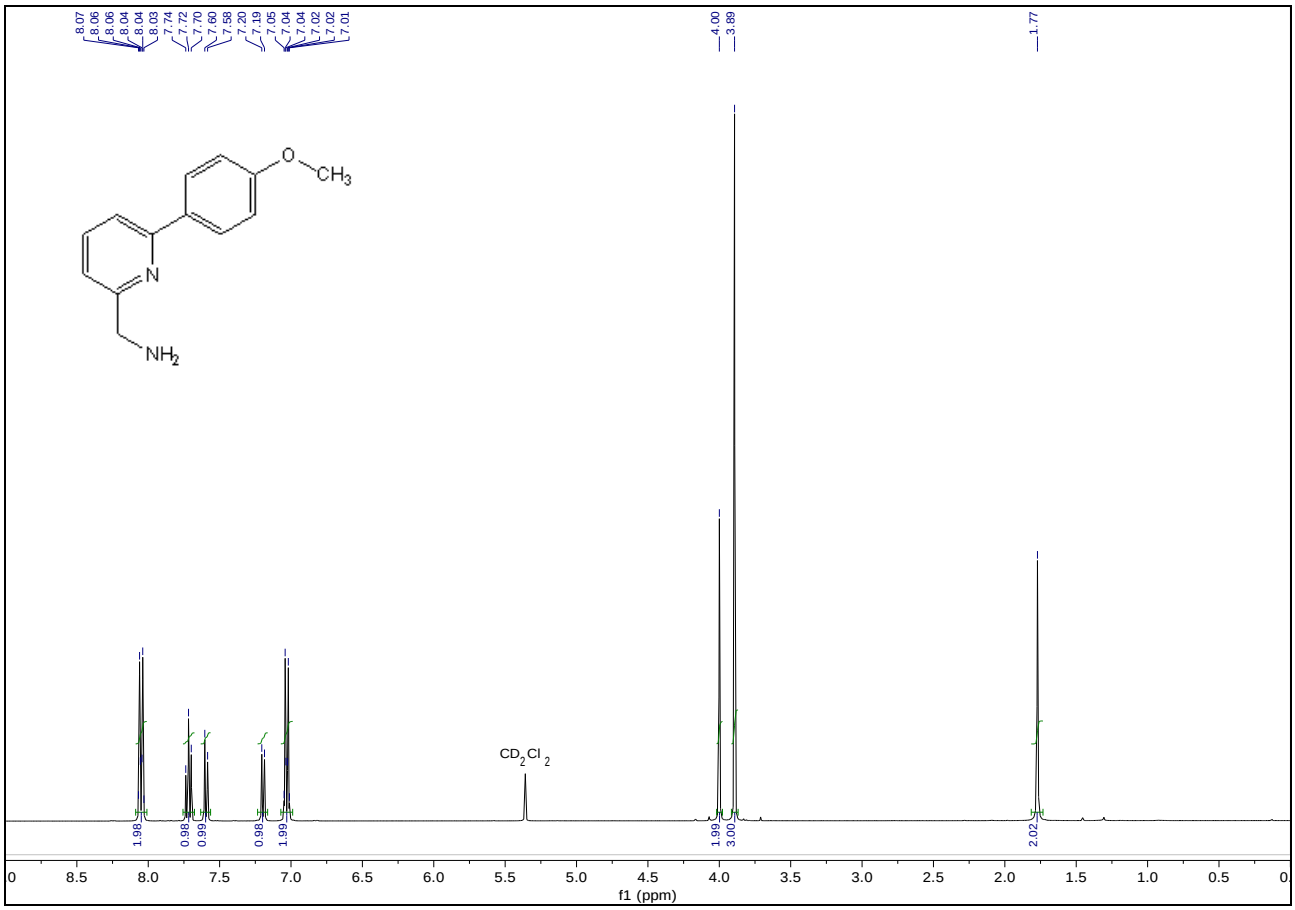

Figure S4. ^{1}H NMR spectrum (400.1 MHz) of (6-(4-methoxyphenyl)pyridin-2-yl)methanamine ($HCNN^{OMe}$) in CD_2Cl_2 at 25 °C.

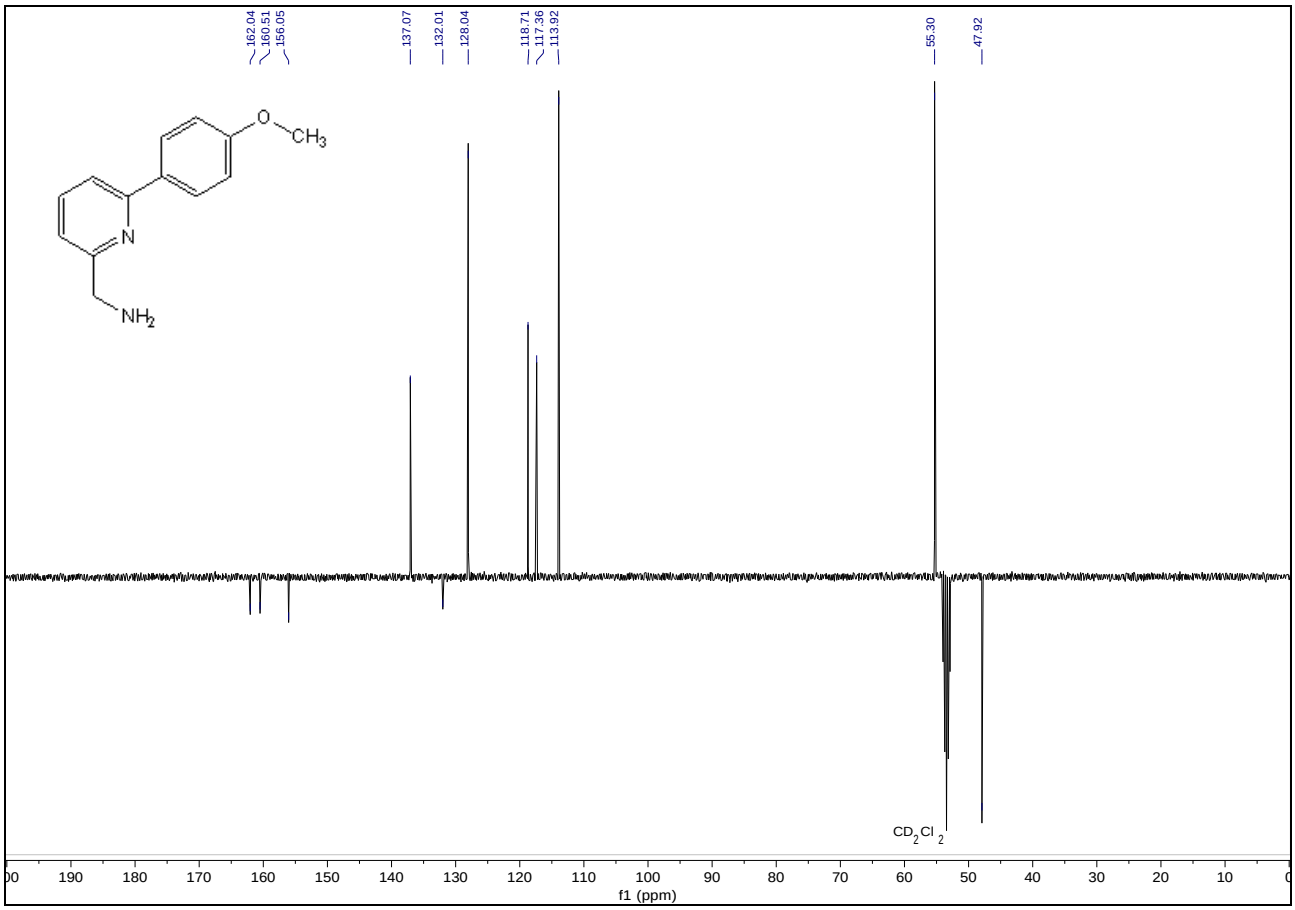

Figure S5. $^{13}C\{^{1}H\}$ DEPTQ NMR spectrum (100.6 MHz) of (6-(4-methoxyphenyl)pyridin-2-yl)methanamine ($HCNN^{OMe}$) in CD_2Cl_2 at 25 °C.

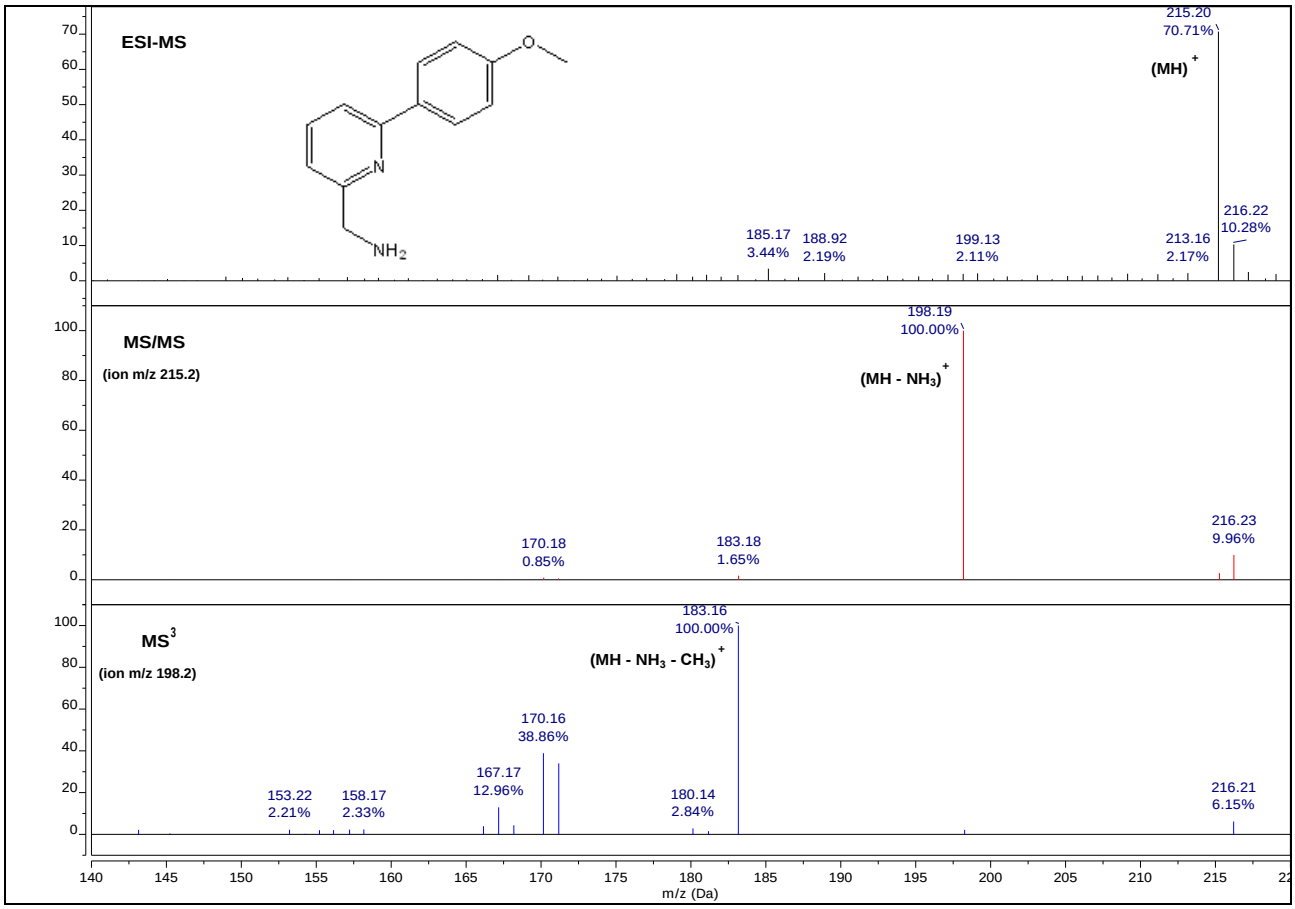

Figure S6. (+)-ESI-MS and MS^n spectra of (6-(4-methoxyphenyl)pyridin-2-yl)methanamine ($HCNN^{OMe}$) in CH_3OH

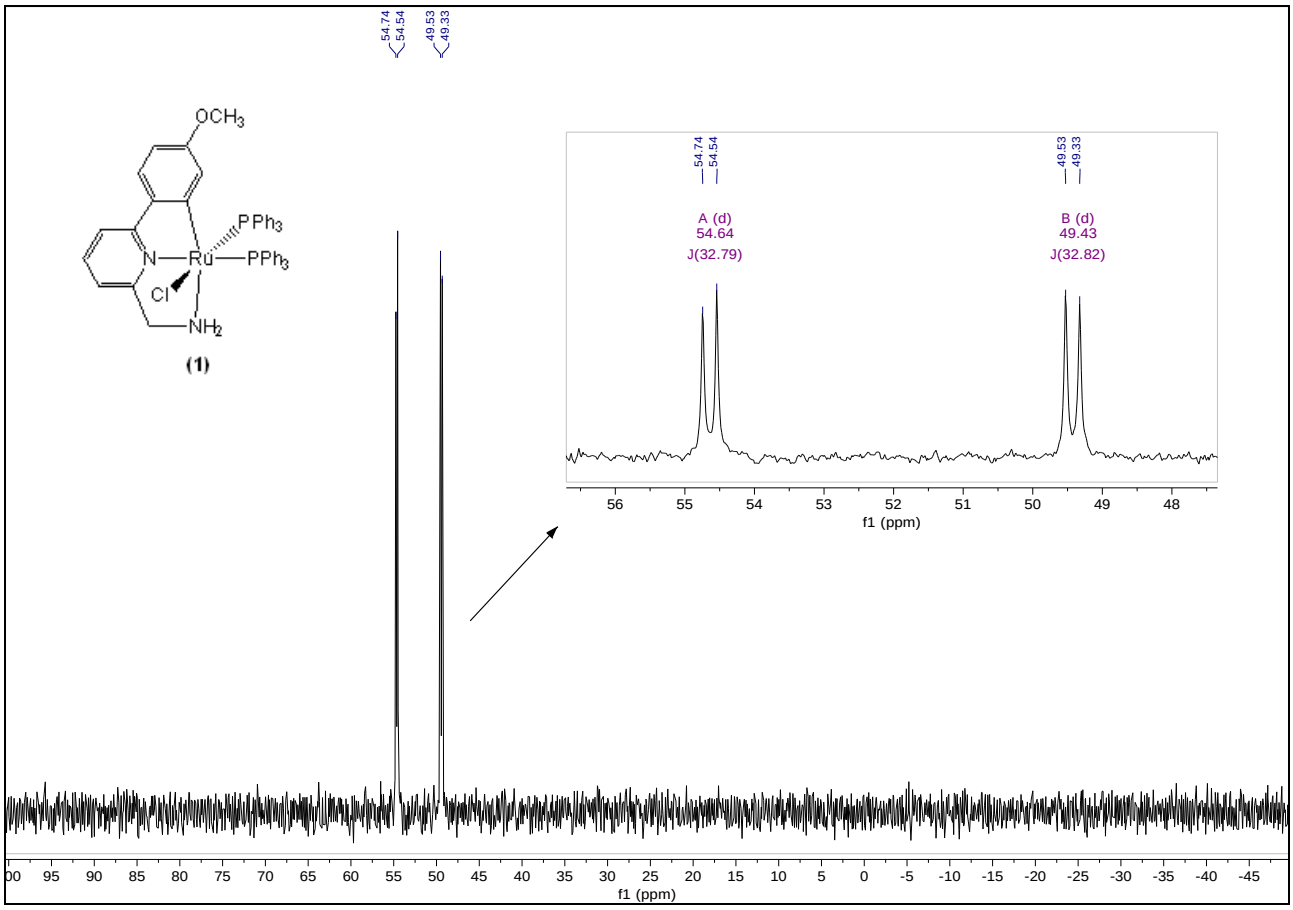

Figure S7. $^{31}P\{^{1}H\}$ NMR spectrum (162.0 MHz) of *cis*-[RuCl(CNN^{OMe})(PPh_3)$_2$] (**1**) in CD_2Cl_2 at 25 °C.

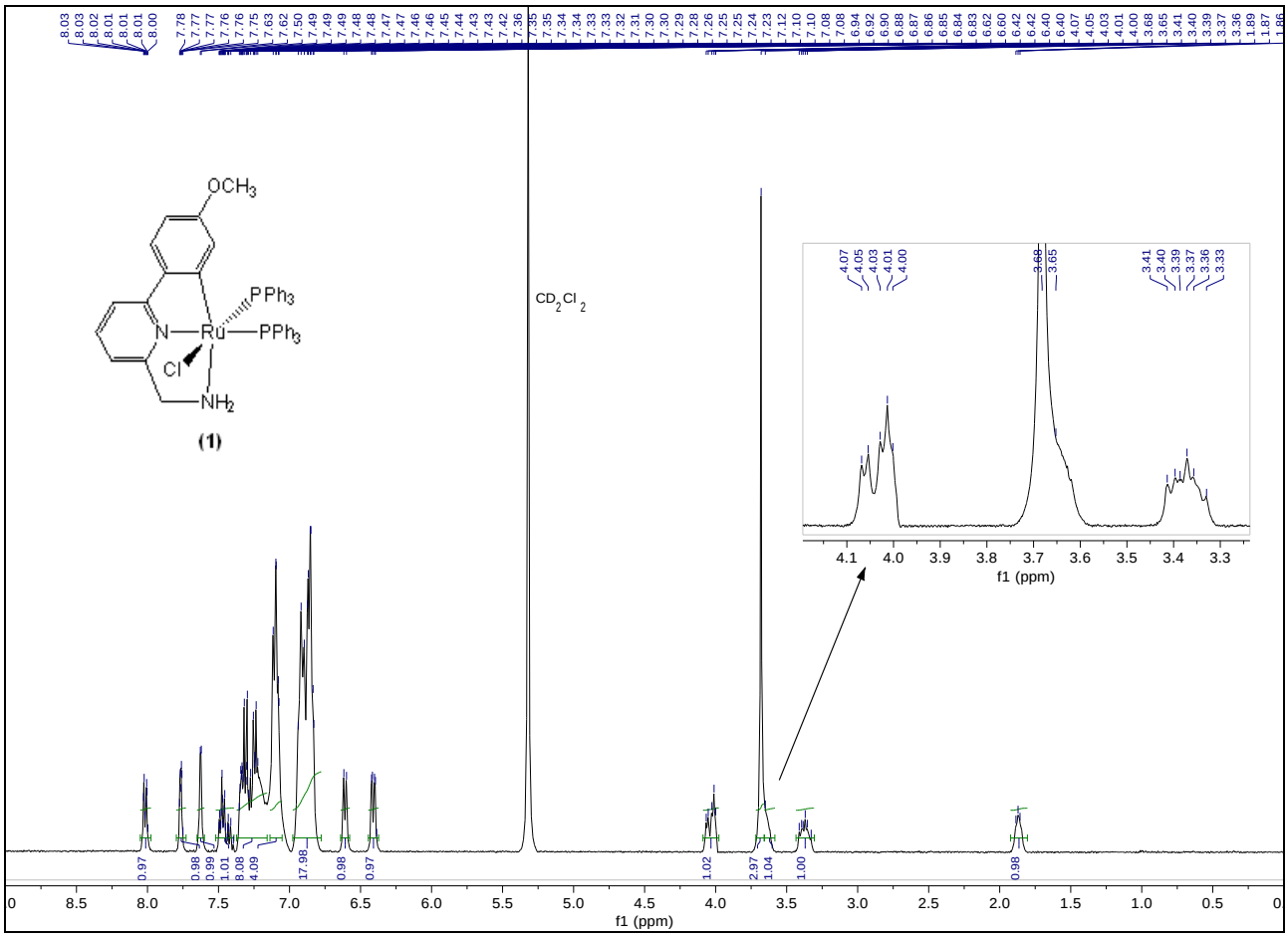

Figure S8. ^{1}H NMR spectrum (400.1 MHz) of *cis*-[RuCl(CNN^{OMe})(PPh$_3$)$_2$] (**1**) in CD_2Cl_2 at 25 °C.

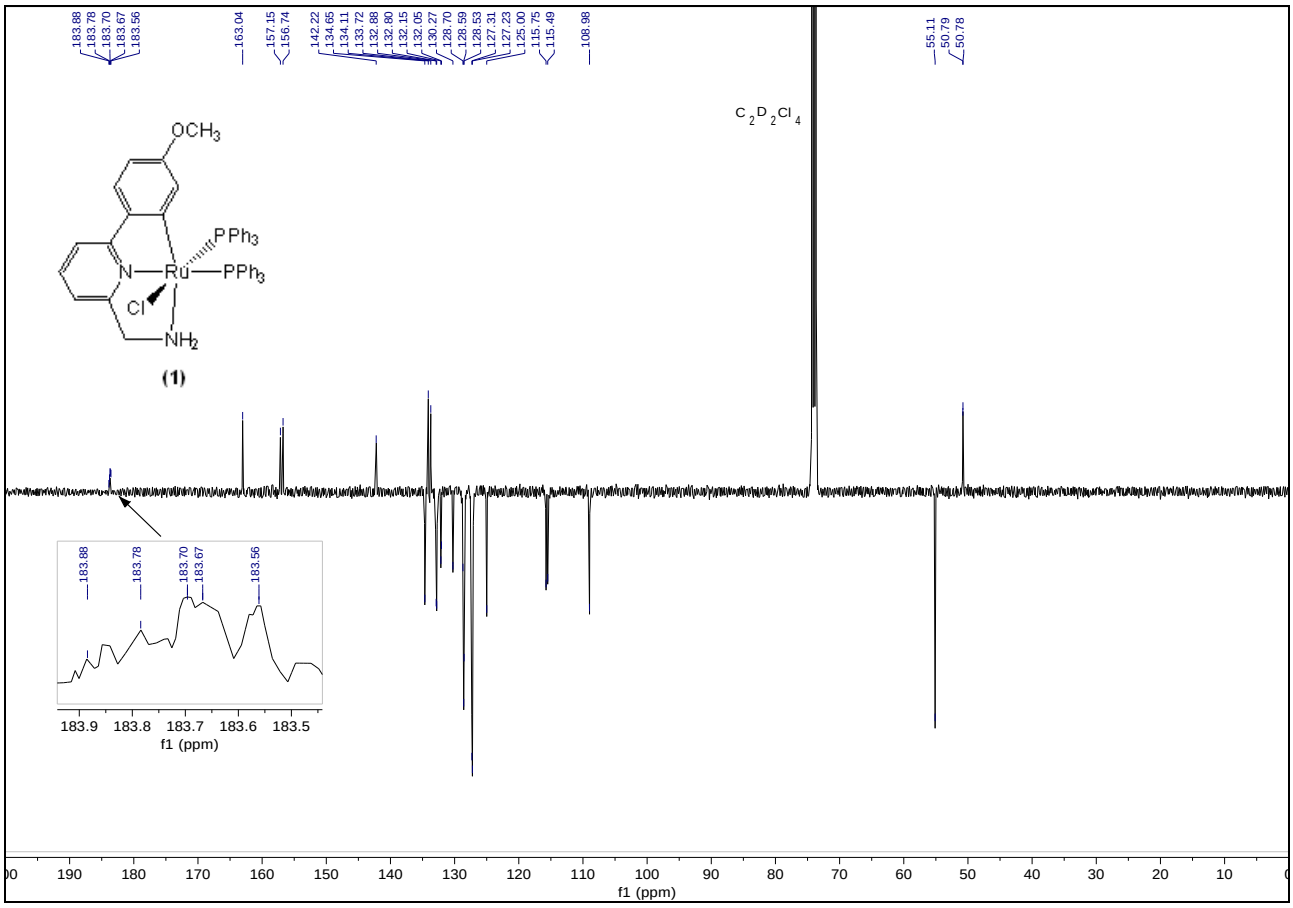

Figure S9. $^{13}C\{^{1}H\}$ DEPTQ NMR spectrum (100.6 MHz) of *cis*-[RuCl(CNN^{OMe})(PPh$_3$)$_2$] (**1**) in $C_2D_2Cl_4$ at 25 °C.

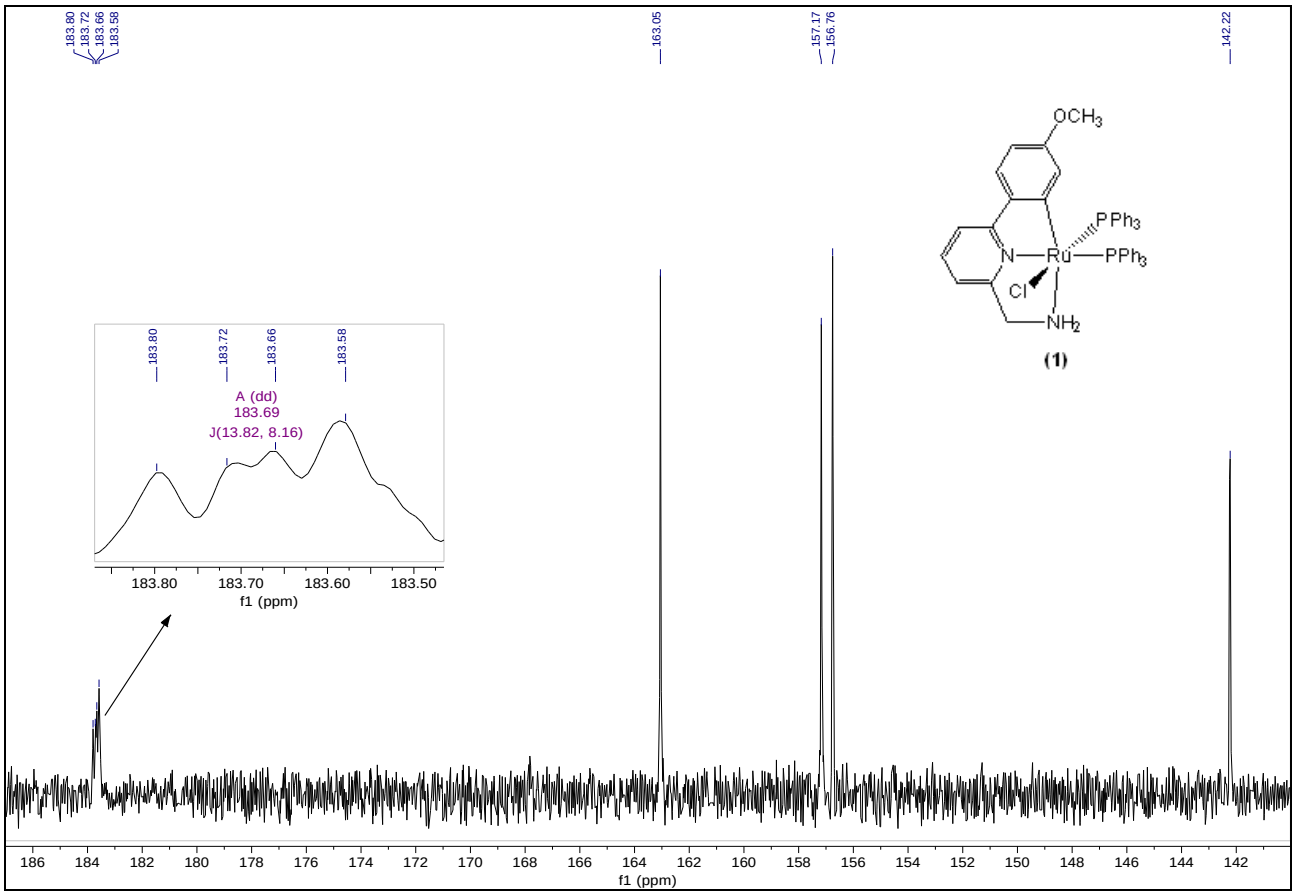

Figure S10. $^{13}C\{^{1}H\}$ QUATD NMR spectrum (100.6 MHz) of *cis*-[RuCl(CNN^{OMe})(PPh$_3$)$_2$] (**1**) in $C_2D_2Cl_4$ at 25 °C.

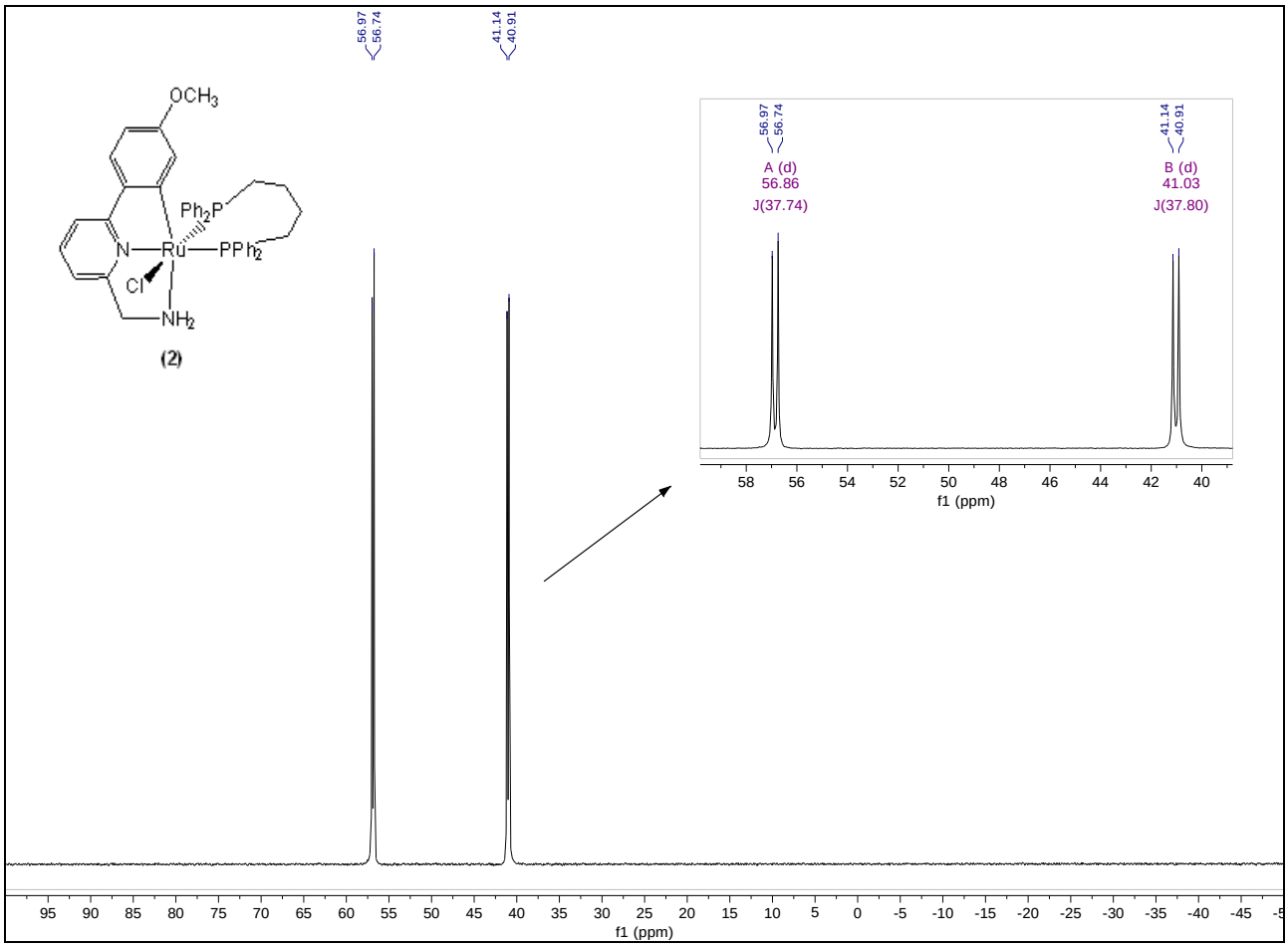

Figure S11. $^{31}P\{^{1}H\}$ NMR spectrum (162.0 MHz) of [RuCl(CNN^{OMe})(dppb)] (**2**) in CD_2Cl_2 at 25 °C.

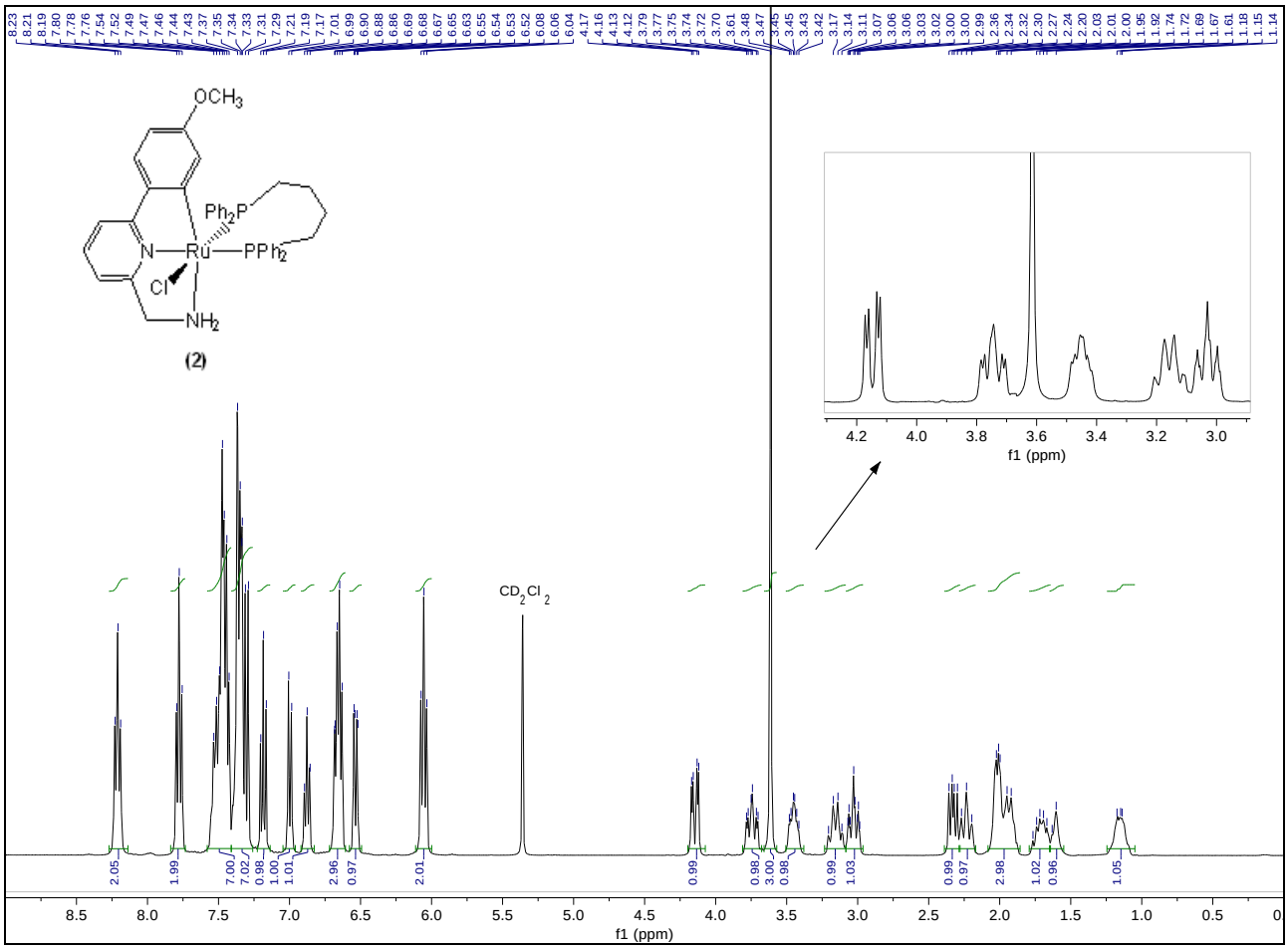

Figure S12. ^{1}H NMR spectrum (400.1 MHz) of [RuCl(CNN^{OMe})(dppb)] (**2**) in CD_2Cl_2 at 25 °C.

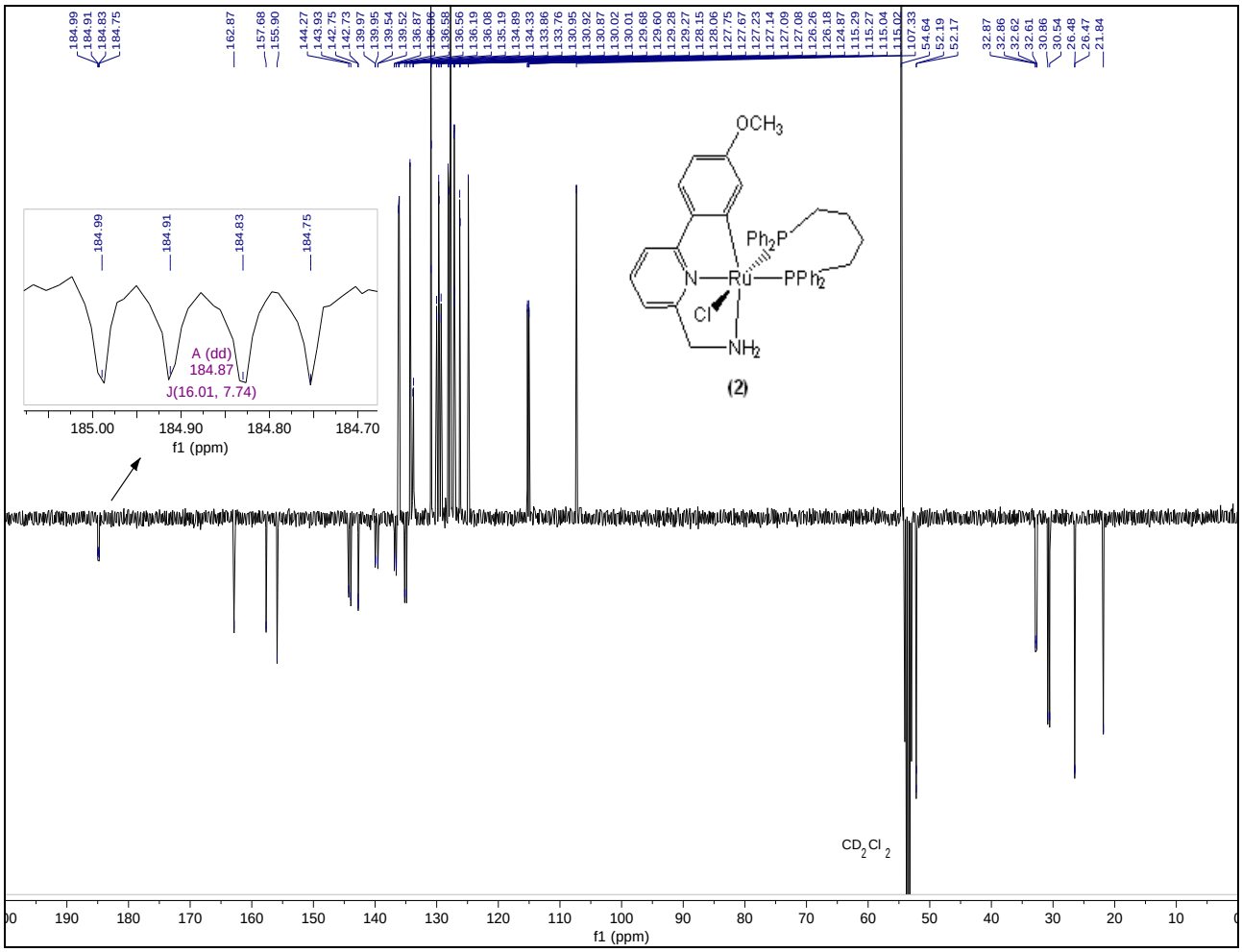

Figure S13. $^{13}C\{^{1}H\}$ DEPTQ NMR spectrum (100.6 MHz) of [RuCl(CNN^{OMe})(dppb)] (**2**) in CD_2Cl_2 at 25 °C.

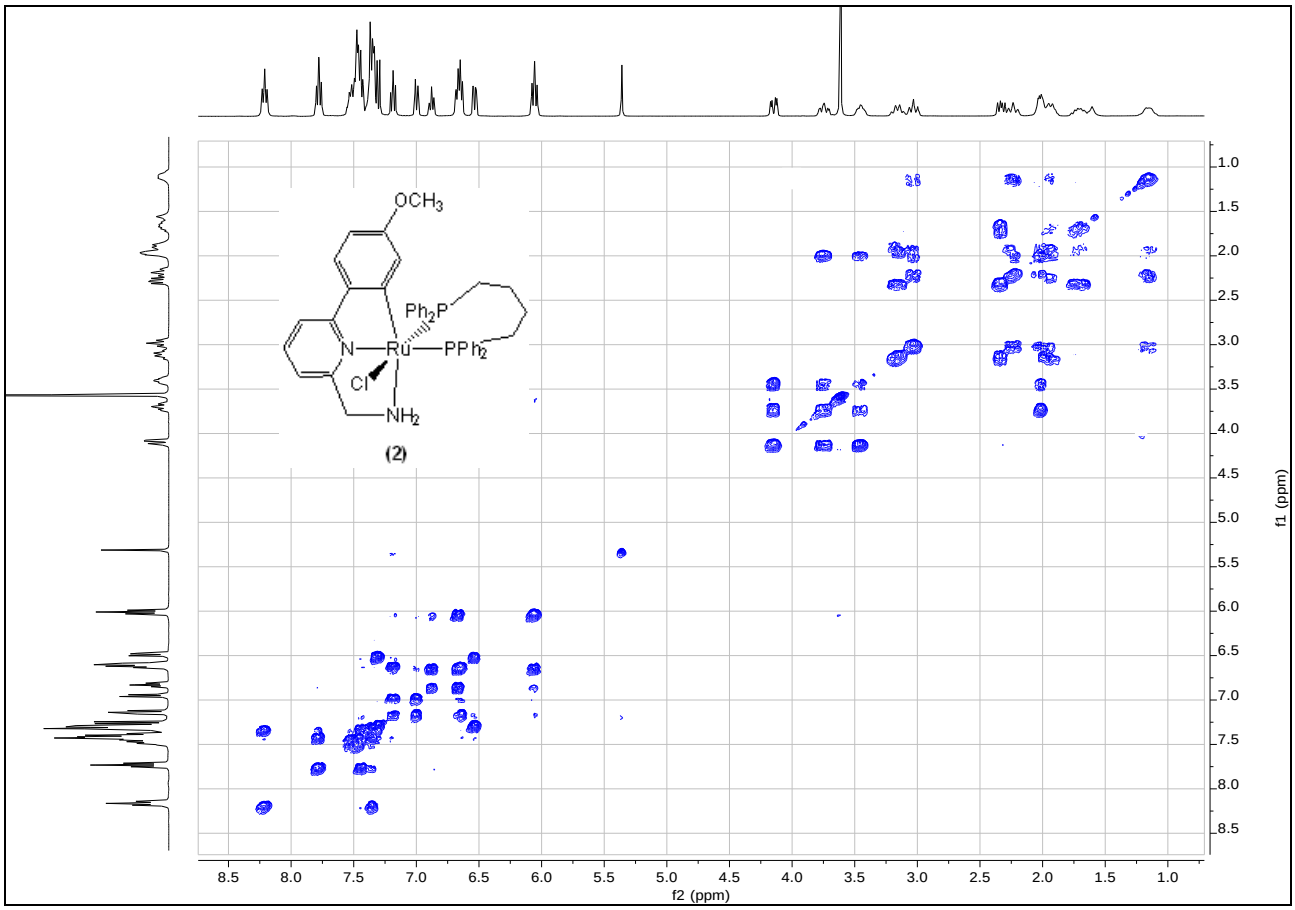

Figure S14. ^{1}H-^{1}H COSY 2D NMR spectrum (400.1 MHz) of [RuCl(CNN^{OMe})(dppb)] (**2**) in CD_2Cl_2 at 25 °C.

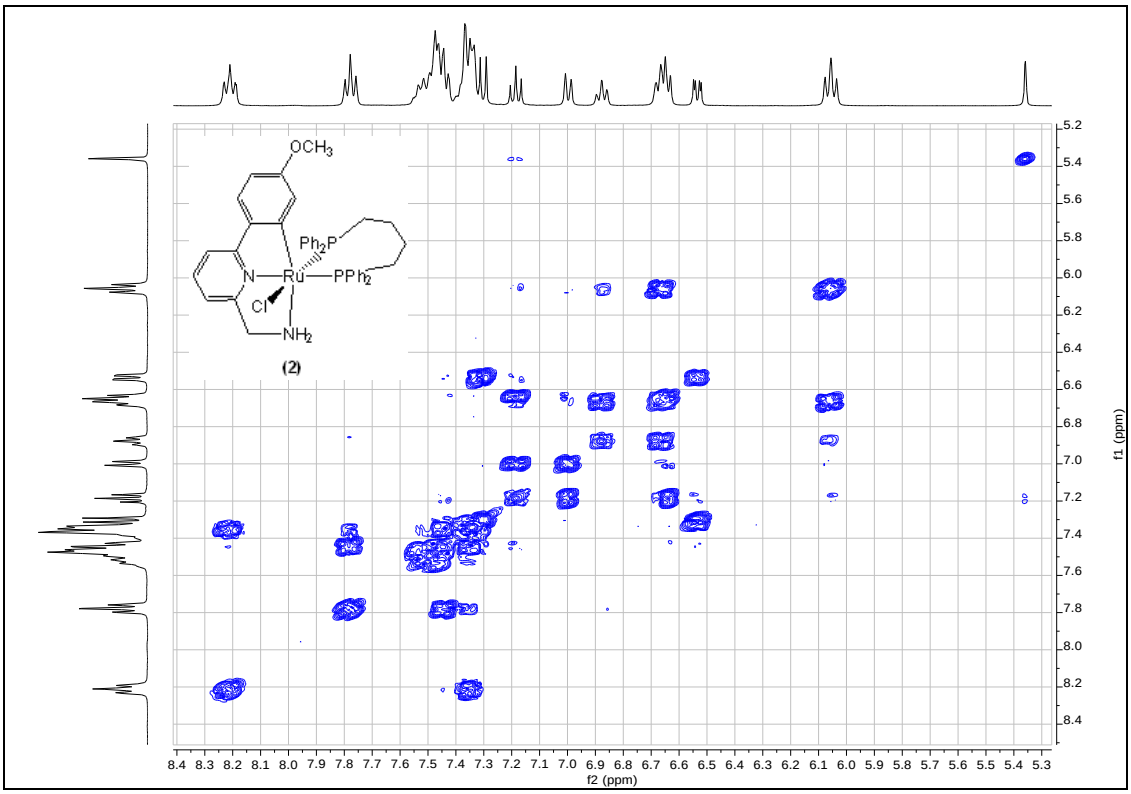

Figure S15. Aromatic region of the ^{1}H-^{1}H COSY 2D NMR spectrum (400.1 MHz) of [RuCl(CNN^{OMe})(dppb)] (**2**) in CD_2Cl_2 at 25 °C.

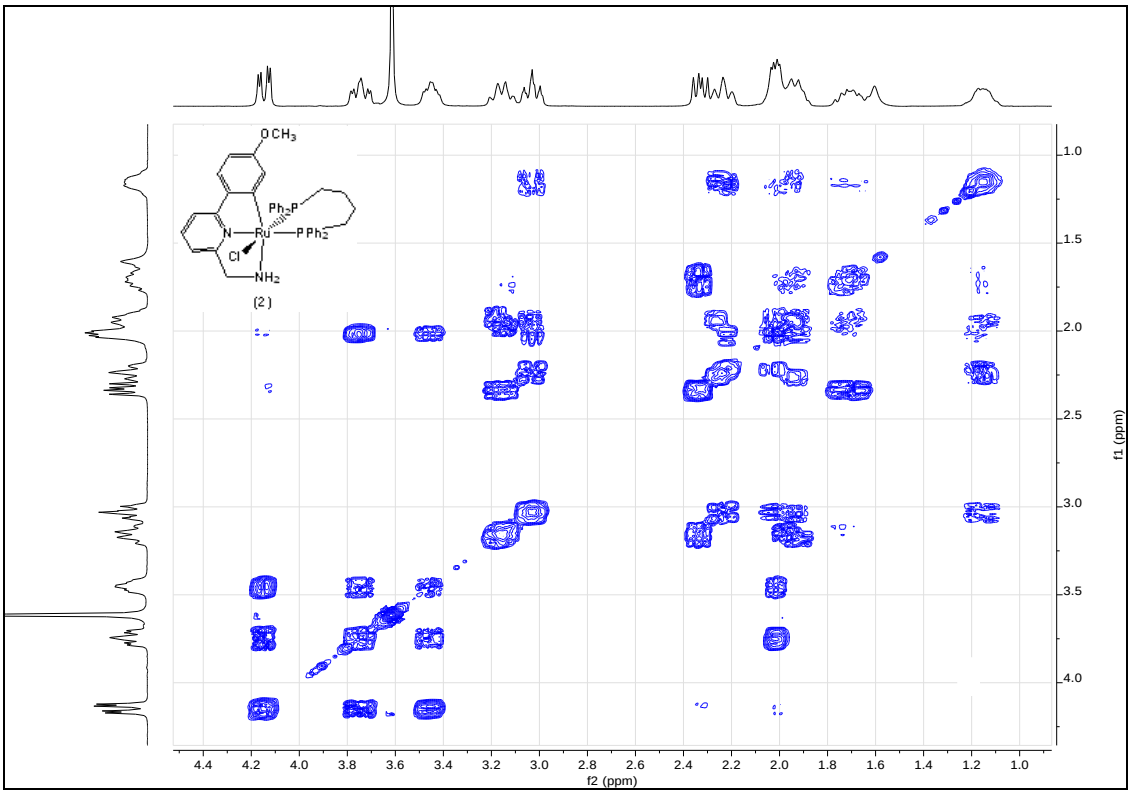

Figure S16. Alkylic region of the ^{1}H-^{1}H COSY 2D NMR spectrum (400.1 MHz) of [RuCl(CNN^{OMe})(dppb)] (**2**) in CD_2Cl_2 at 25 °C.

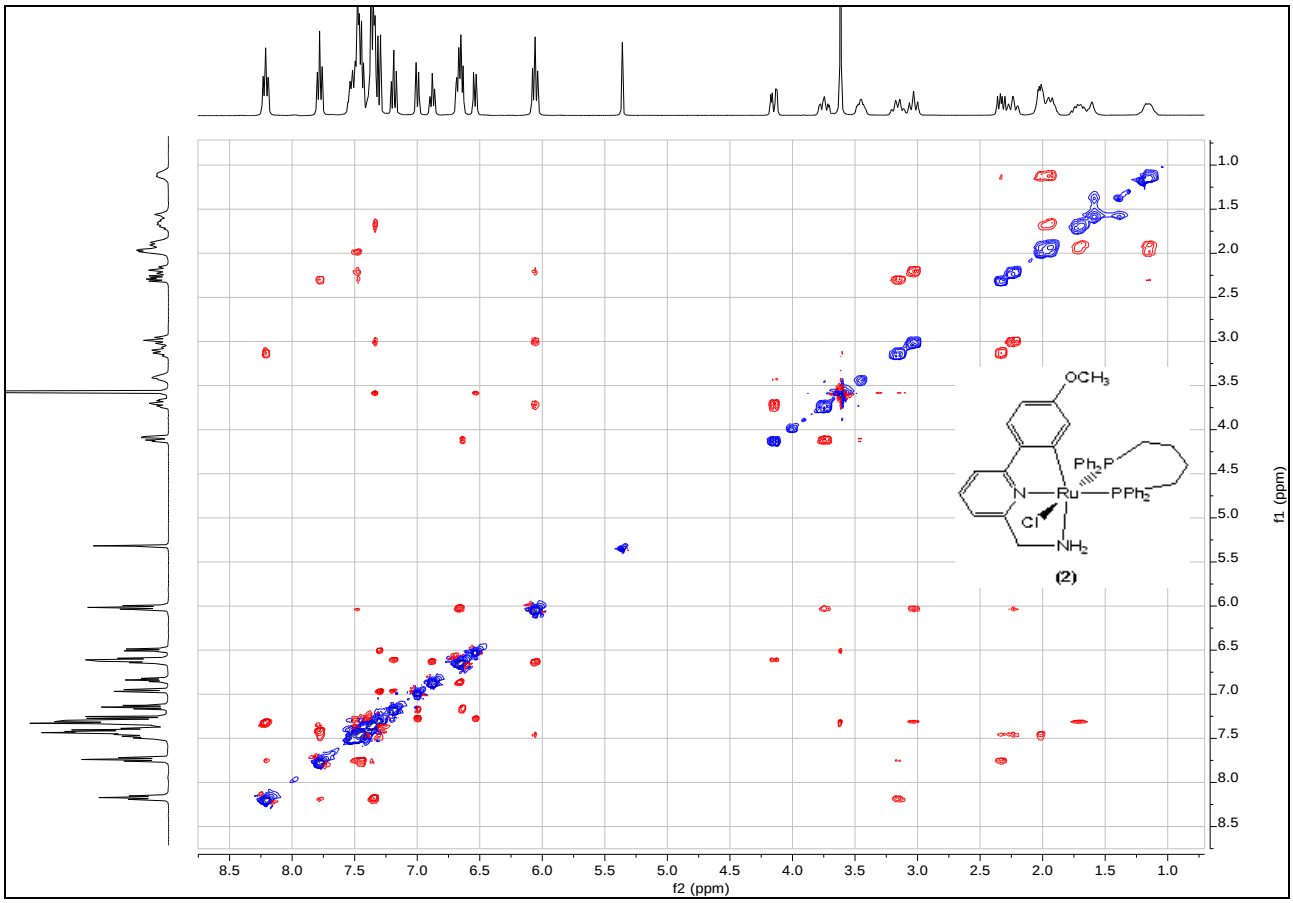

Figure S17. ^{1}H-^{1}H NOESY 2D NMR spectrum (400.1 MHz) of [RuCl(CNN^{OMe})(dppb)] (**2**) in CD_2Cl_2 at 25 °C.

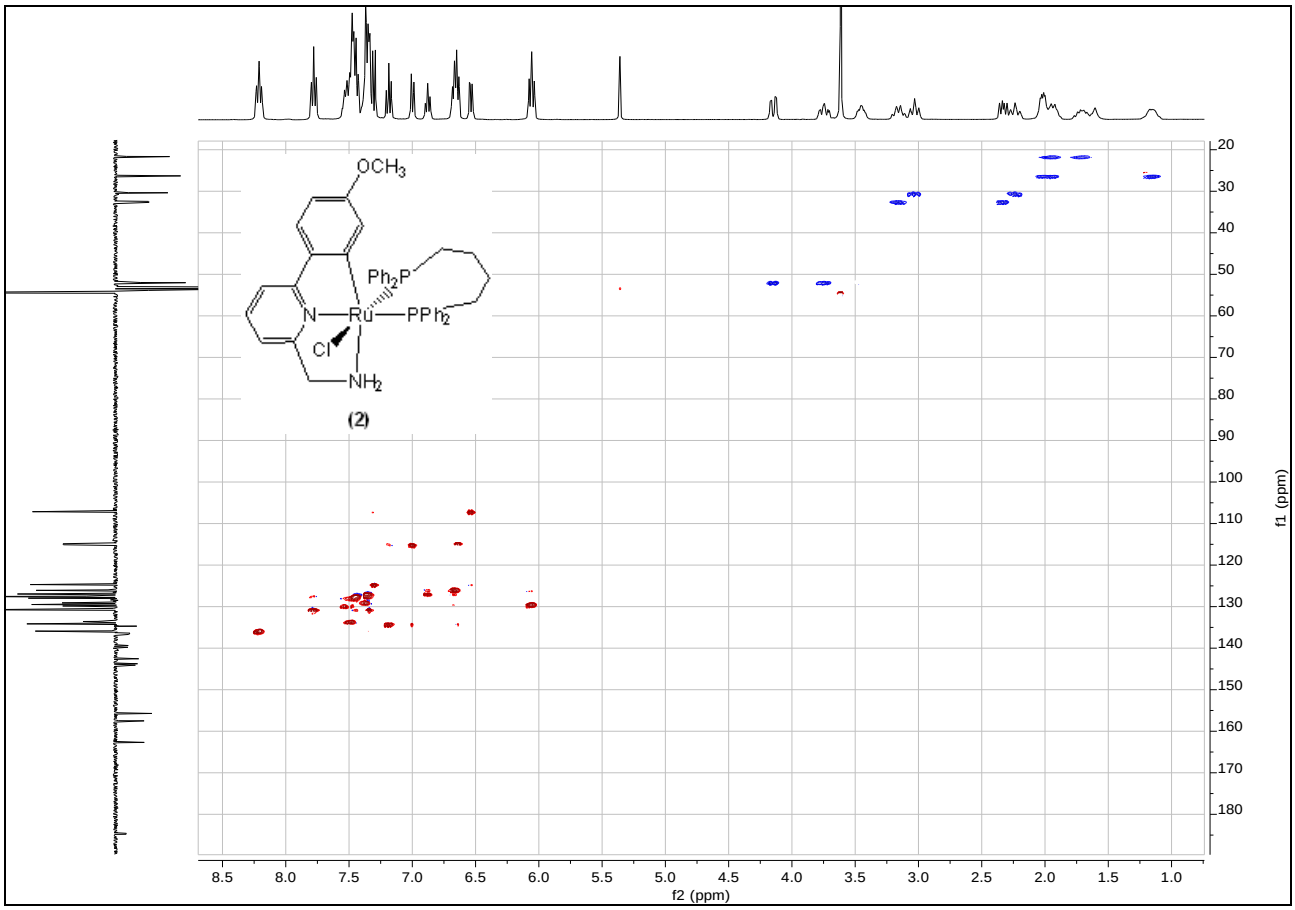

Figure S18. ^{1}H-^{13}C HSQC 2D NMR spectrum of [RuCl(CNN^{OMe})(dppb)] (**2**) in CD_2Cl_2 at 25 °C.

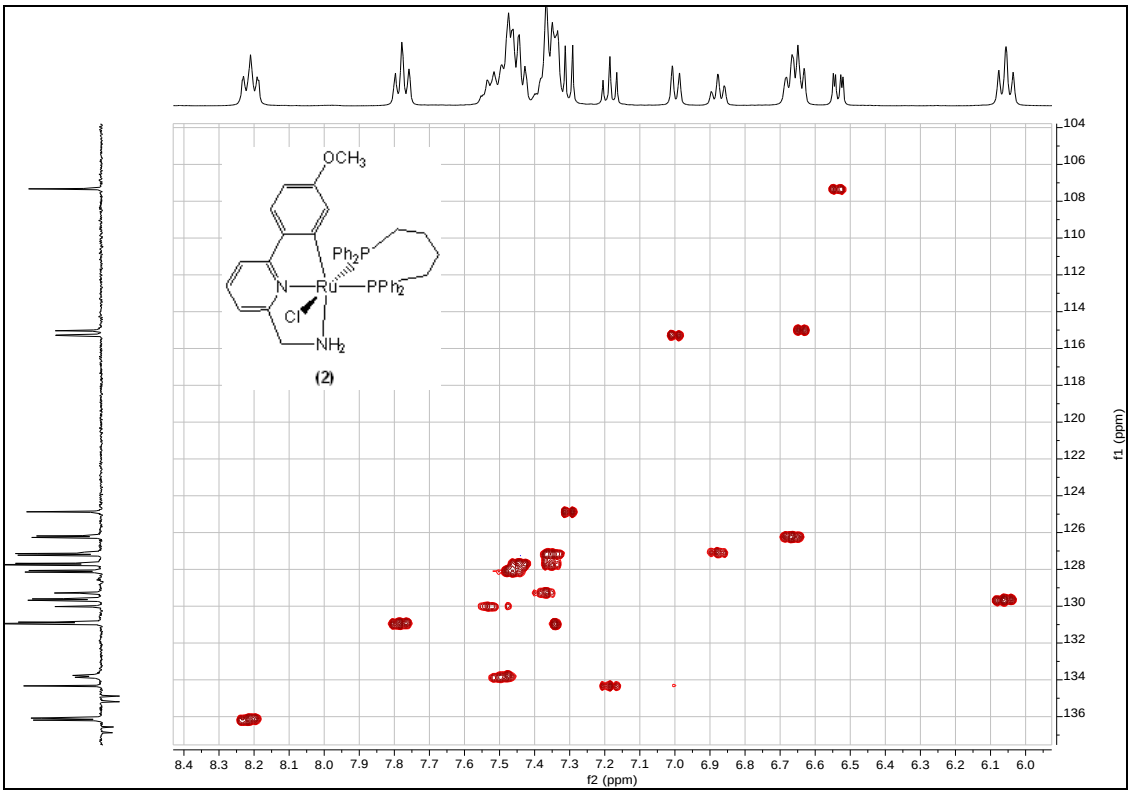

Figure S19. Aromatic region of the ^{1}H-^{13}C HSQC 2D NMR spectrum of [RuCl(CNN^{OMe})(dppb)] (**2**) in CD_2Cl_2 at 25 °C.

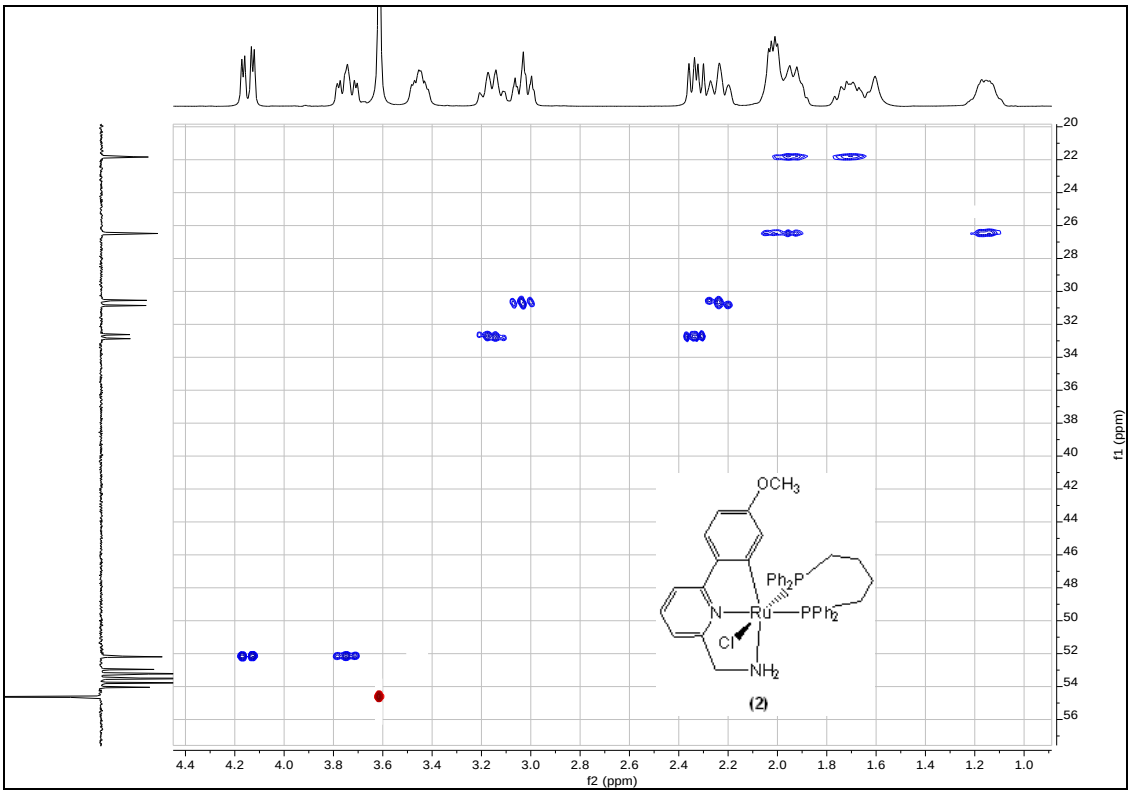

Figure S20. Alkylic region of the ^{1}H-^{13}C HSQC 2D NMR spectrum of [RuCl(CNN^{OMe})(dppb)] (**2**) in CD_2Cl_2 at 25 °C.

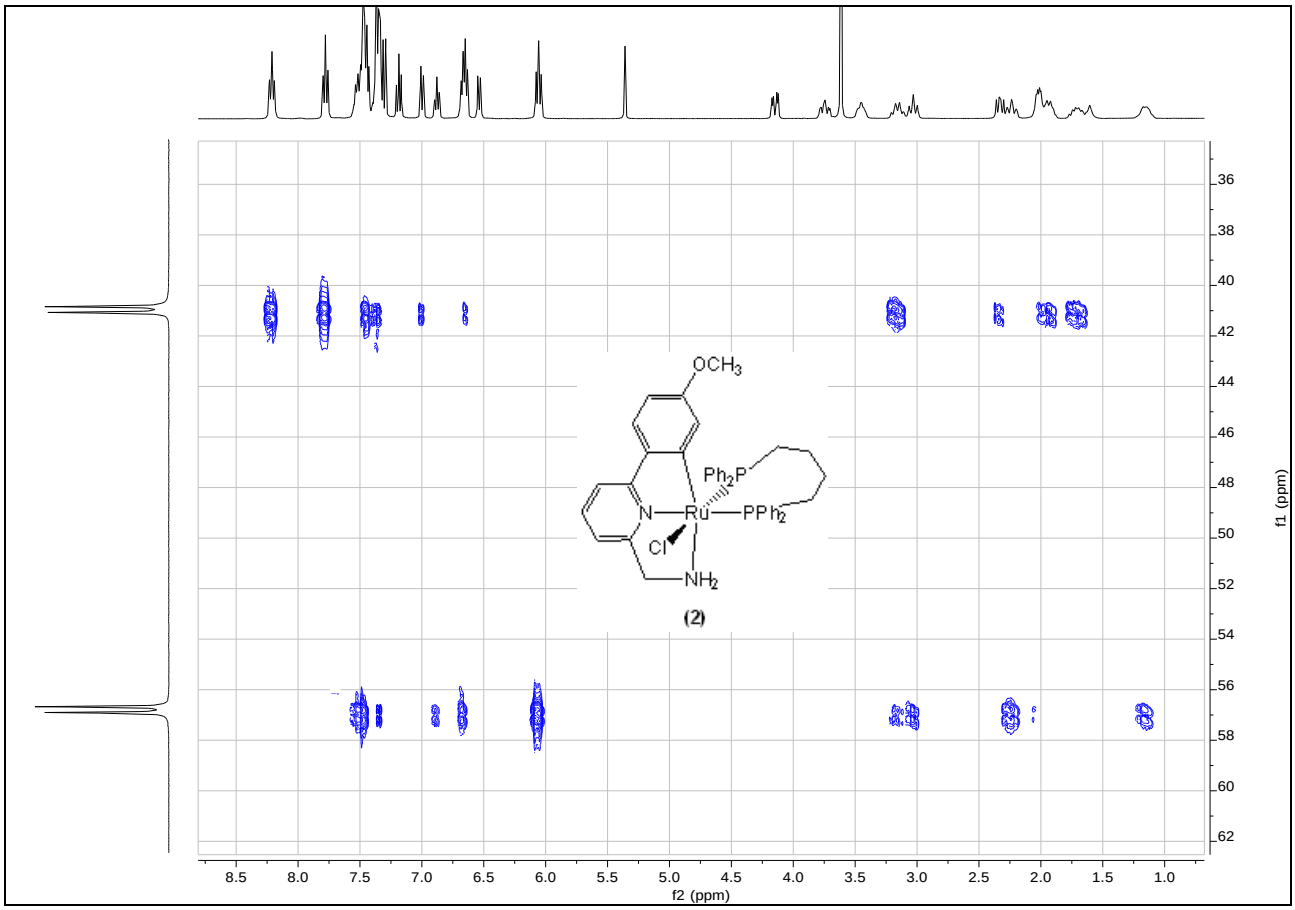

Figure S21. ^{1}H-^{31}P HMBC 2D NMR spectrum of [RuCl(CNN^{OMe})(dppb)] (**2**) in CD_2Cl_2 at 25 °C.

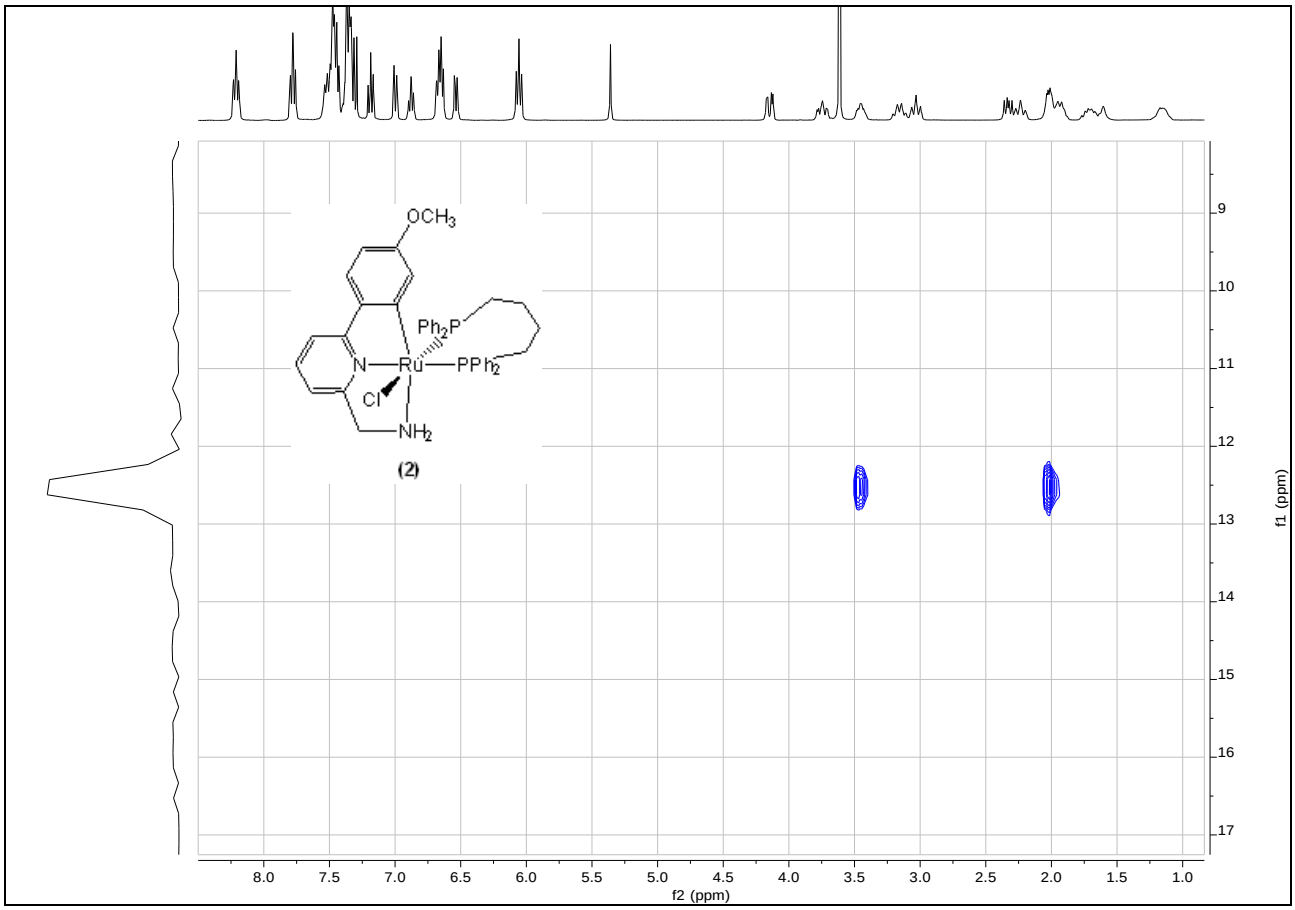

Figure S22. ^{1}H-^{15}N HSQC 2D NMR spectrum of [RuCl(CNN^{OMe})(dppb)] (**2**) in CD_2Cl_2 at 25 °C.

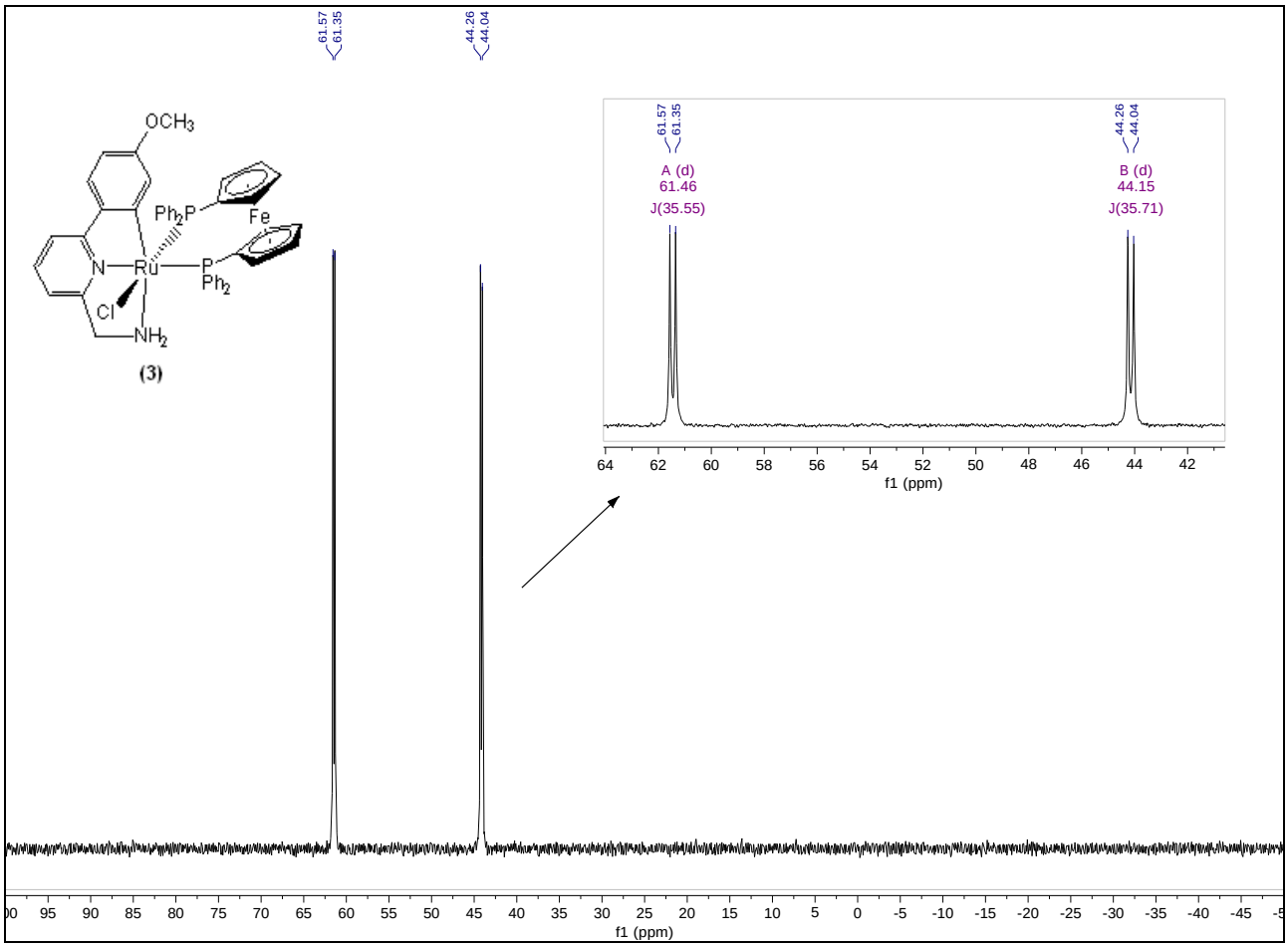

Figure S23. $^{31}P\{^{1}H\}$ NMR spectrum (162.0 MHz) of [RuCl(CNN^{OMe})(dppf)] (**3**) in CD_2Cl_2 at 25 °C.

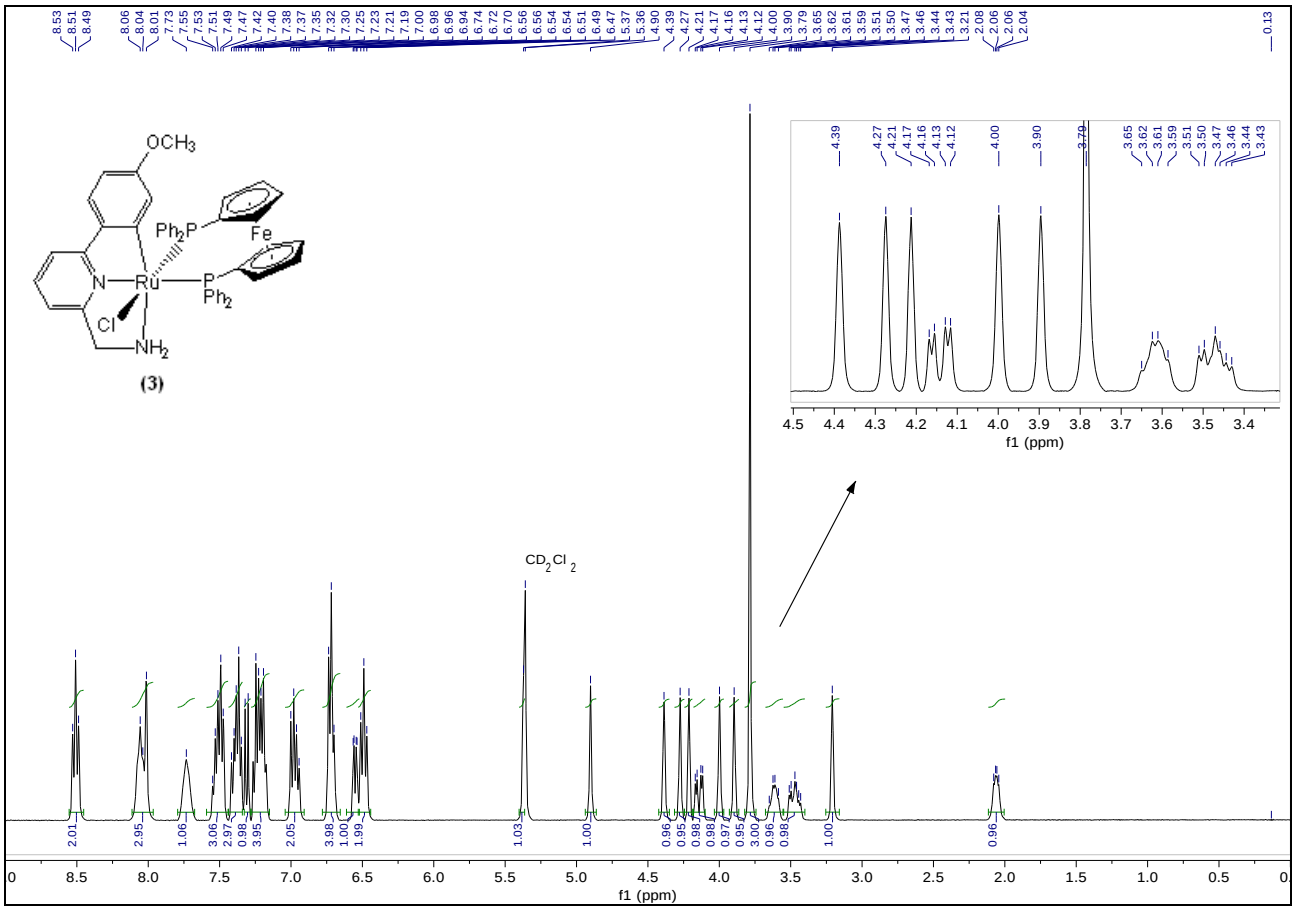

Figure S24. ^{1}H NMR spectrum (400.1 MHz) of [RuCl(CNN^{OMe})(dppf)] (**3**) in CD_2Cl_2 at 25 °C.

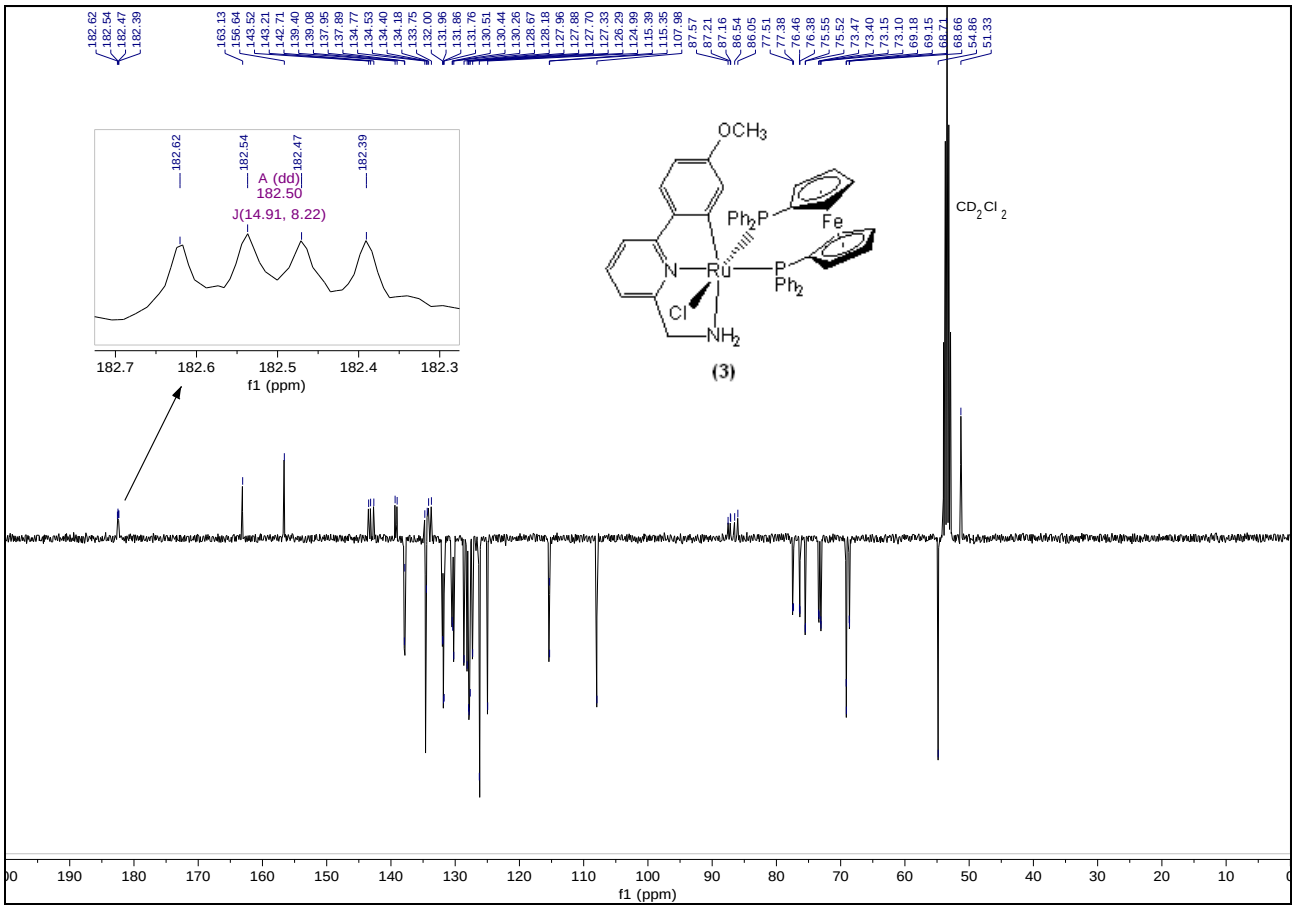

Figure S25. $^{13}C\{^{1}H\}$ DEPTQ NMR spectrum (100.6 MHz) of [RuCl(CNN^{OMe})(dppf)] (**3**) in CD_2Cl_2 at 25 °C.

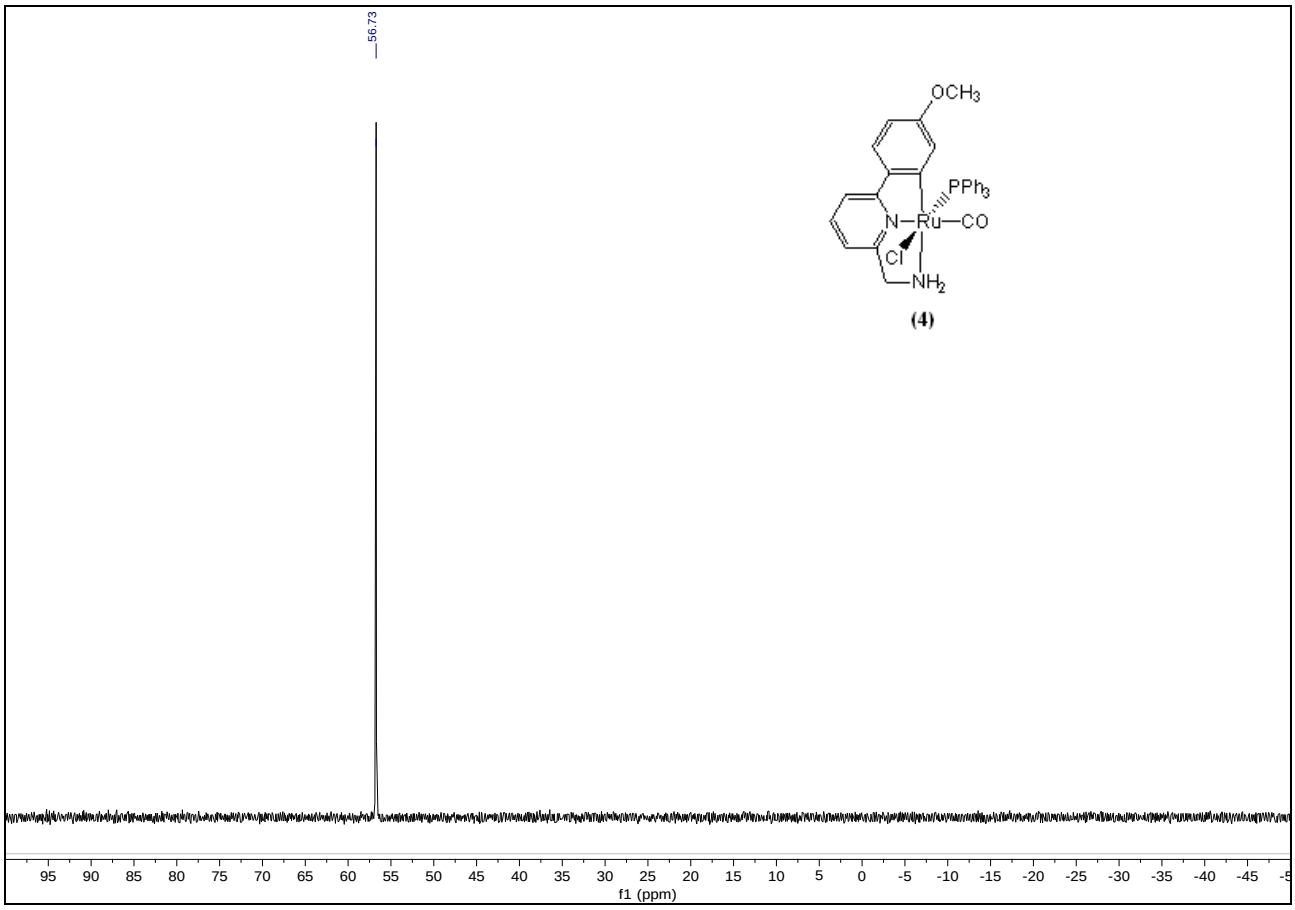

Figure S26. $^{31}P\{^{1}H\}$ NMR spectrum (162.0 MHz) of [RuCl(CNN^{OMe})(CO)(PPh_3)] (**4**) in CD_2Cl_2 at 25 °C.

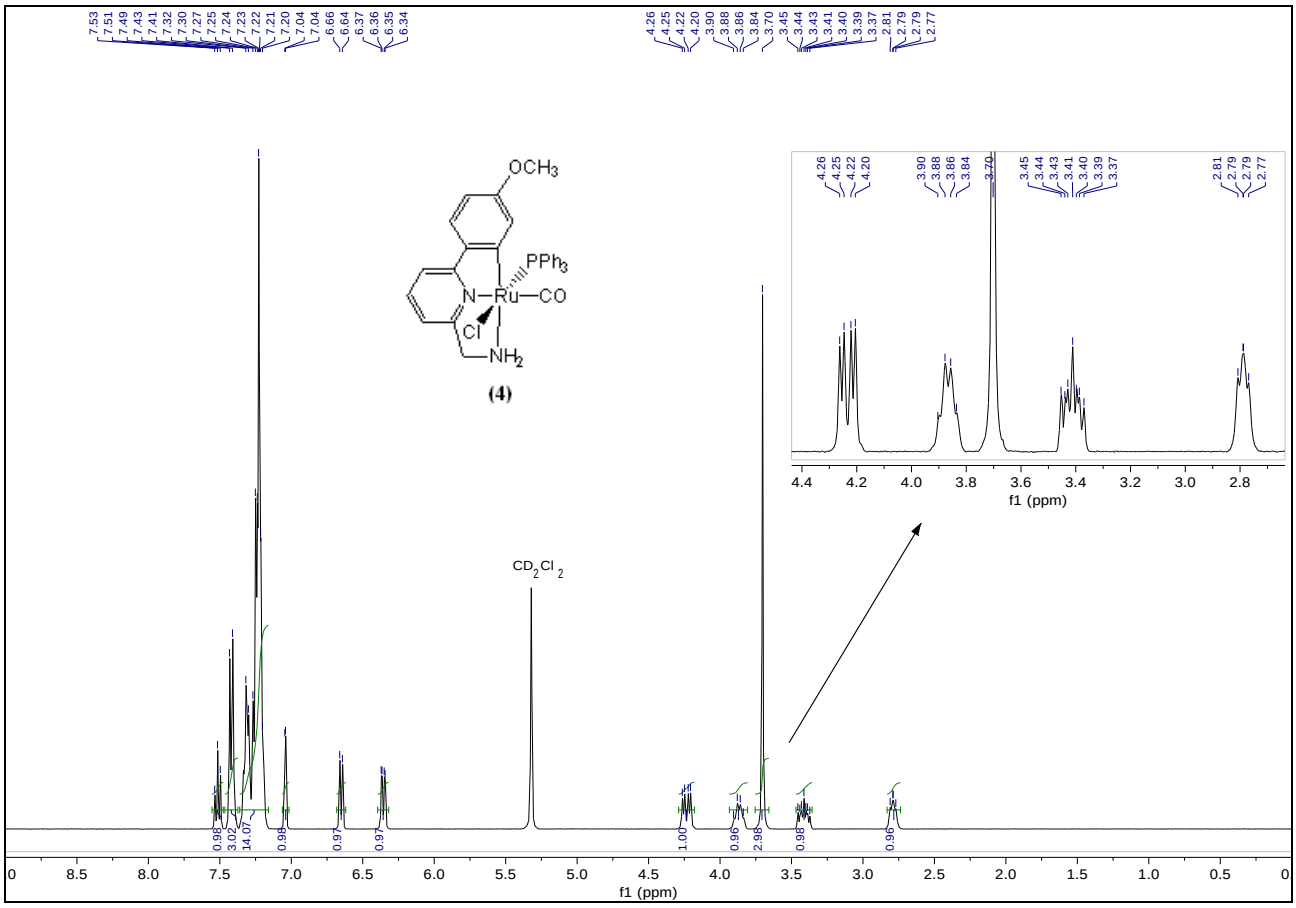

Figure S27. ^{1}H NMR spectrum (400.1 MHz) of [RuCl(CNN^{OMe})(CO)(PPh$_3$)] (**4**) in CD_2Cl_2 at 25 °C.

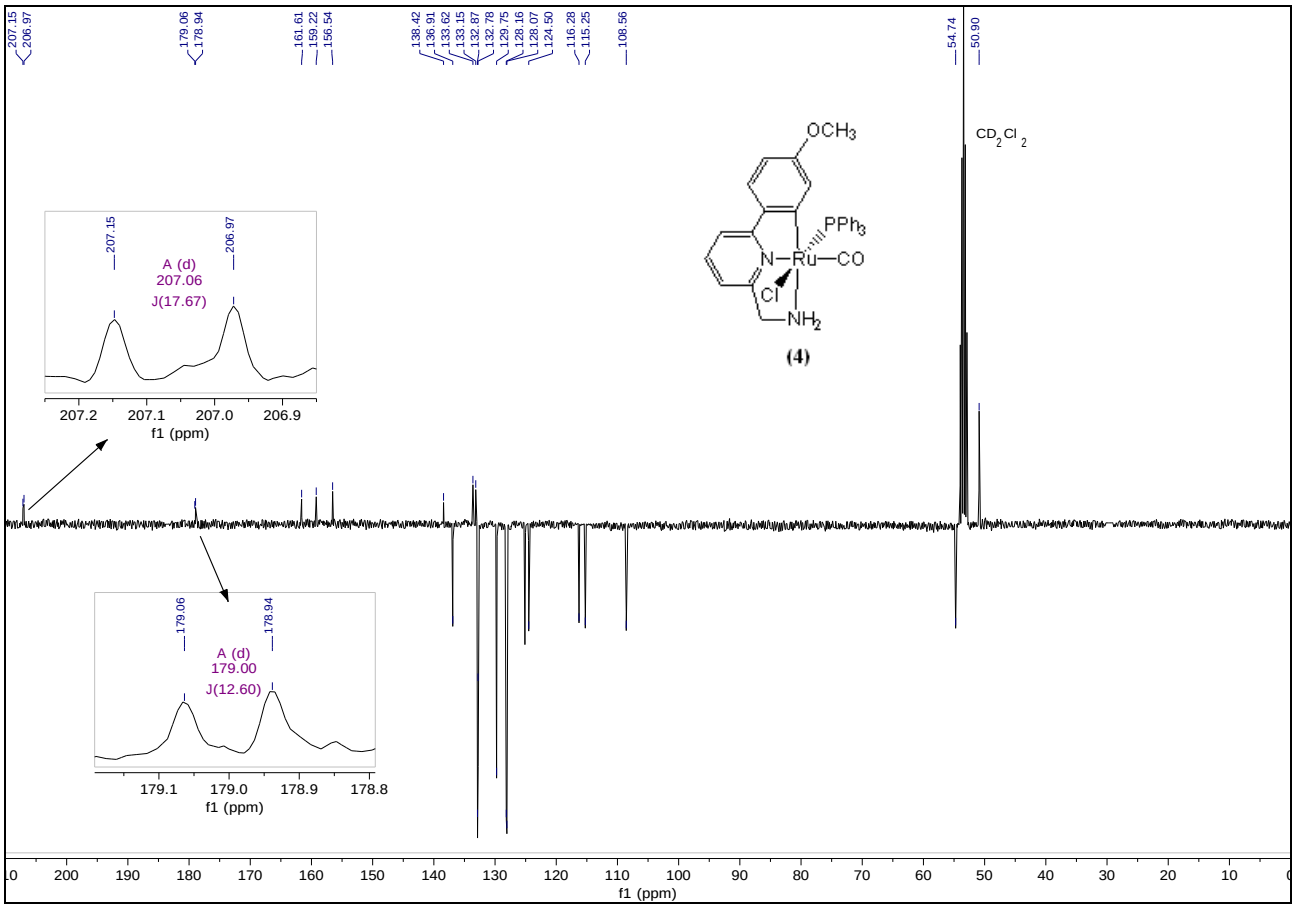

Figure S28. $^{13}C\{^{1}H\}$ NMR spectrum (100.6 MHz) of [RuCl(CNN^{OMe})(CO)(PPh$_3$)] (**4**) in CD_2Cl_2 at 25 °C.

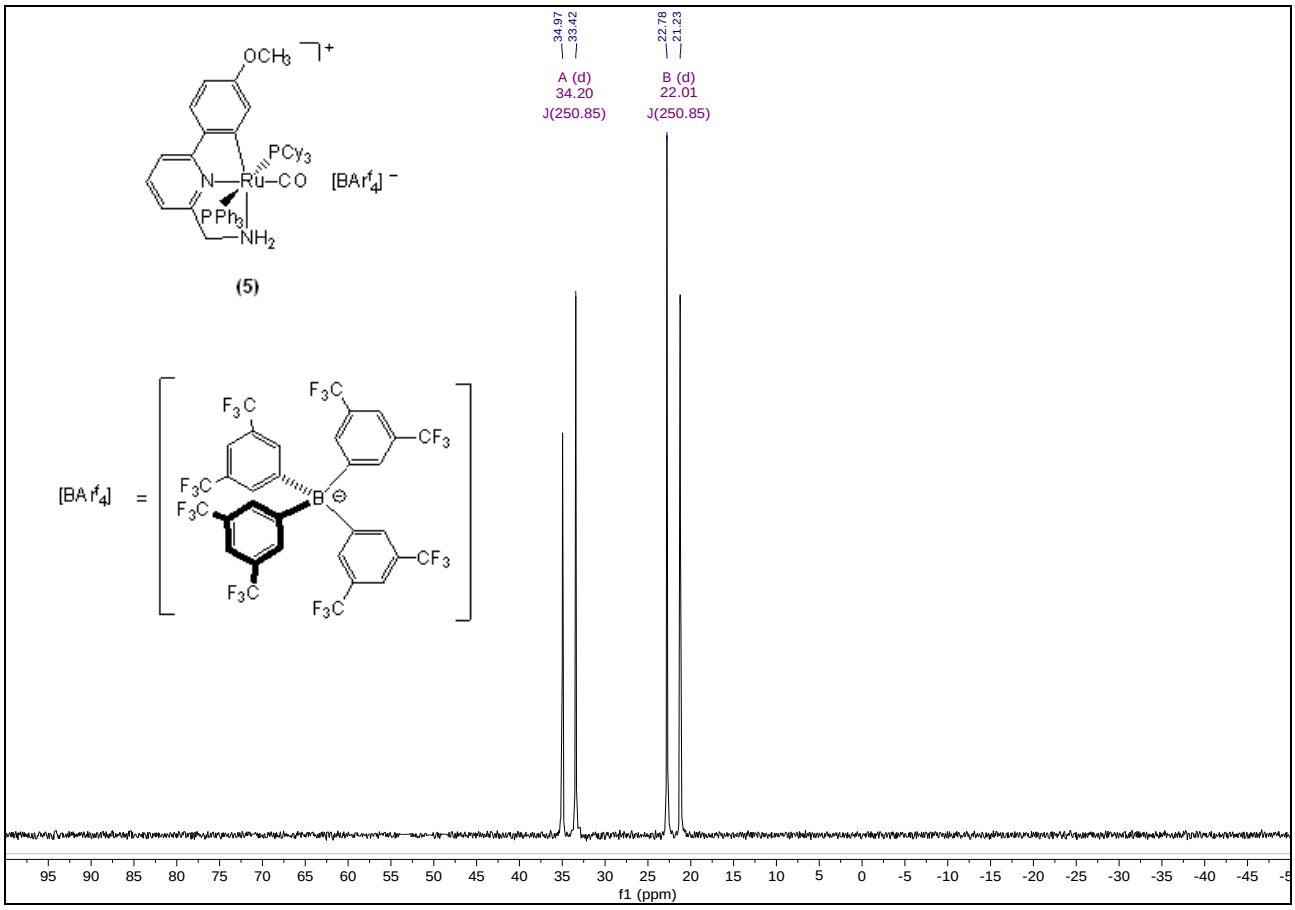

Figure S29. $^{31}P\{^{1}H\}$ NMR spectrum (162.0 MHz) of *trans*-[Ru(CNN^{OMe})(CO)(PCy$_3$)(PPh$_3$)][BAr$^f{}_4$] (**5**) in CD_2Cl_2 at 25 °C.

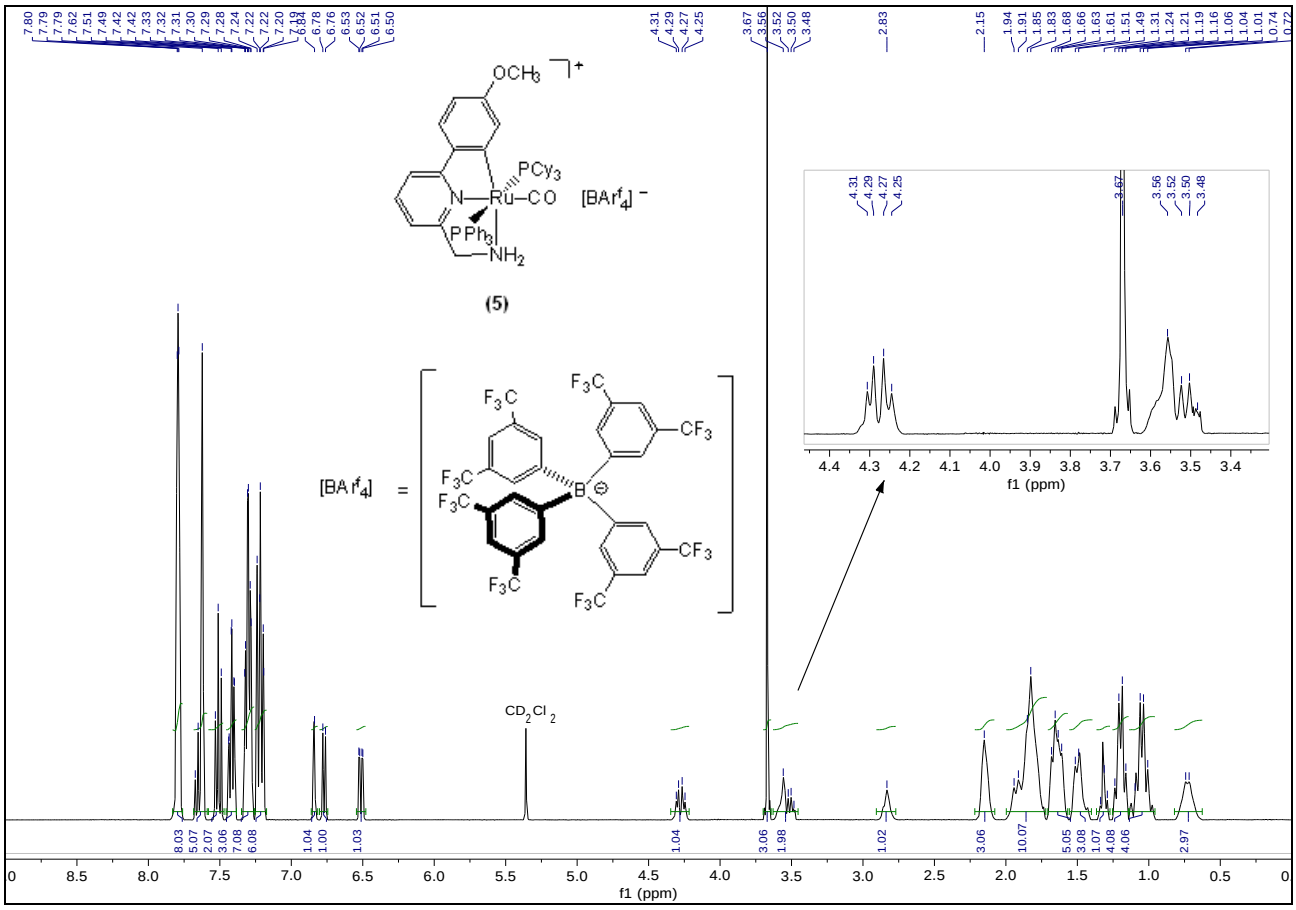

Figure S30. ^{1}H NMR spectrum (400.1 MHz) of *trans*-[Ru(CNN^{OMe})(CO)(PCy$_3$)(PPh$_3$)][BAr$^f_4$] (**5**) in CD_2Cl_2 at 25 °C.

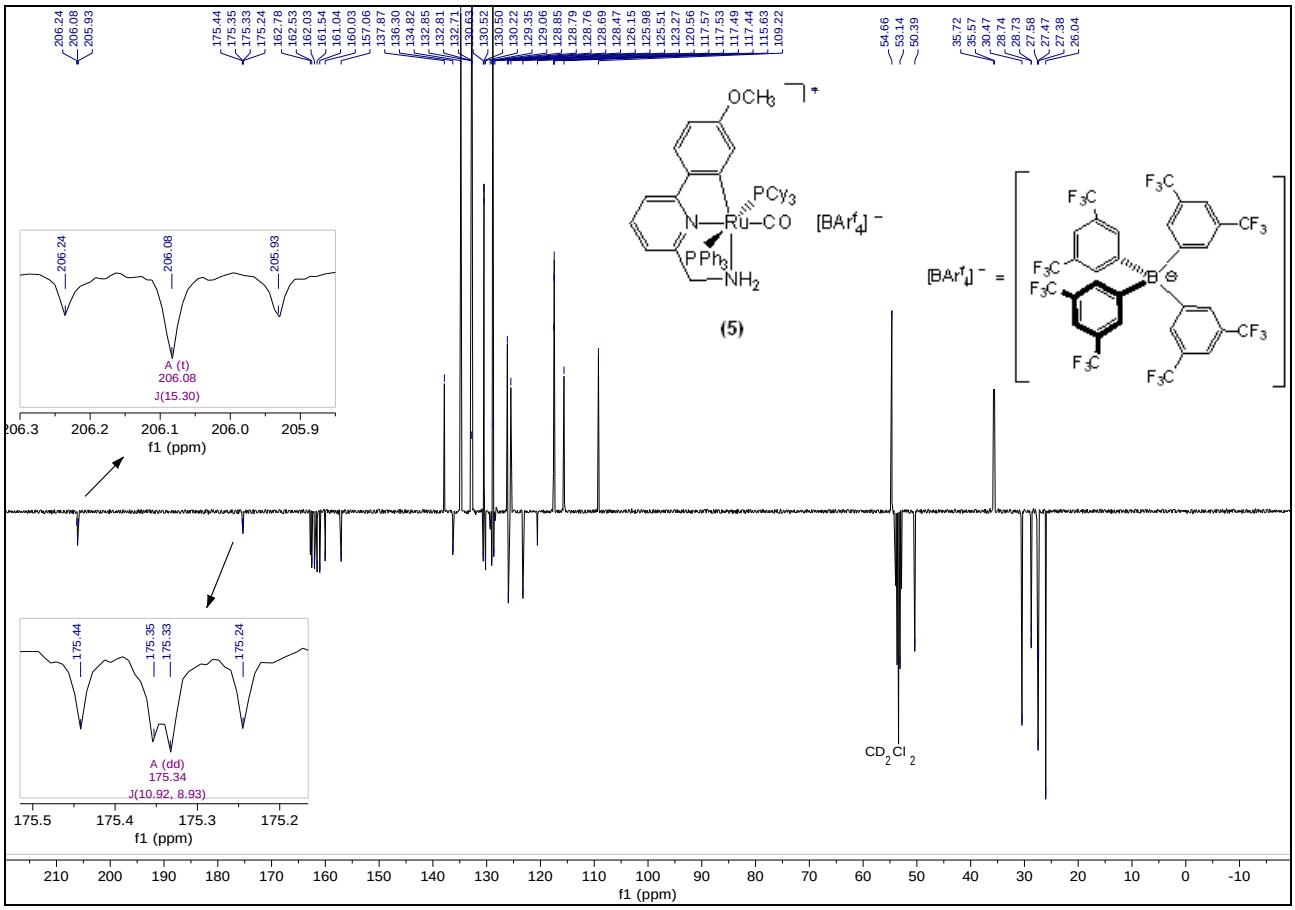

Figure S31. $^{13}C\{^{1}H\}$ DEPTQ NMR spectrum (100.6 MHz) of *trans*-[Ru(CNN^{OMe})(CO)(PCy$_3$)(PPh$_3$)][BAr$^f{}_4$] (**5**) in CD_2Cl_2 at 25 °C.

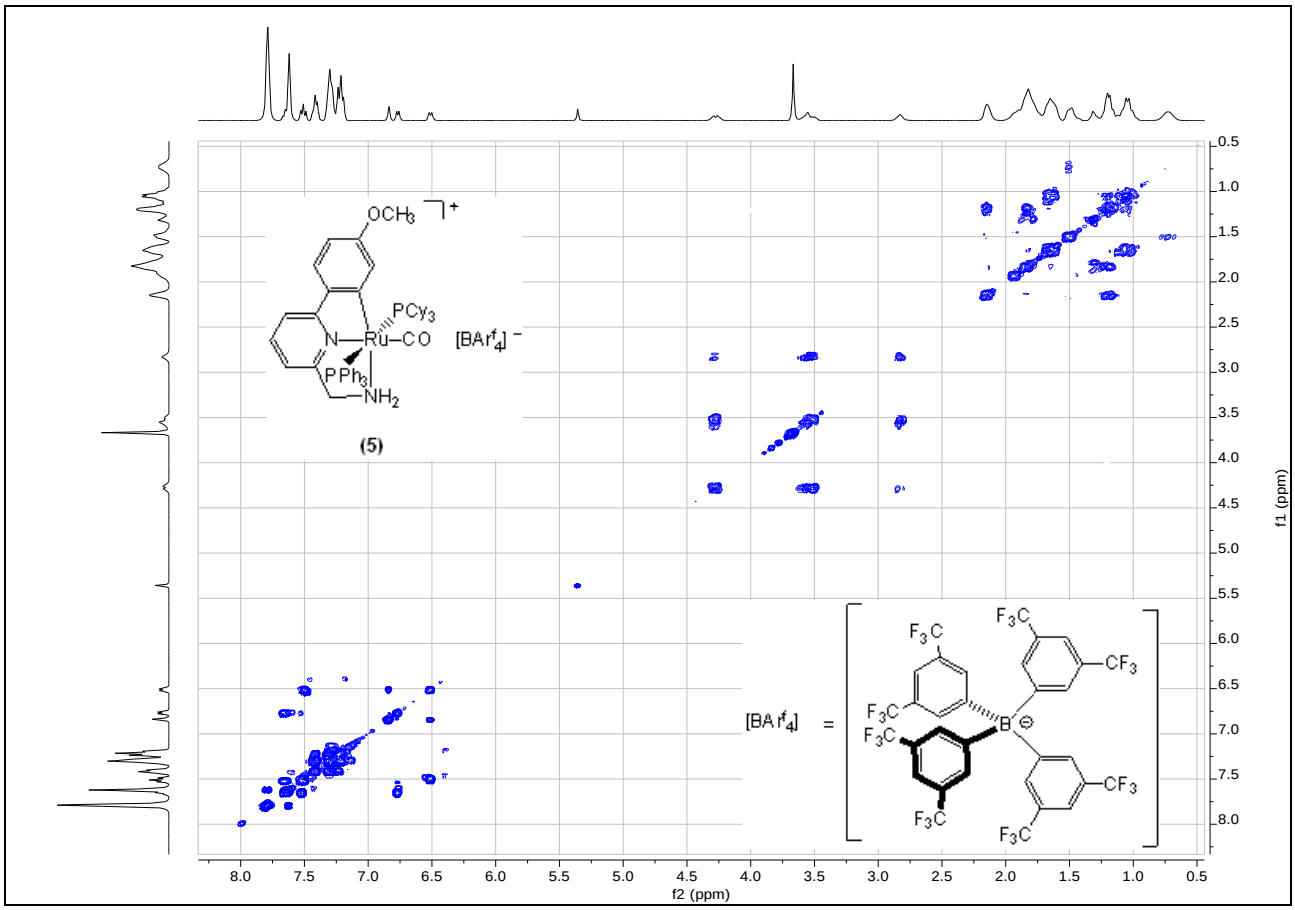

Figure S32. ^{1}H-^{1}H COSY 2D NMR spectrum (400.1 MHz) of *trans*-[Ru(CNN^{OMe})(CO)(PCy$_3$)(PPh$_3$)][BAr$^f_4$] (**5**) in CD_2Cl_2 at 25 °C.

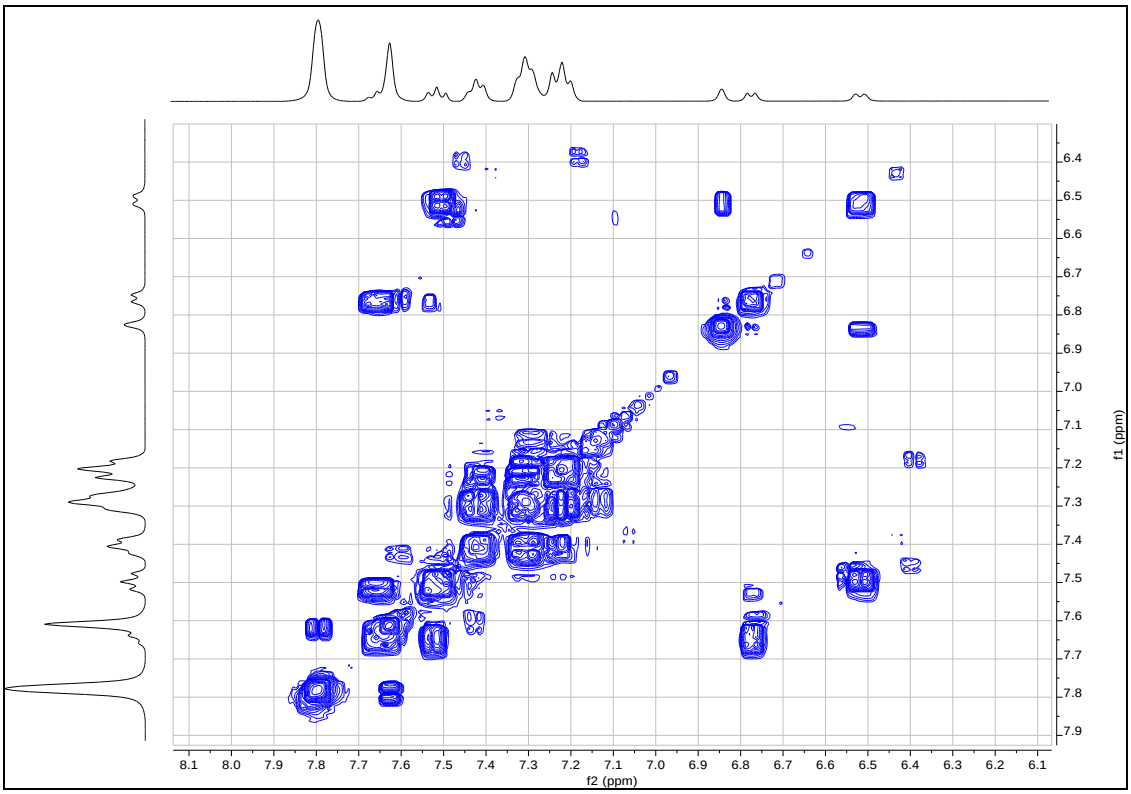

Figure S33. Aromatic region of the ^{1}H-^{1}H COSY 2D NMR spectrum (400.1 MHz) of *trans*-[Ru(CNN^{OMe})(CO)(PCy$_3$)(PPh$_3$)][BAr$^f_4$] (**5**) in CD_2Cl_2 at 25 °C.

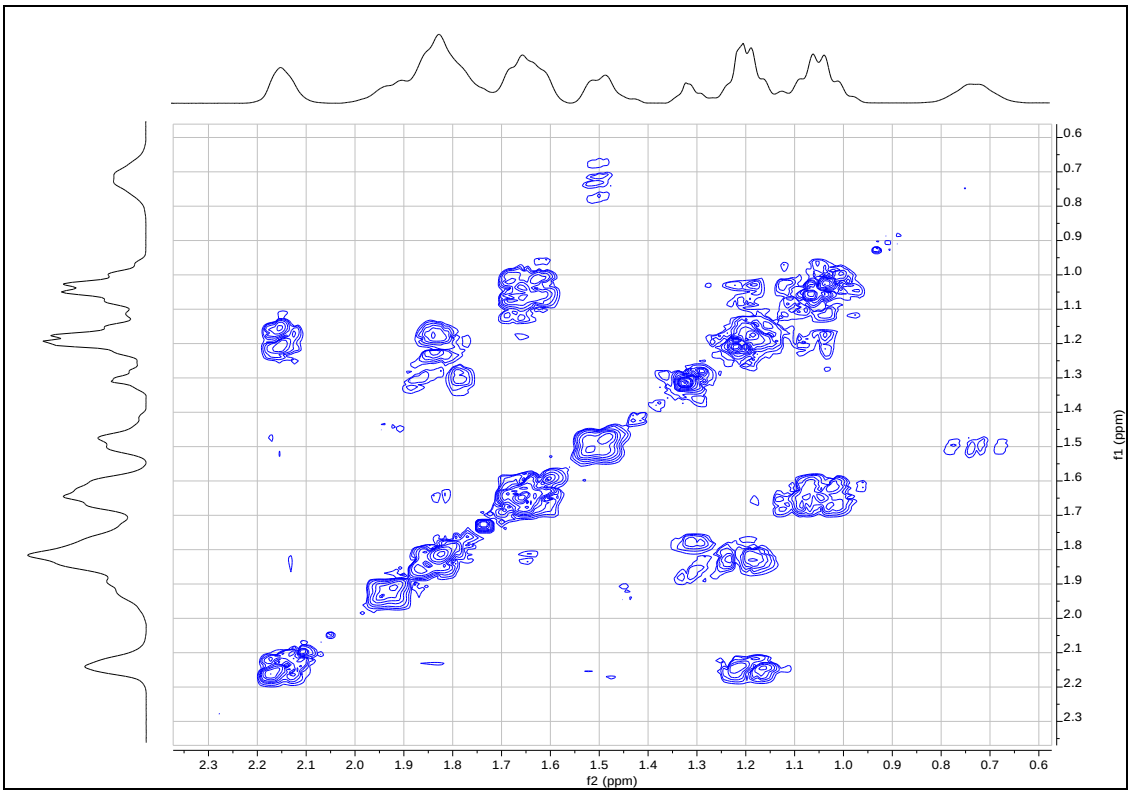

Figure S34. Alkylic region of the ^{1}H-^{1}H COSY 2D NMR spectrum (400.1 MHz) of *trans*-[Ru(CNN^{OMe})(CO)(PCy$_3$)(PPh$_3$)][BAr$^f_4$] (**5**) in CD_2Cl_2 at 25 °C.

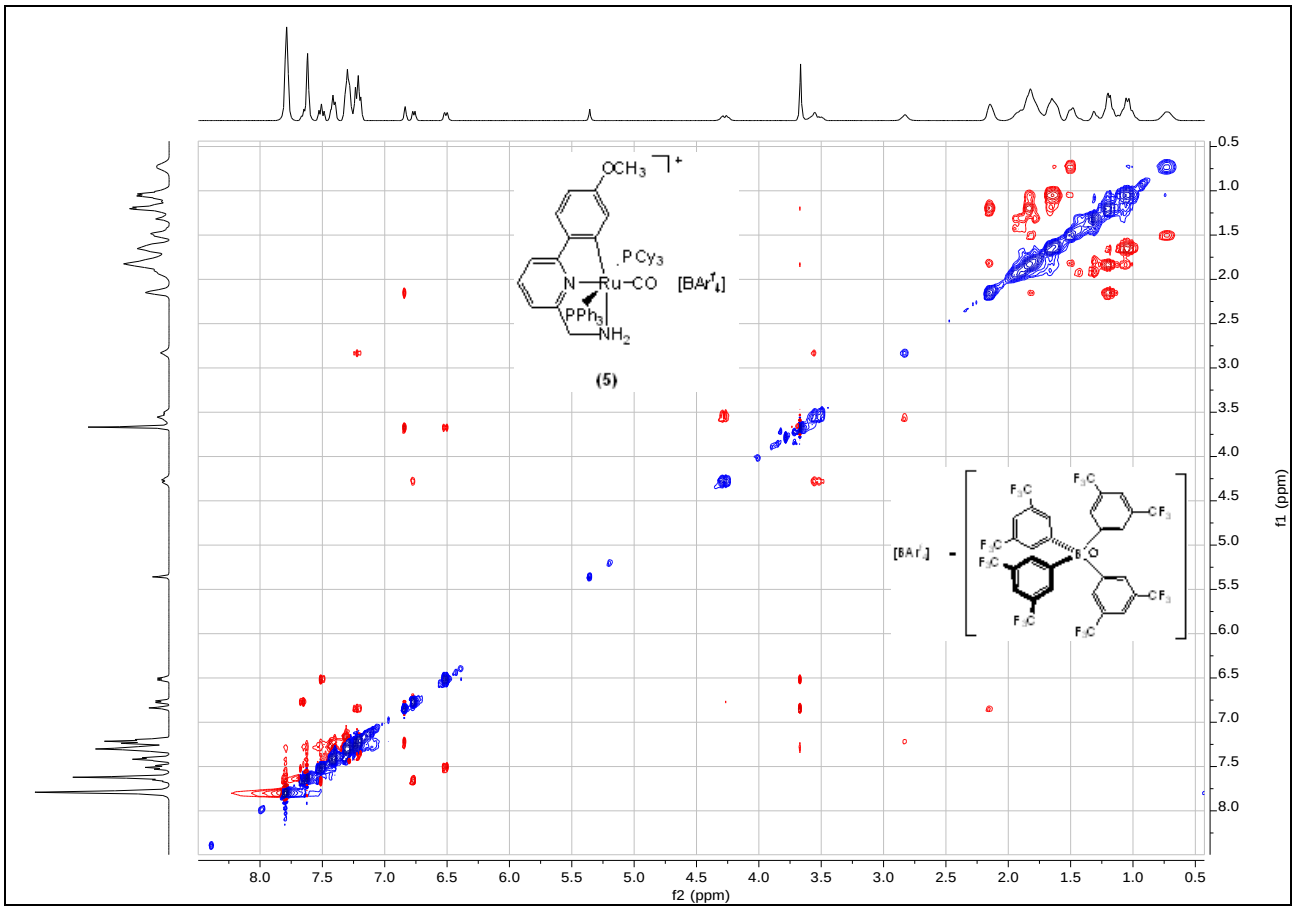

Figure S35. ^{1}H-^{1}H NOESY 2D NMR spectrum (400.1 MHz) of *trans*-[Ru(CNN^{OMe})(CO)(PCy$_3$)(PPh$_3$)][BAr$^f_4$] (**5**) in CD_2Cl_2 at 25 °C.

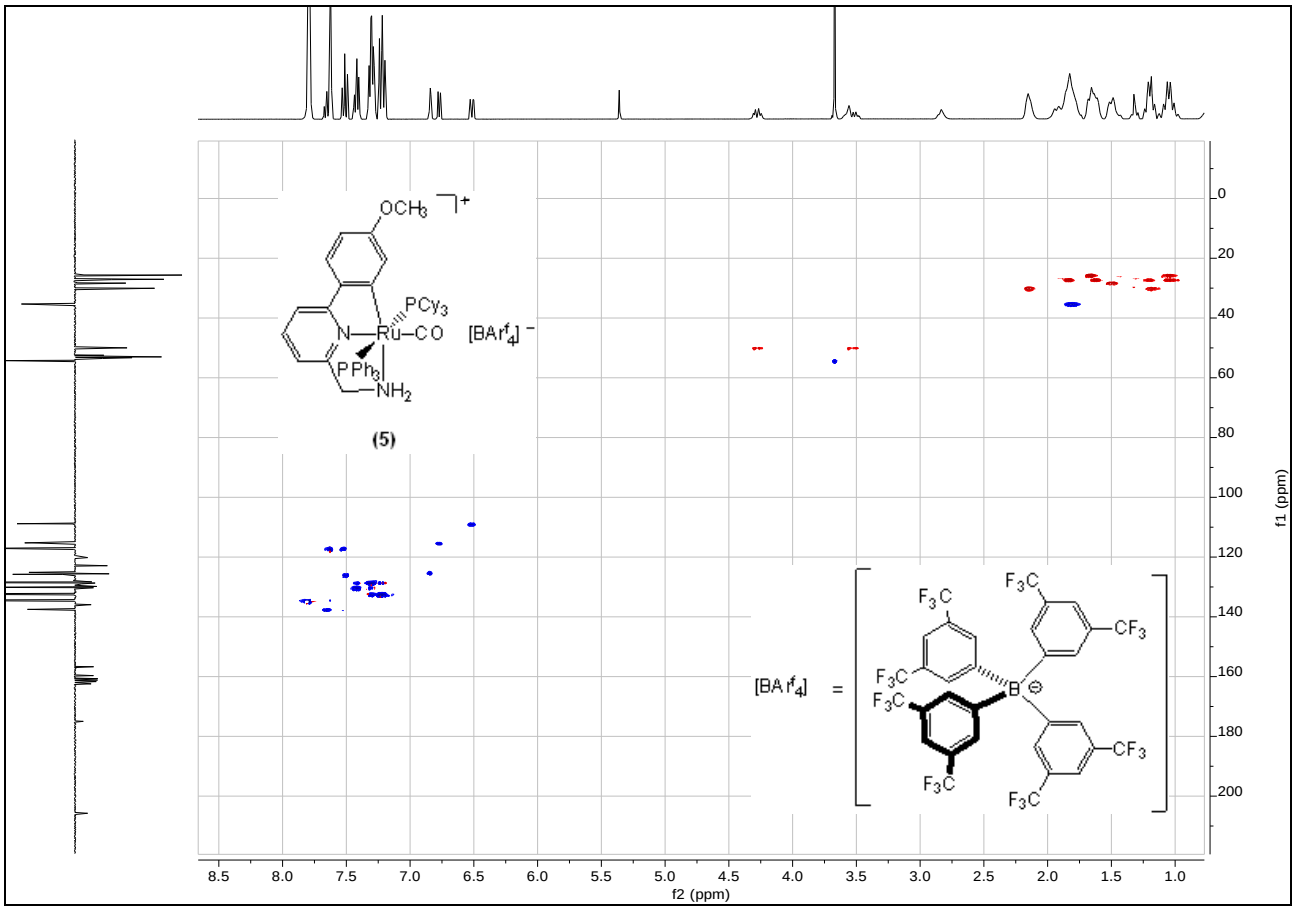

Figure S36. ^{1}H-^{13}C HSQC 2D NMR spectrum of *trans*-[Ru(CNN^{OMe})(CO)(PCy$_3$)(PPh$_3$)][BAr^f$_4$] (**5**) in CD_2Cl_2 at 25 °C.

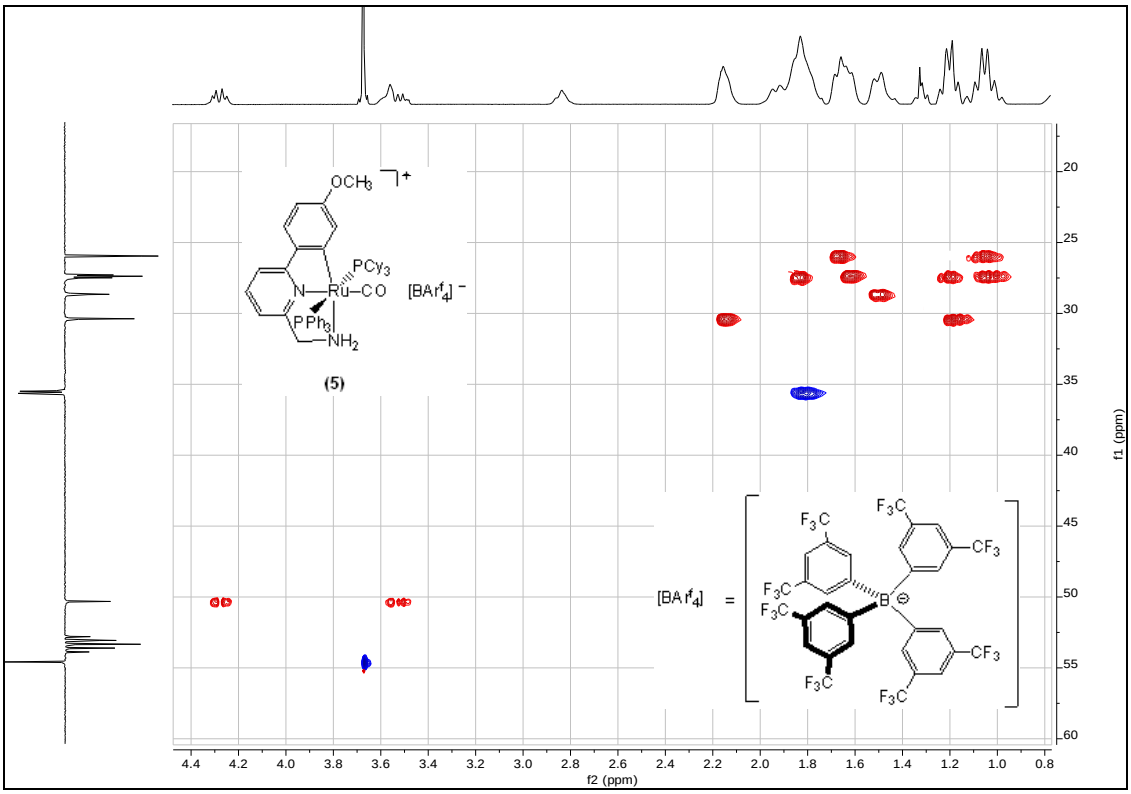

Figure S37. Alkylic region of the ^{1}H-^{13}C HSQC 2D NMR spectrum of *trans*-[Ru(CNN^{OMe})(CO)(PCy$_3$)(PPh$_3$)][BAr$^f_4$] (**5**) in CD_2Cl_2 at 25 °C.

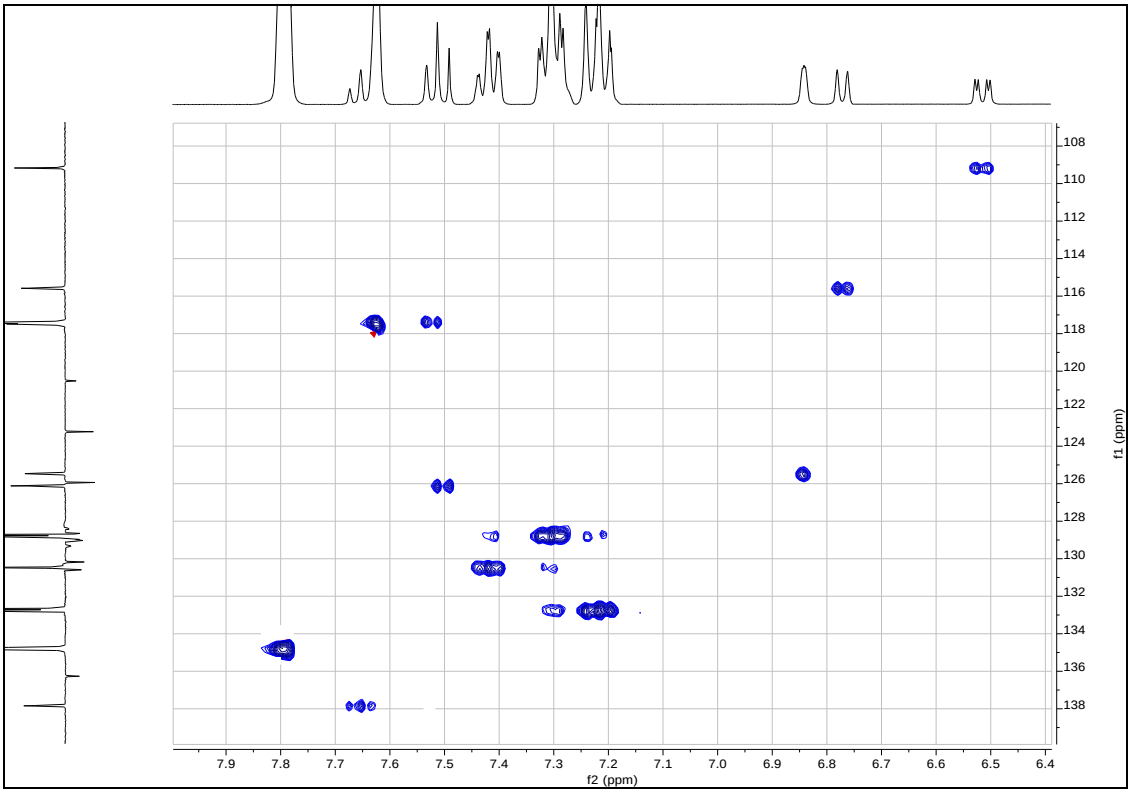

Figure S38. Aromatic region of the ^{1}H-^{13}C HSQC 2D NMR spectrum of *trans*-[Ru(CNN^{OMe})(CO)(PCy$_3$)(PPh$_3$)][BAr$^f_4$] (**5**) in CD_2Cl_2 at 25 °C.

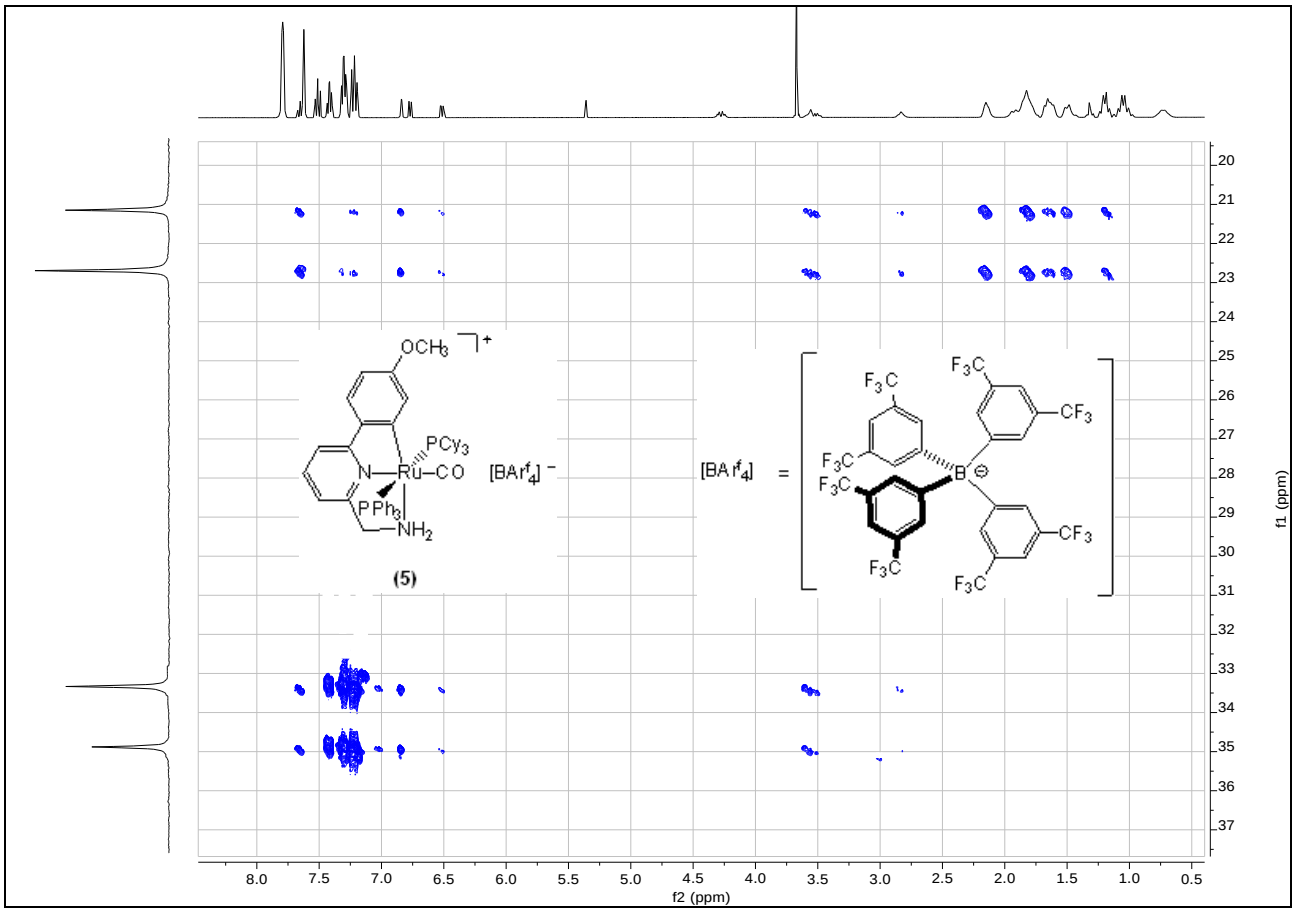

Figure S39. ^{1}H-^{31}P HMBC 2D NMR of *trans*-[Ru(CNN^{OMe})(CO)(PCy$_3$)(PPh$_3$)][BAr$^f{}_4$] (**5**) in CD_2Cl_2 at 25 °C.

Table S1. Further data regarding the catalytic TH of lignocellulose biomass carbonyl compounds (0.1 M) to alcohols with **2**, **3**, **5** (S/C = 1000-10000) in 2-propanol at 82 °C.

Entry	Substrate	Complex	S/C	Base[a]	Time [min]	Conv.[b] [%]	Alcohol [%]	By-prod. [%]
1	**b**	**2**	1000	NaO*i*Pr	5	97	97	-
2	**b**	**2**	10000	K_2CO_3	24 h	47	47	-
3	**c**	**3**	1000	NaOiPr	1	99[c]	98	<1
4	**d**	**3**	1000	K_2CO_3	180	60[c]	4	56[d]
5	**f**	**3**	10000	K_2CO_3	30	64	62[e]	2[f]
6	**g**	**2**	1000	K_2CO_3	5	98	96	2[g]
7	**g**	**2**	1000	K_2CO_3	60	98	63	35[g]
8	**g**	**3**	1000	K_2CO_3	10	98	95	3[g]
9	**g**	**5**	1000	K_2CO_3	15	99	94	5[g]
10	**h**	**5**	1000	K_2CO_3	5	99[c]	98	<1
11	**h**	**5**	10000	K_2CO_3	20	99[c]	90	9[h]
12	**i**	**2**	1000	NaO*i*Pr	60	99[c]	97	2[i]
13	**i**	**3**	1000	NaOiPr	1	99[c]	99	-

[a]Base: NaO*i*Pr (2 mol%) or K_2CO_3 (5 mol%). [b]Conversions have been determined by GC analyses. [c]Conversions have been determined by NMR analyses. [d]5-(hydroxymethyl)furfural (5-HMF). [e]% of γ-valerolactone (GVL). [f]isopropyl 4-hydroxypentanoate. [g]3-phenylpropan-1-ol. [h]4-(isopropoxymethyl)-1,2-dimethoxybenzene. [i]4-(2-(4-(hydroxymethyl)-2-methoxyphenoxy)ethoxy)-3-methoxybenzaldehyde.

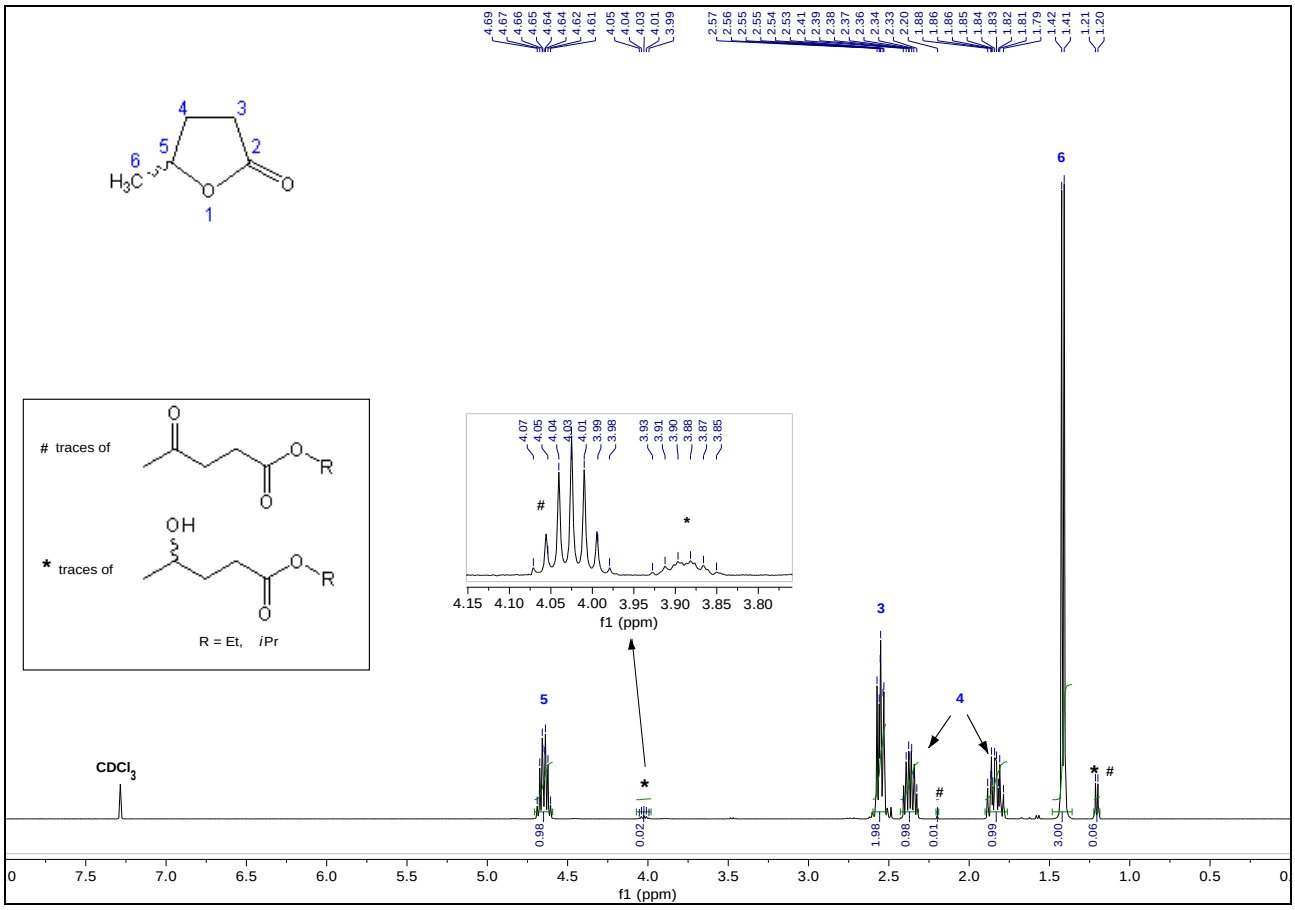

Figure S40. ^{1}H NMR spectrum (400.1 MHz) in $CDCl_3$ at 25 °C of γ-valerolactone (GVL) obtained from TH reduction of ethyl levulinate in 2-propanol catalyzed by ruthenium pincer complexes **2**, **3** and **5**.

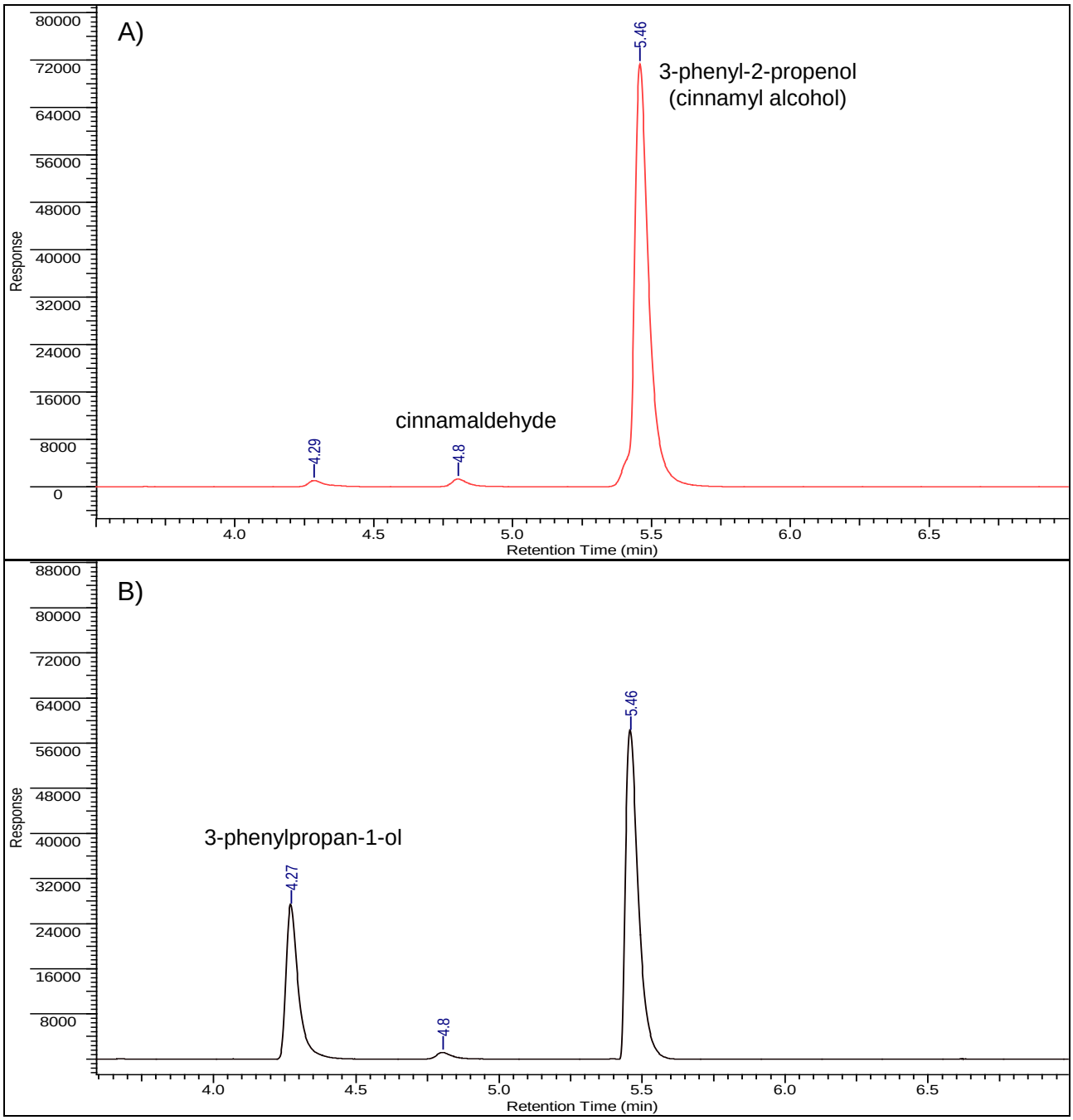

Figure S41. GC-FID chromatograms of the reaction mixture of the TH of cinnamaldehyde **g** in 2-propanol at reflux promoted by complex **2** at S/C 1000 after 5 min (A) and 1 h (B).

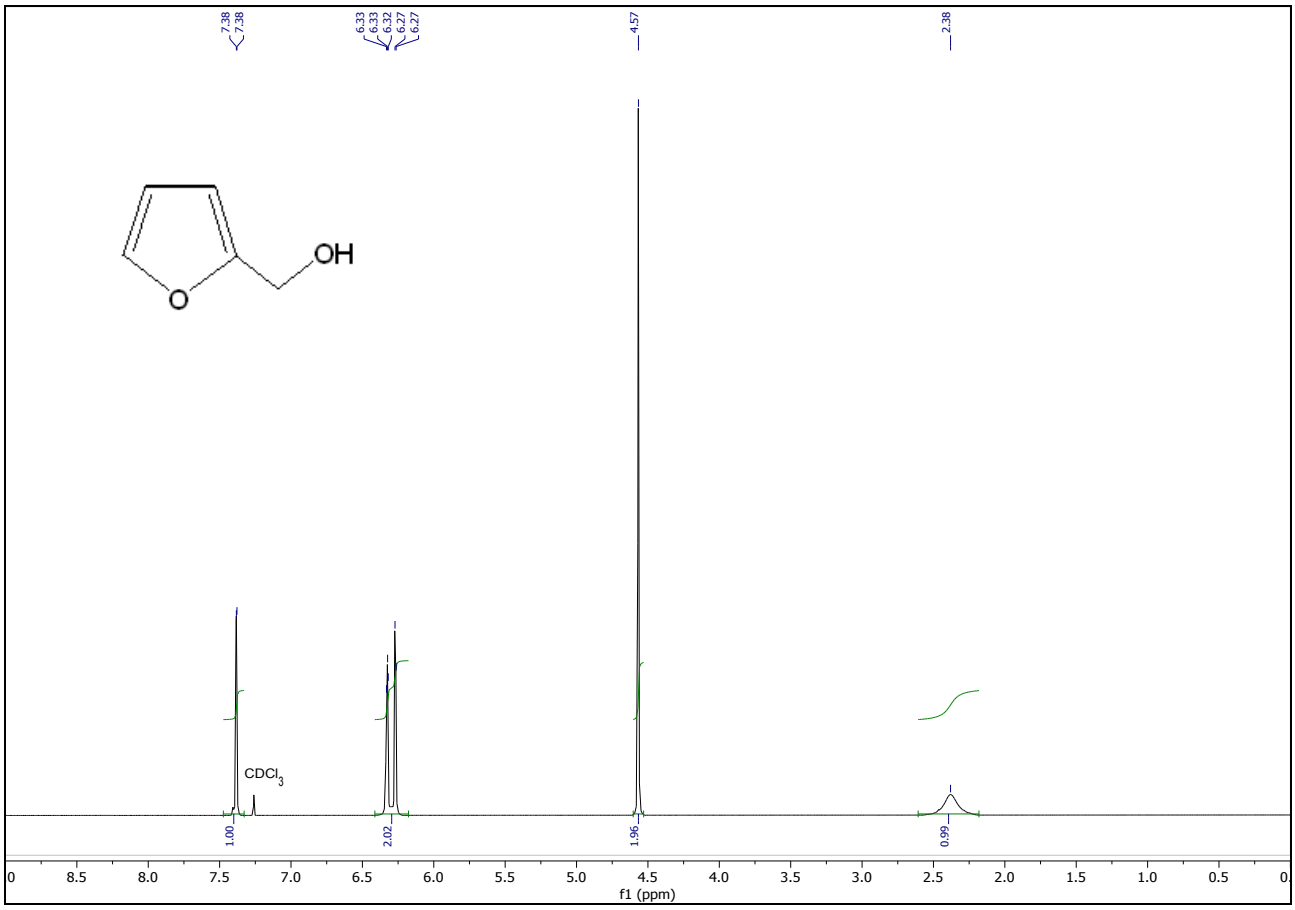

Figure S42. ^{1}H NMR spectrum (400.1 MHz) of furfuryl alcohol obtained from TH of furfural in $CDCl_3$ at 25 °C.

^{1}H NMR (400 MHz, $CDCl_3$, 25 °C): δ = 7.38 (m, 1H; aromatic proton), 6.33 (dd, $^{3}J_{HH}$ = 3.2 Hz, $^{3}J_{HH}$ = 1.8 Hz, 1H; aromatic proton), 6.27 (d, $^{3}J_{HH}$ = 3.2 Hz, 1H; aromatic proton), 4.57 (s, 2H; CH_2), 2.38 ppm (s, 2H; OH).

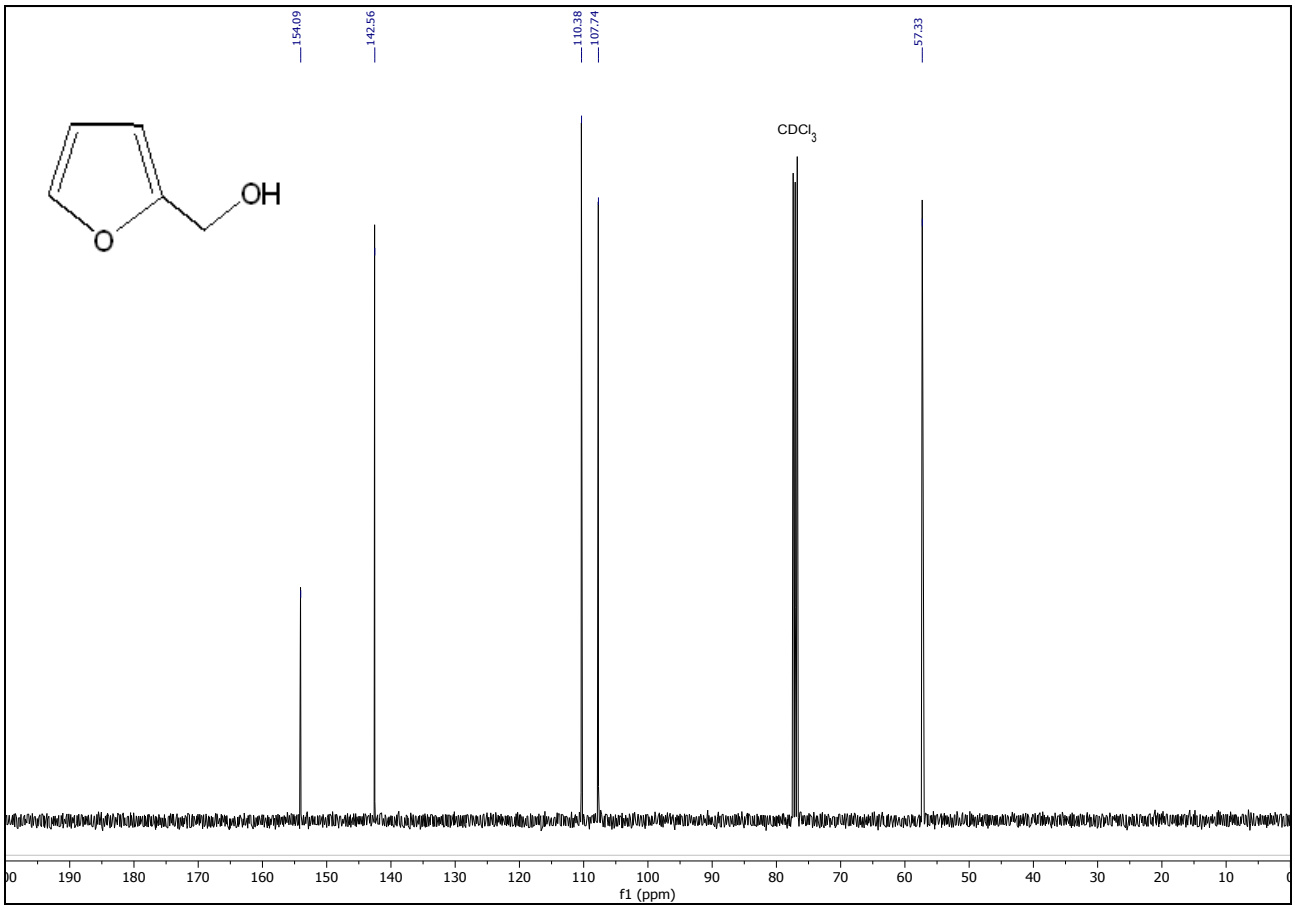

Figure S43. $^{13}C\{^{1}H\}$NMR spectrum (100.6 MHz) of furfuryl alcohol obtained from TH of furfural in $CDCl_3$ at 25 °C.

$^{13}C\{^{1}H\}$ NMR (100.6 MHz, $CDCl_3$, 25 °C): δ = 154.1 (s; ipso aromatic carbon), 142.6 (s; aromatic carbon atom), 110.4 (s; aromatic carbon atom), 107.7 (s; aromatic carbon atom), 57.3 ppm (s; CH_2).

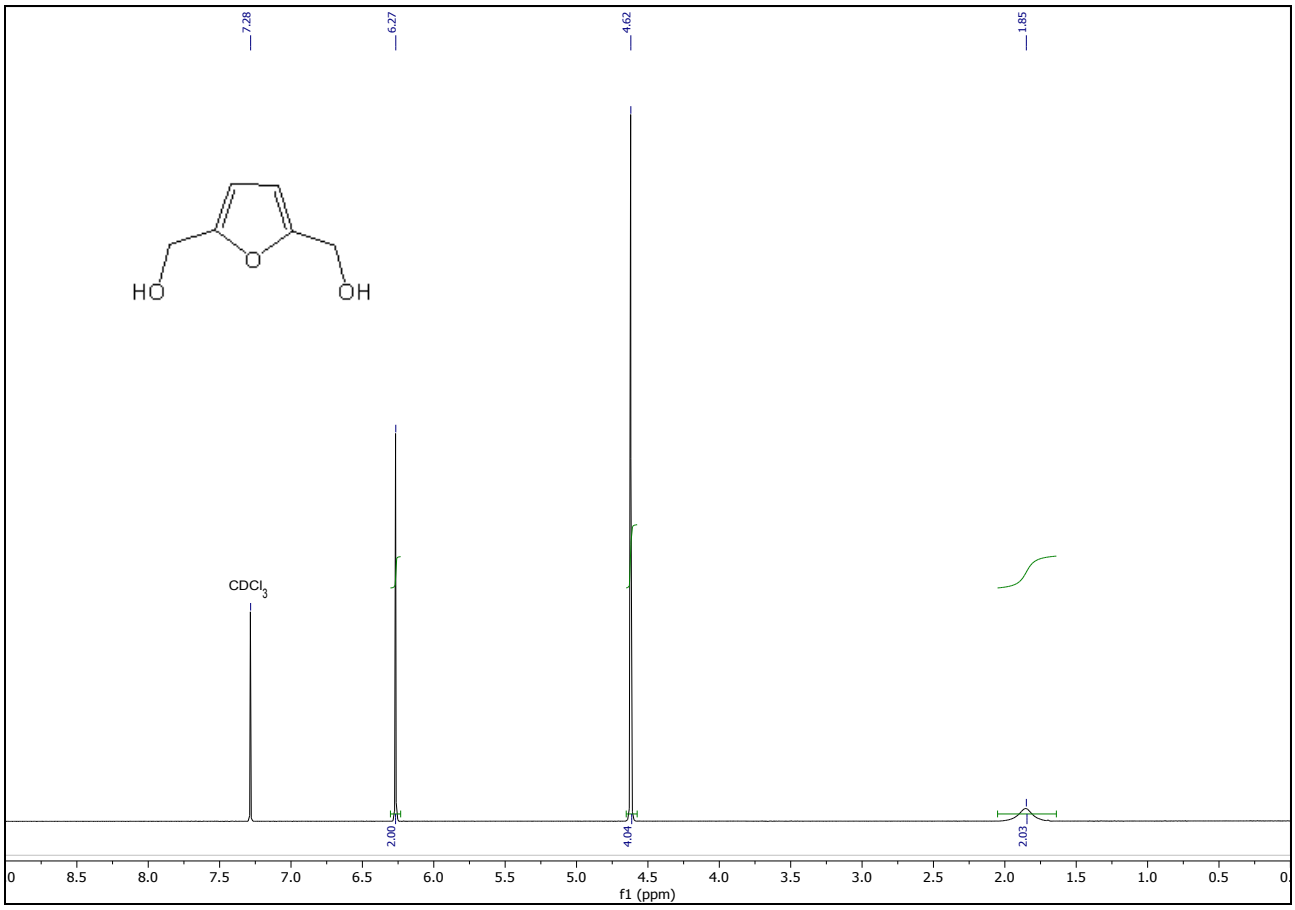

Figure S44. ^{1}H NMR spectrum (400.1 MHz) of 2,5-bis(hydroxymethyl)furan (BHMF) obtained from TH of 5-HMF in $CDCl_3$ at 25 °C.

^{1}H NMR (400 MHz, $CDCl_3$, 25 °C): δ = 6.27 (s, 2H; aromatic protons), 4.62 (s, 4H; CH_2), 1.85 ppm (s, 2H; OH).

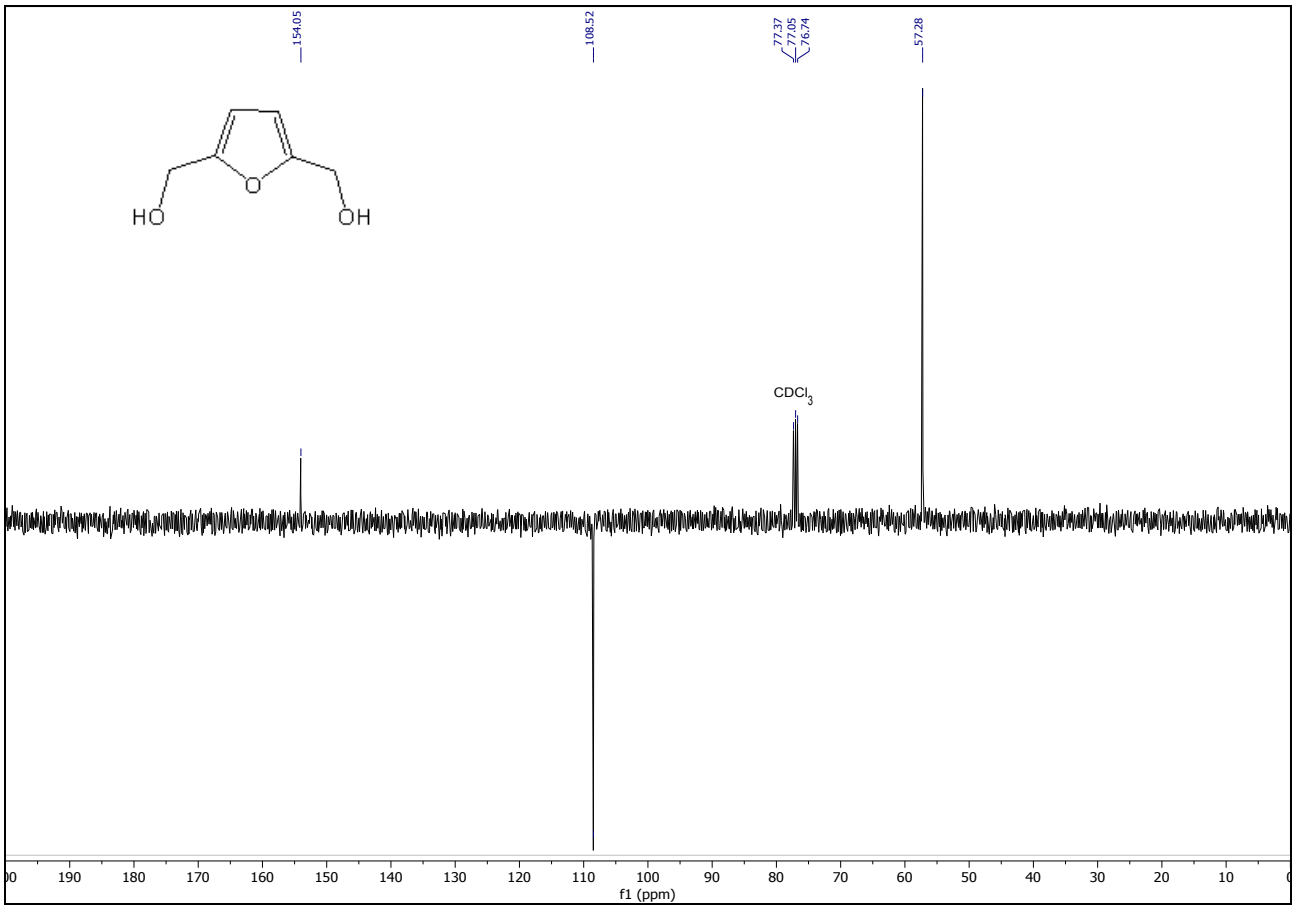

Figure S45. $^{13}C\{^{1}H\}$ DEPTQ NMR spectrum (100.6 MHz) of 2,5-bis(hydroxymethyl)furan (BHMF) obtained from TH of 5-HMF in $CDCl_3$ at 25 °C.

$^{13}C\{^{1}H\}$ NMR (100.6 MHz, $CDCl_3$, 25 °C): δ = 154.1 (s; *C*CH_2), 108.5 (s; *C*H), 57.3 ppm(s; *C*H_2).

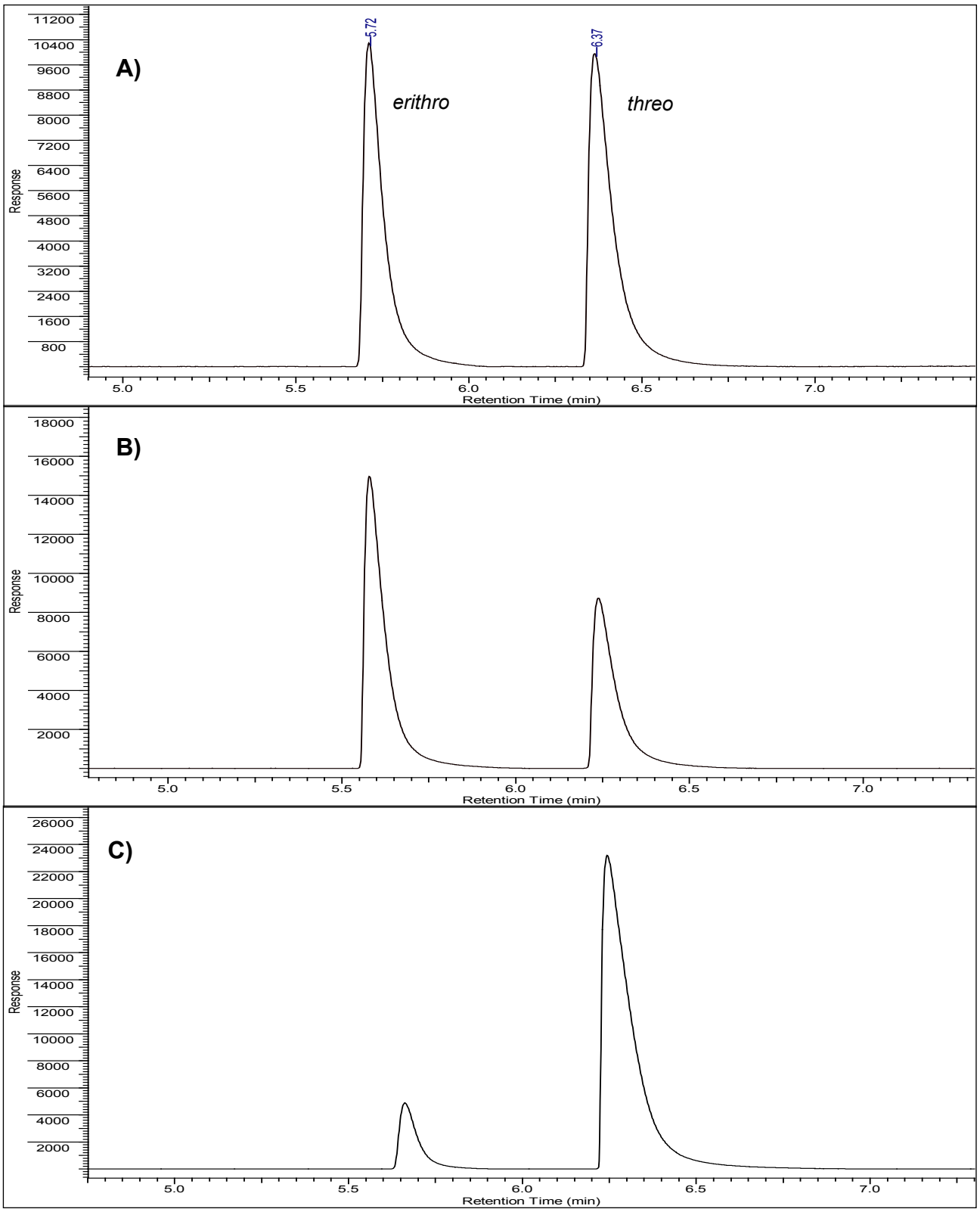

Figure S46. Comparison between the GC-FID chromatograms of levoglucosanol obtained from TH of Cyrene **e** in 2-propanol at reflux and NaO*i*Pr 2 mol% promoted by complex **2** (A), **3** (B) and **5** (C) at S/C 10000.

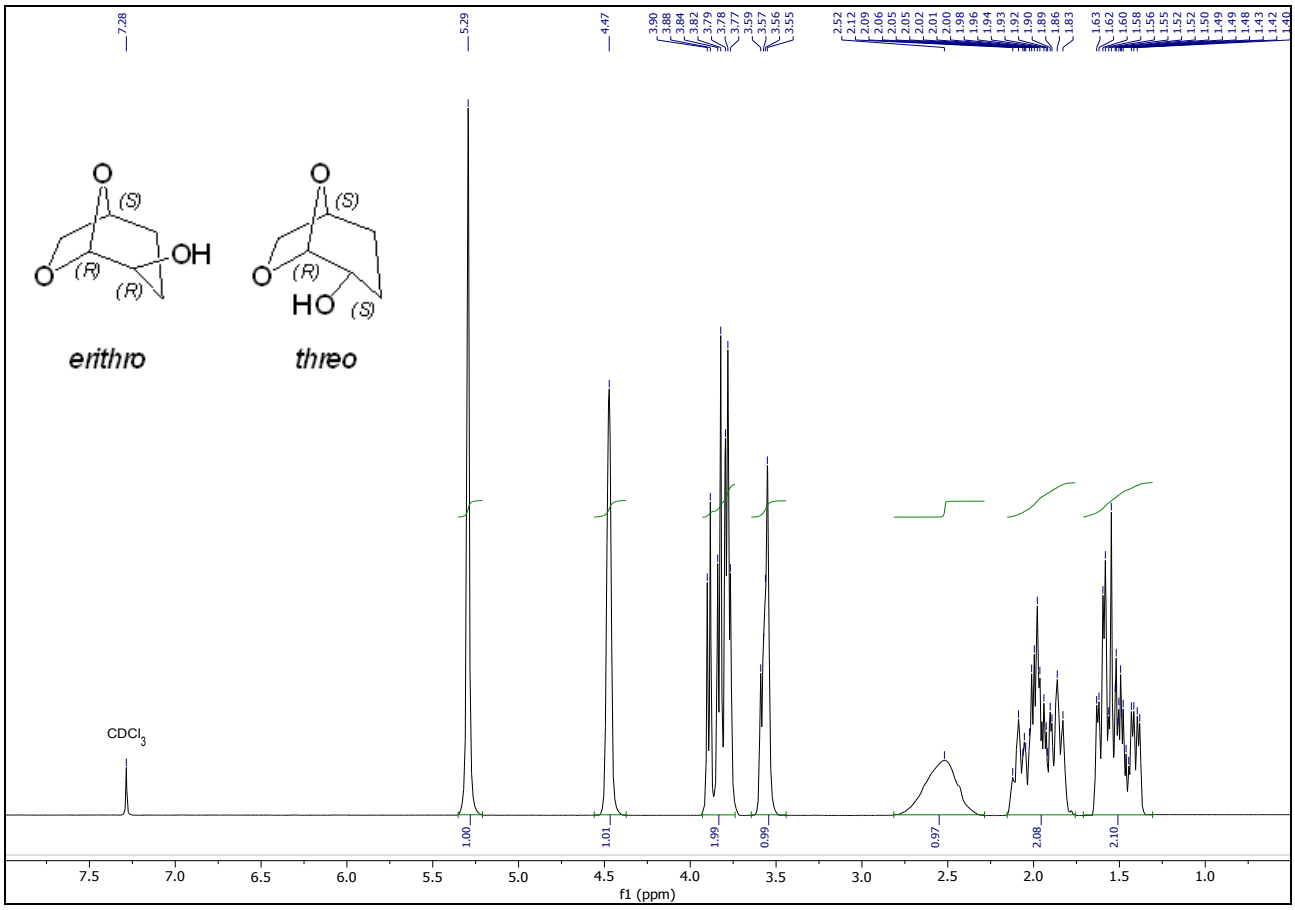

Figure S47. ^{1}H NMR spectrum (400.1 MHz) of levoglucosanol obtained from TH of Cyrene **e** promoted by complex **2** at S/C 10000 (*erithro*/*threo* ratio 1/1.2) in $CDCl_3$ at 25 °C.

^{1}H NMR (400 MHz, $CDCl_3$, 25 °C): δ = 5.29 (s, 1H; CH(O)O), 4.47 (br s, 1H; $CH_2C\mathit{H}(O)CH_2$), 3.91-3.75 (m, 2H; OCH_2), 3.57 (m, 1H; C*H*OH), 2.52 (s, 1H; OH), 2.14-1.79 (m, 2H; $CHC\mathit{H}_2CH_2$), 1.67-1.35 ppm (m, 2H; $CHCH_2C\mathit{H}_2$).

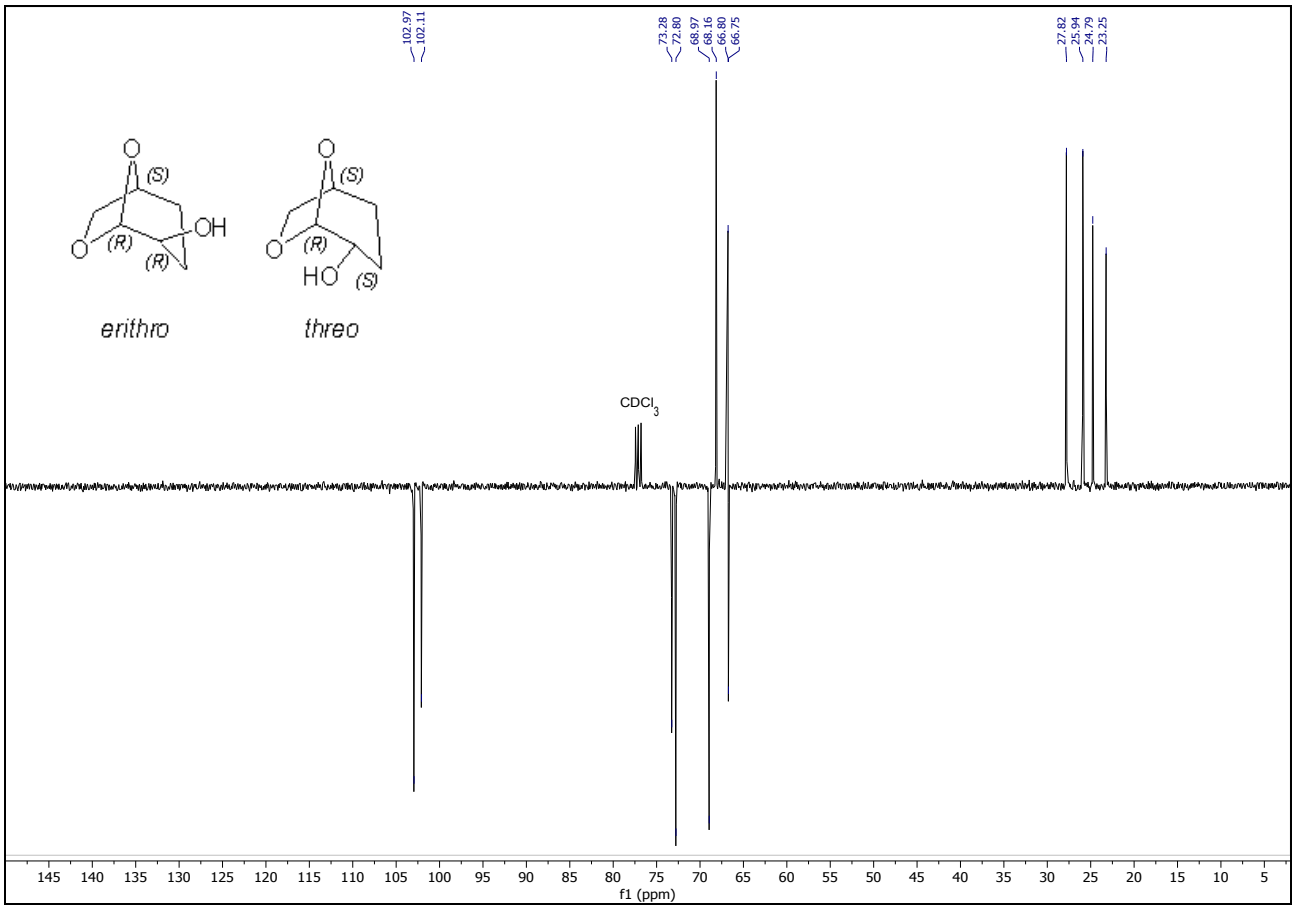

Figure S48. $^{13}C\{^{1}H\}$ DEPTQ NMR spectrum (100.6 MHz) of levoglucosanol obtained from TH of Cyrene **e** promoted by complex **2** at S/C 10000 (*erithro*/*threo* ratio 1/1.2) in $CDCl_3$ at 25 °C.

$^{13}C\{^{1}H\}$ NMR (100.6 MHz, $CDCl_3$, 25 °C): δ = 103.0 (s; *C*H(O)O *threo* isomer), 102.1 (s; *C*H(O)O *erithro* isomer), 73.3 (s; CH_2*C*H(O)CH_2 *erithro* isomer), 72.8 (s; CH_2*C*H(O)CH_2 *threo* isomer), 69.0 (s; *C*HOH *threo* isomer), 68.2 (s; O*C*H_2 *threo* isomer), 66.8 (s; O*C*H_2 *erithro* isomer), 66.7 (s; *C*HOH *erithro* isomer), 27.8 (s; CH*C*$H_2$$CH_2$ *threo* isomer), 25.9 (s; CHCH_2*C*H_2 *threo* isomer), 24.8 (s; CH*C*$H_2$$CH_2$ *erithro* isomer), 23.3 ppm (s; CHCH_2*C*H_2 *erithro* isomer).

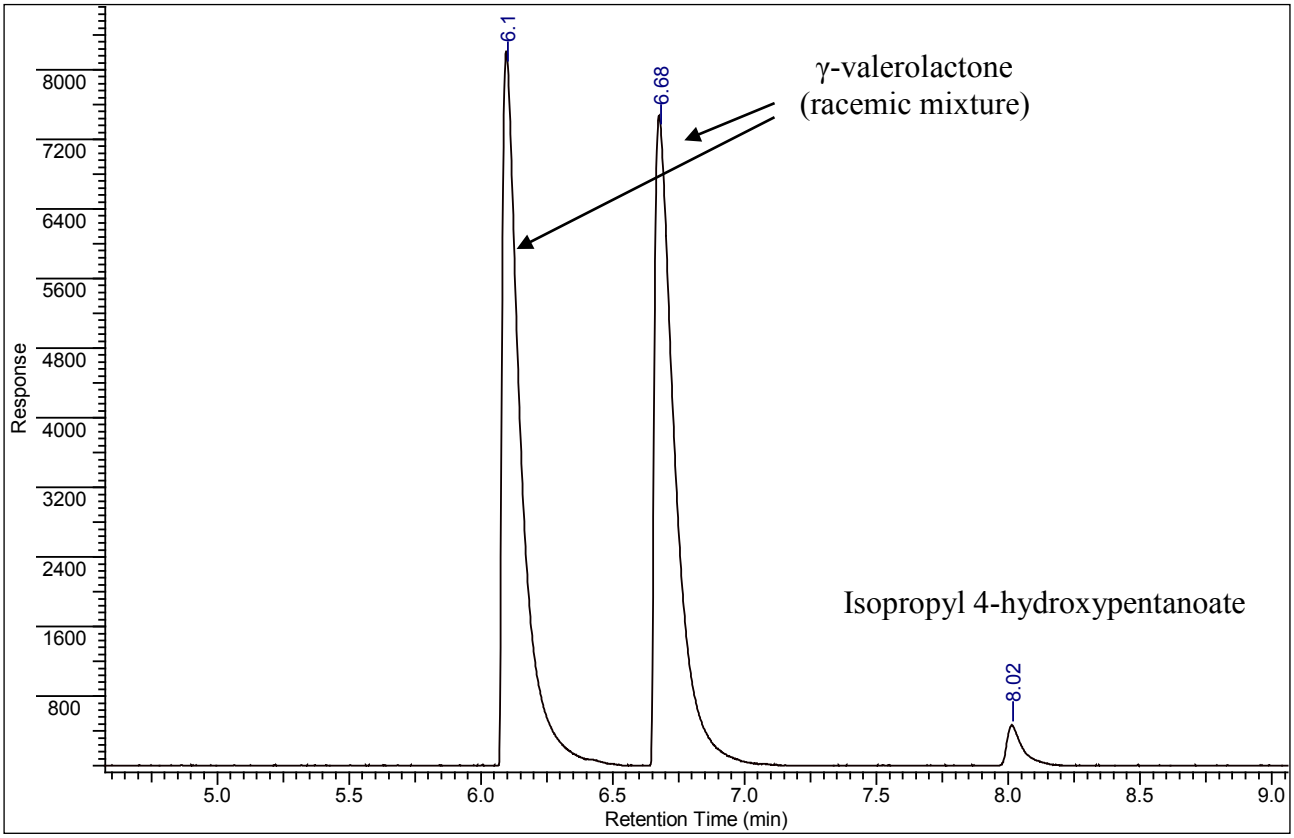

Figure S49. GC-FID chromatogram of γ-valerolactone (GVL) obtained from TH of ethyl levulinate **f** in 2-propanol at reflux and K_2CO_3 5 mol% promoted by complex **2** at S/C 1000.

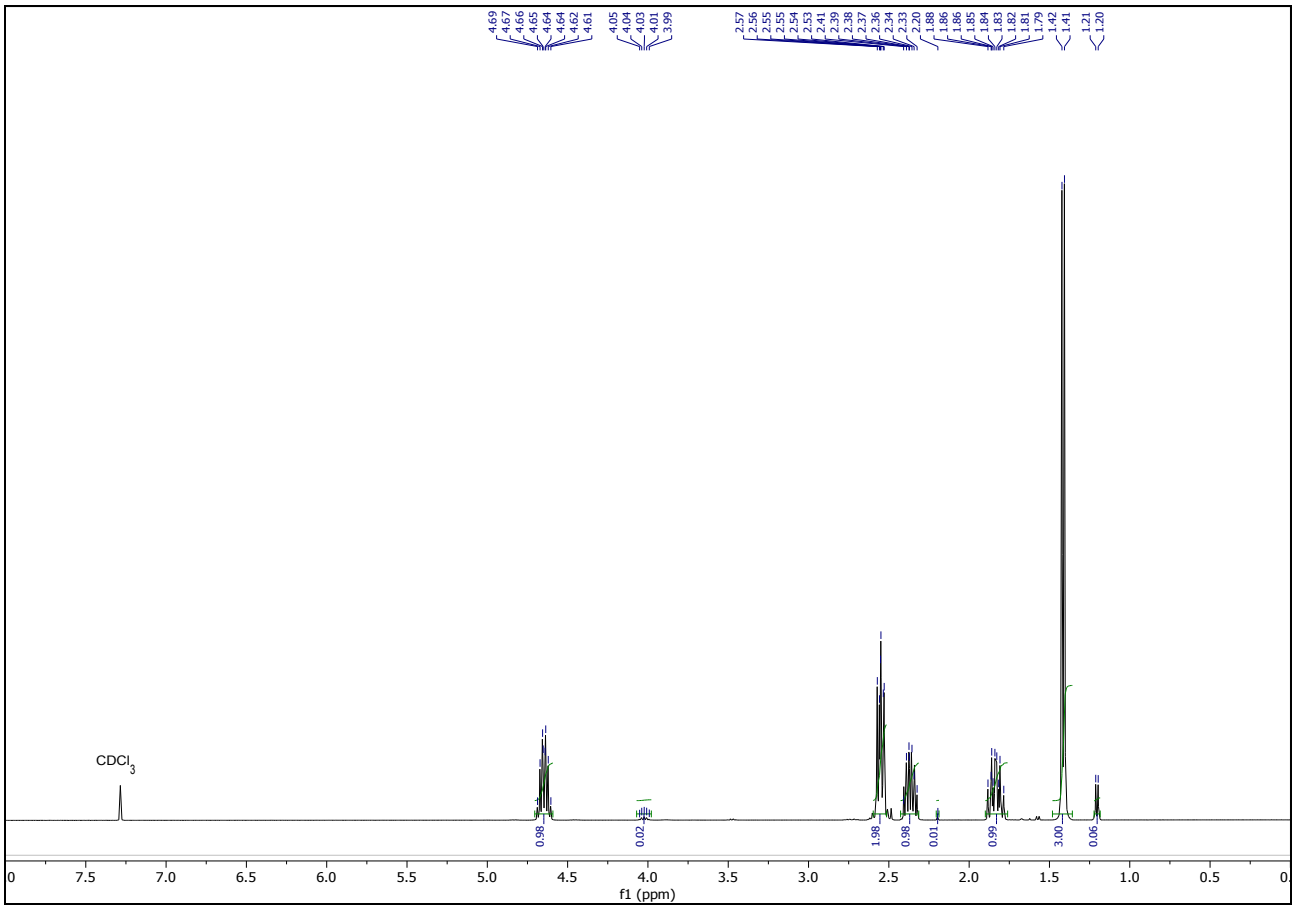

Figure S50. ^{1}H NMR spectrum (400.1 MHz) of γ-valerolactone (GVL) obtained from TH of ethyl levulinate **f** in $CDCl_3$ at 25 °C.

^{1}H NMR (400 MHz, $CDCl_3$, 25 °C): δ = 4.65 (dt, $^{3}J_{HH}$ = 7.8 Hz, $^{3}J_{HH}$ = 6.3Hz, 1H; C*H*CH_3), 2.60-2.52 (m, 2H; CH_2C*H*$_2$CO), 2.43-2.29 (m, 1H; C*H*$_2$$CH_2$CO), 1.91-1.76 (m, 1H; C*H*$_2$$CH_2$CO), 1.42 ppm (d, $^{3}J_{HH}$ = 6.2 Hz, 3H; CH_3).

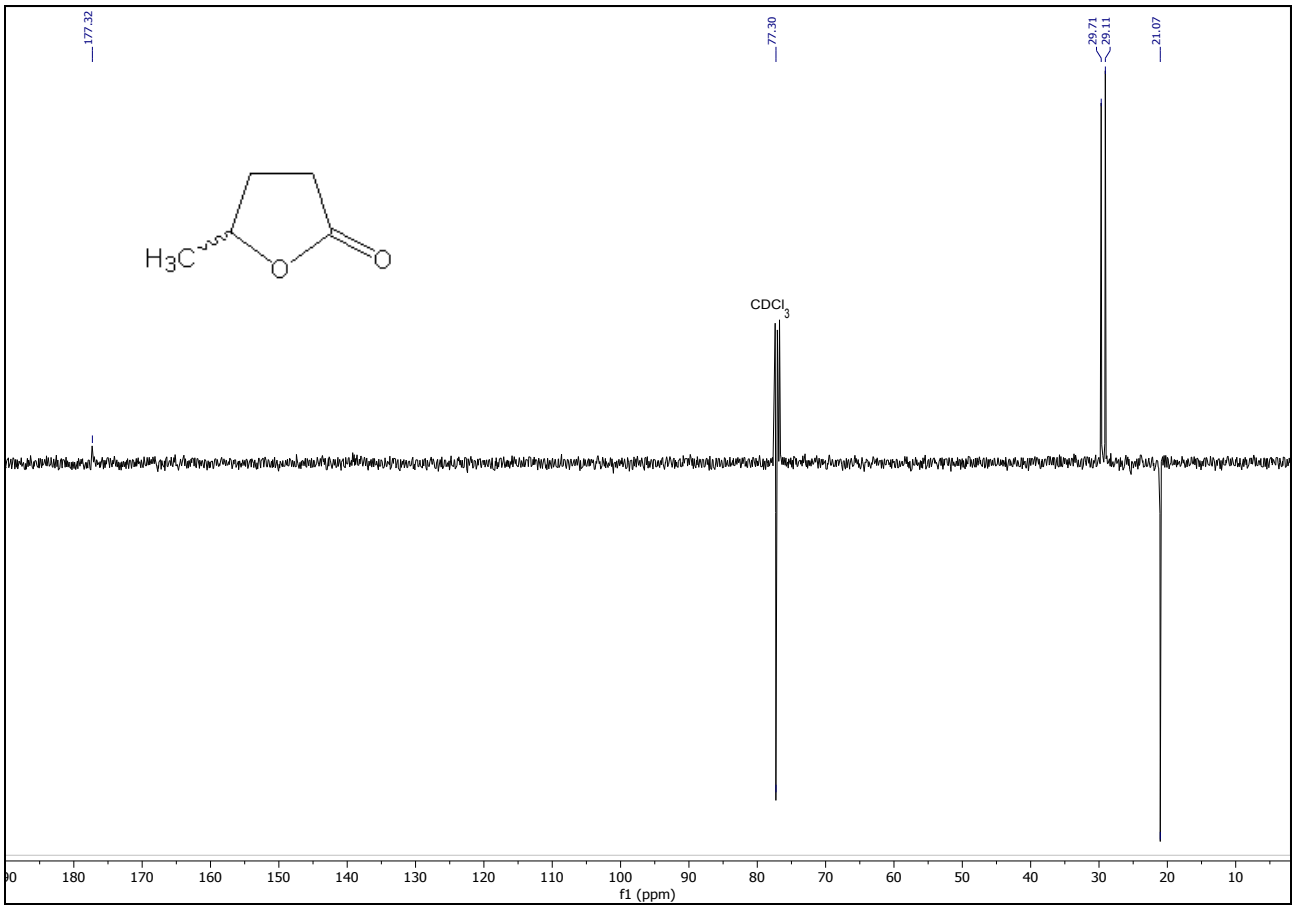

Figure S51. $^{13}C\{^{1}H\}$ DEPTQ NMR spectrum (100.6 MHz) of γ-valerolactone (GVL) obtained from TH of ethyl levulinate **f** in $CDCl_3$ at 25 °C.

$^{13}C\{^{1}H\}$ NMR (100.6 MHz, $CDCl_3$, 25 °C): δ = 177.3 (s; CO), 77.3 (s; *C*HCH$_3$), 29.7 (s; CH*C*H$_2$), 29.1 (s; *C*H$_2$CO), 21.1 ppm (s; CH$_3$).

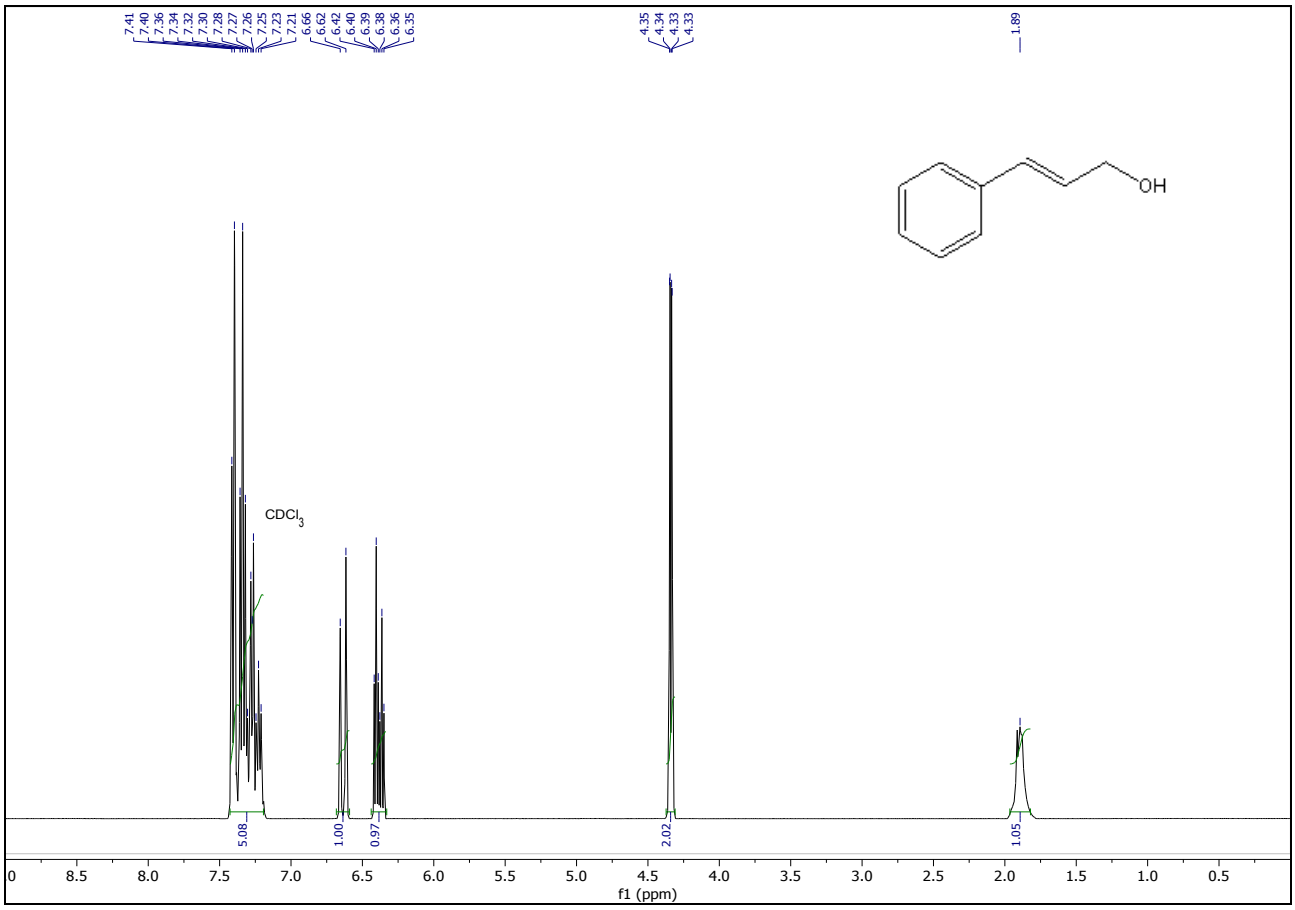

Figure S52. ^{1}H NMR spectrum (400.1 MHz) of cinnamyl alcohol obtained from TH of *trans*-cinnamaldehyde **g** in $CDCl_3$ at 25 °C.

^{1}H NMR (400 MHz, $CDCl_3$, 25 °C): δ = 7.41 (d, $^{3}J_{HH}$ = 7.5 Hz, 2H; aromatic protons), 7.37-7.17 (m, 3H; aromatic protons), 6.64 (d, $^{3}J_{HH}$ = 15.9 Hz, 1H; PhC*H*=CH), 6.38 (dt, $^{3}J_{HH}$ = 15.9 Hz, $^{3}J_{HH}$ = 5.7 Hz, 1H; PhCH=C*H*), 4.34 (dd, $^{3}J_{HH}$ = 5.7 Hz, $^{3}J_{HH}$ = 1.3 Hz, 2H; CH_2), 1.89 ppm (br s, 1H; OH).

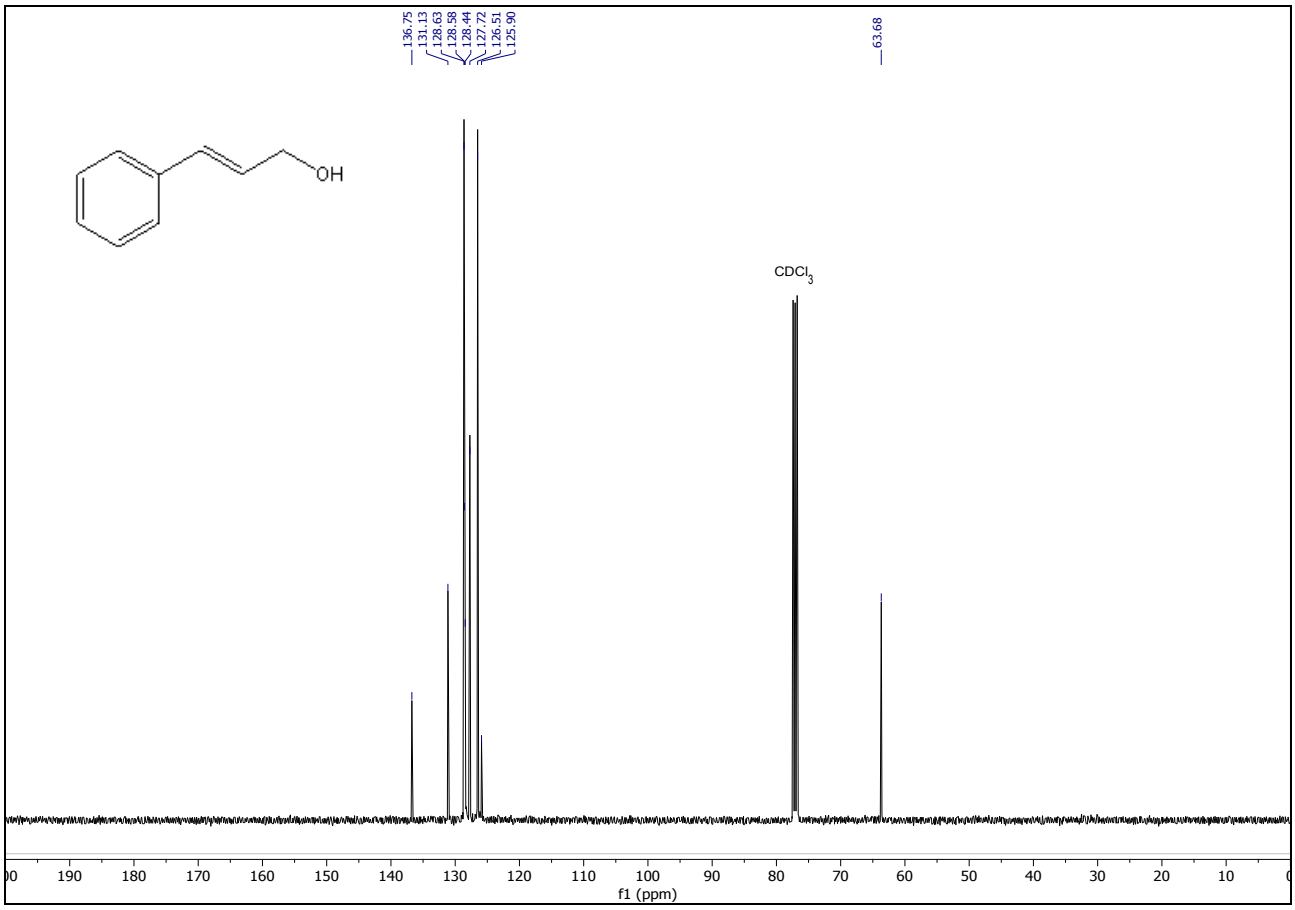

Figure S53. $^{13}C\{^{1}H\}$ NMR spectrum (100.6 MHz) of cinnamyl alcohol obtained from TH of *trans*-cinnamaldehyde **g** in $CDCl_3$ at 25 °C.

$^{13}C\{^{1}H\}$ NMR (100.6 MHz, $CDCl_3$, 25 °C): δ = 136.7 (s; aromatic ipso carbon), 131.1 (s; Ph*C*H=CH), 128.6 (s; PhCH=*C*H), 128.7-125.9 (m; aromatic carbon atoms), 63.7 ppm (s; CH_2).

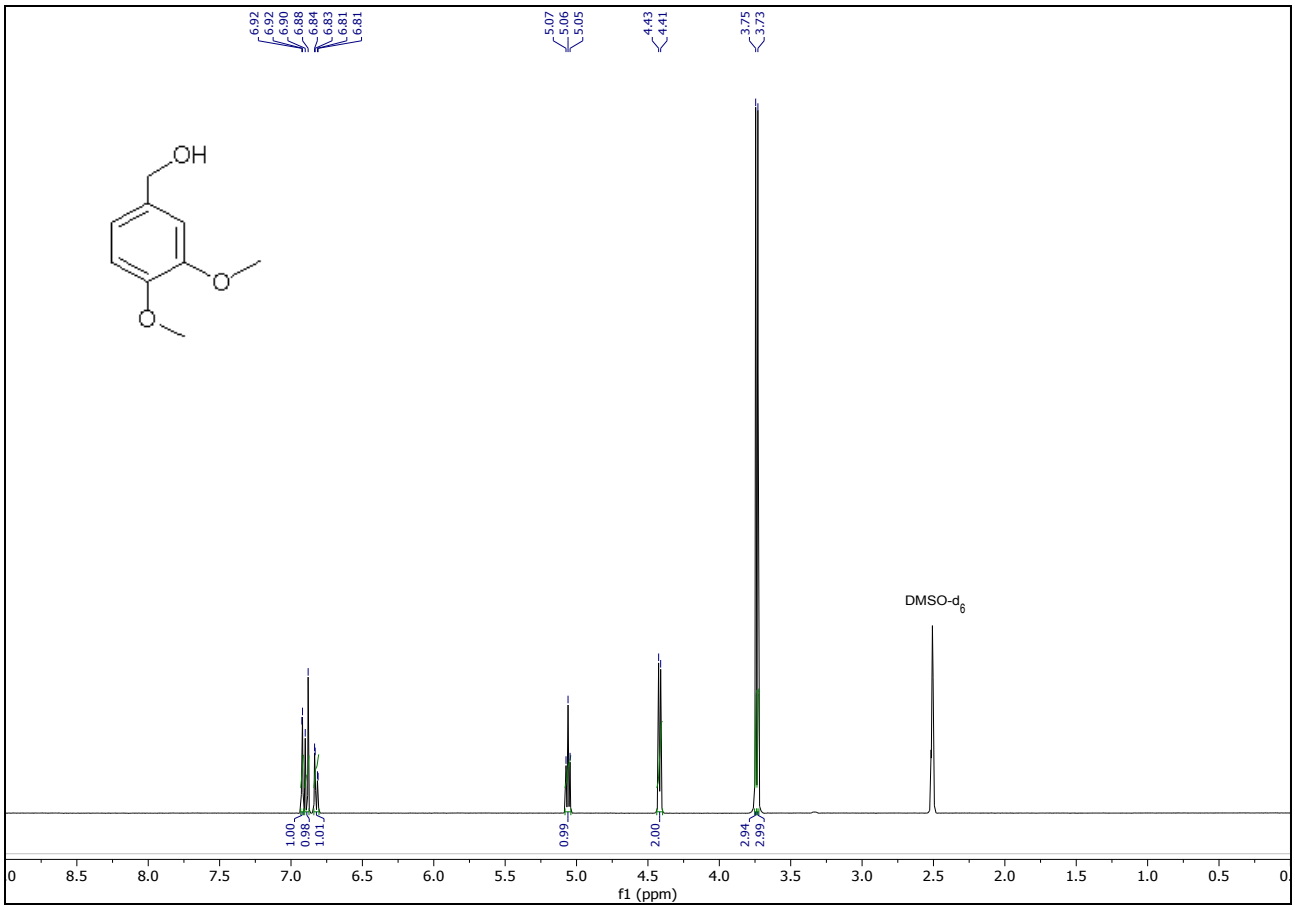

Figure S54. ^{1}H NMR spectrum (400.1 MHz) of veratryl alcohol obtained from TH of veratraldehyde **h** in DMSO-d$_6$ at 25 °C.

^{1}H NMR (400 MHz, DMSO-d$_6$, 25 °C): δ = 6.92 (br d, $^{3}J_{HH}$ = 1.8 Hz, 1H; aromatic proton), 6.89 (d, $^{3}J_{HH}$ = 8.1 Hz, 1H; aromatic proton), 6.82 (dd, $^{3}J_{HH}$ = 8.1 Hz, $^{3}J_{HH}$ = 1.8 Hz, 1H; aromatic proton), 5.06 (t, $^{3}J_{HH}$ = 5.7 Hz, 1H; OH), 4.42 (d, $^{3}J_{HH}$ = 5.7 Hz, 2H; CH_2OH), 3.75 (s, 3H; OCH$_3$), 3.73 ppm (s, 3H; OCH$_3$).

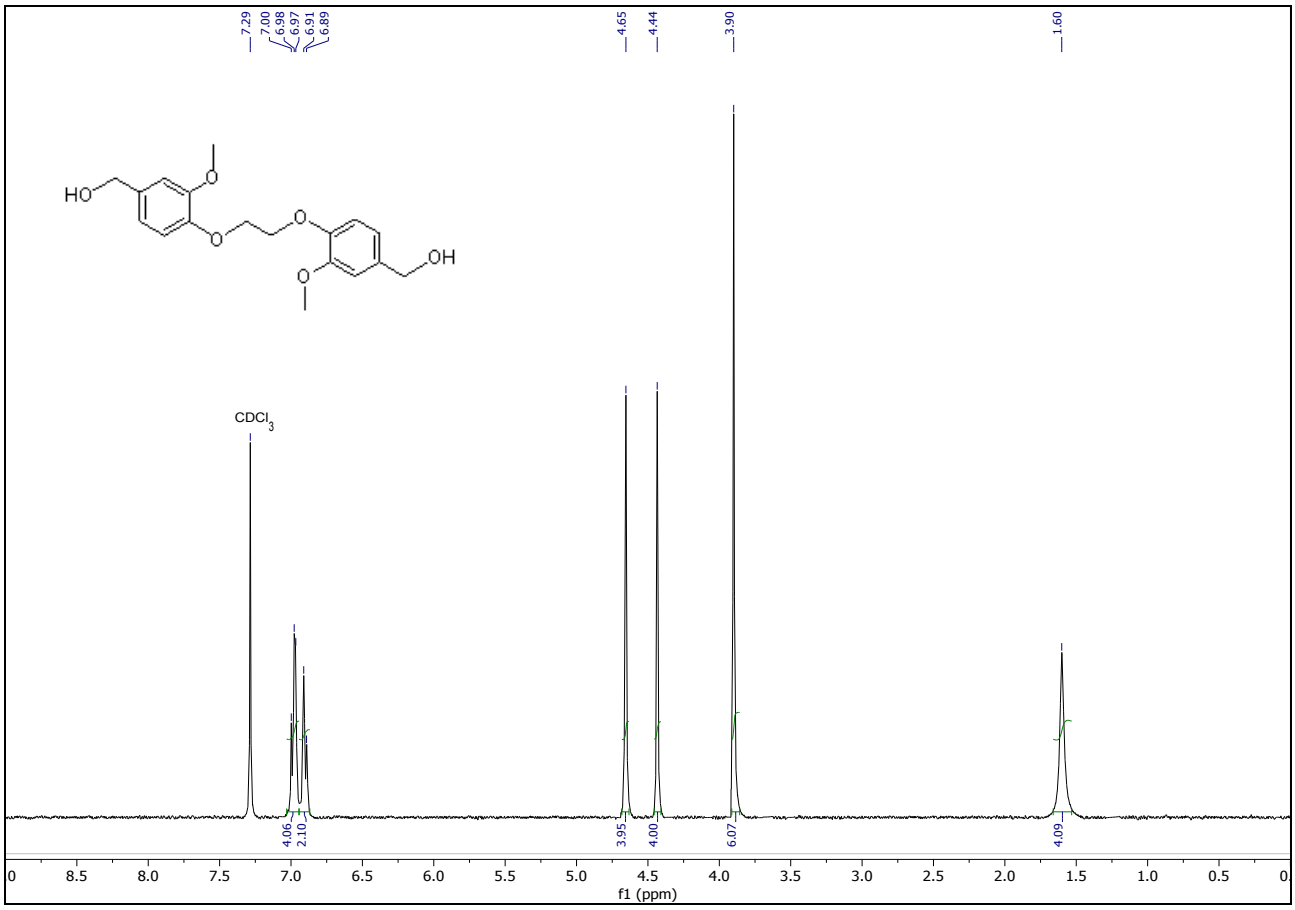

Figure S55. ^{1}H NMR spectrum (400.1 MHz) of the dibenzyl alcohol obtained from TH of 4,4'-[ethane-1,2-diylbis(oxy)]bis(3-methoxybenzaldehyde) (EDOMB) **i** in $CDCl_3$ at 25 °C.

^{1}H NMR (400 MHz, $CDCl_3$, 25 °C): δ = 6.98 (m, 4H; aromatic protons), 6.90 (m, 2H; aromatic protons), 4.65 (s, 4H; OCH_2CH_2O), 4.44 (s, 4H; CH_2OH), 3.90 (s, 6H; OCH_3), 1.60 ppm (br s, 4H; OH).

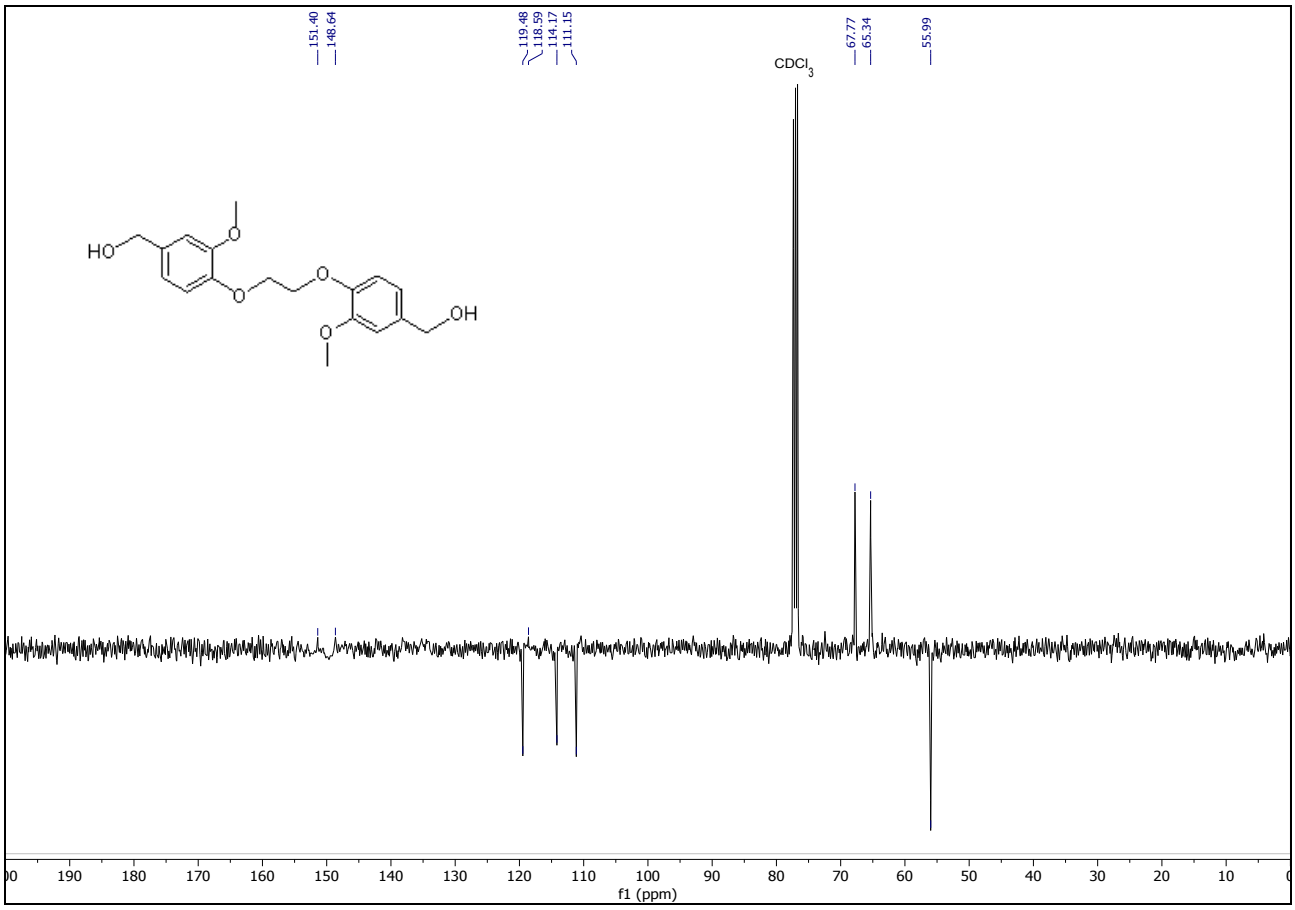

Figure S56. $^{13}C\{^{1}H\}$ DEPTQ NMR spectrum (100.6 MHz) of the dibenzyl alcohol obtained from TH of 4,4'-[ethane-1,2-diylbis(oxy)]bis(3-methoxybenzaldehyde) (EDOMB) **i** in $CDCl_3$ at 25 °C.

$^{3}C\{^{1}H\}$ NMR (100.6 MHz, $CDCl_3$, 25 °C): δ = 151.4 (s; aromatic ipso carbon), 148.6 (s; aromatic ipso carbon), 118.6 (s; aromatic ipso carbon), 119.4-111.2 (m; aromatic carbon atoms), 67.8 (s; OCH_2CH_2O), 65.3 (s; CH_2OH), 56.0 ppm (s; OCH_3).

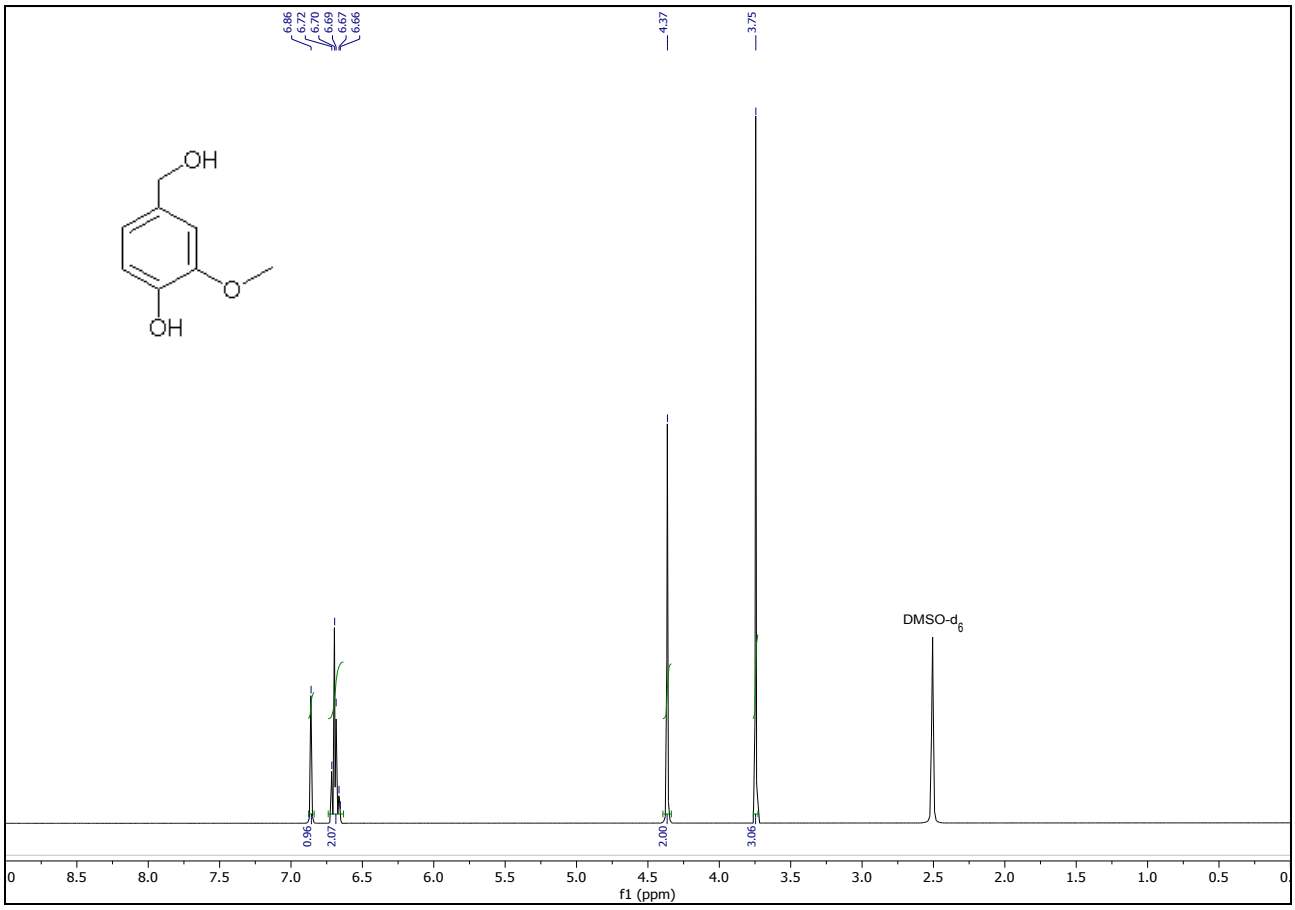

Figure S57. ^{1}H NMR spectrum (400.1 MHz) of vanillyl alcohol obtained from TH of vanillin **j** in DMSO-d_6 at 25 °C.

^{1}H NMR (400 MHz, DMSO-d_6, 25 °C): δ = 6.86 (br d, $^{3}J_{HH}$ = 1.3 Hz, 1H; aromatic proton), 6.73-6.65 (m, 2H; aromatic protons), 4.37 (s, 2H; CH_2OH), 3.75 ppm (s, 3H; CH_3O).

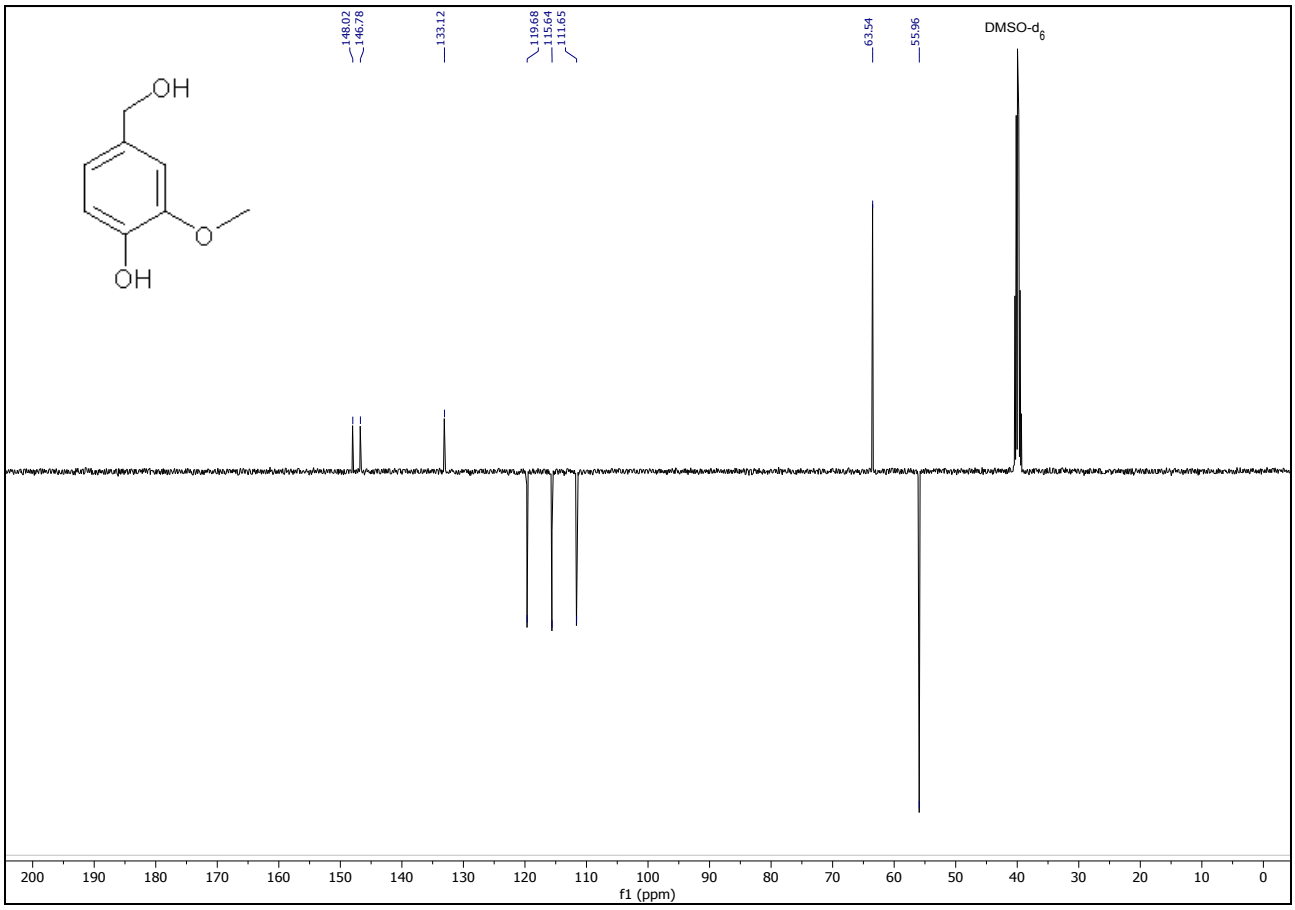

Figure S58. $^{13}C\{^{1}H\}$ DEPTQ NMR spectrum (100.6 MHz) of vanillyl alcohol obtained from TH of vanillin **j** in DMSO-d_6 at 25 °C.

$^{13}C\{^{1}H\}$ NMR (100.6 MHz, DMSO-d_6, 25 °C): δ = 148.0 (s; aromatic ipso carbon), 146.8 (s; aromatic ipso carbon), 133.1 (s; aromatic ipso carbon), 119.7 (s; aromatic carbon), 115.6 (s; aromatic carbon), 111.6 (s; aromatic carbon), 63.5 (s; CH_2O), 56.0 ppm (s; CH_3O).